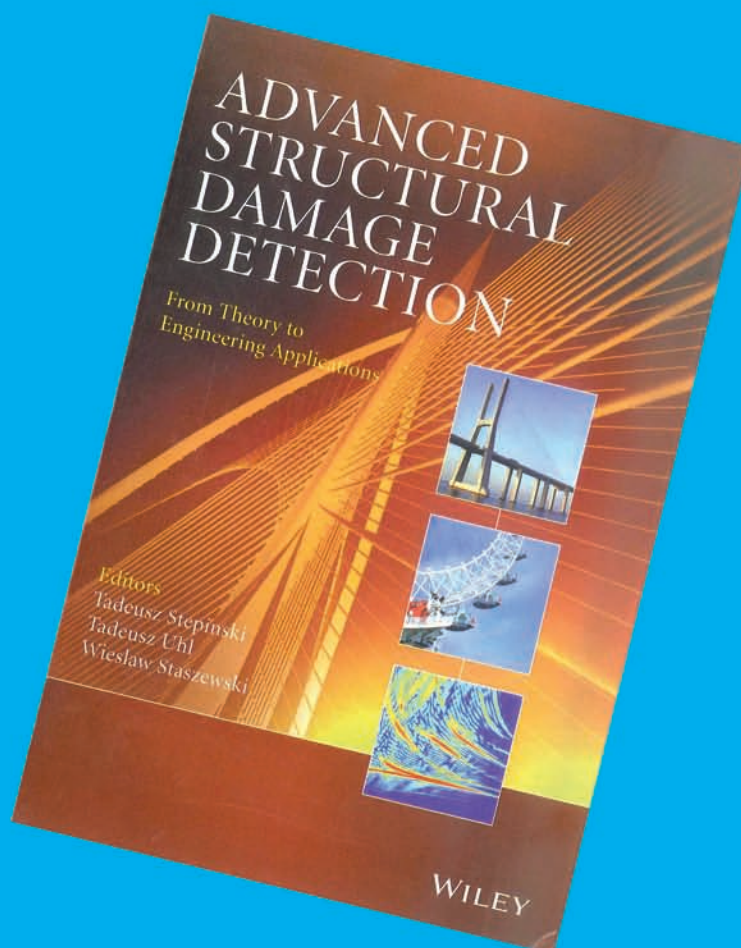




Diagnostyka

Applied Structural Health,
Usage and Condition Monitoring

ISSN 1641-6414



Vol. 14, No 2

PTDT, Warszawa, 2013

RADA PROGRAMOWA / PROGRAM COUNCIL

PRZEWODNICZĄCY / CHAIRMAN:

prof. dr hab. dr h.c. mult. **Czesław CEMPEL** *Politechnika Poznańska*

REDAKTOR NACZELNY / CHIEF EDITOR:

prof. dr hab. inż. **Wiesław STASZEWSKI** *AGH w Krakowie*

CZŁONKOWIE / MEMBERS:

prof. dr hab. inż. **Jan ADAMCZYK**
AGH w Krakowie

prof. **Francesco AYMERICH**
University of Cagliari – Italy

prof. **Jérôme ANTONI**
University of Technology of Compiègne – France

prof. dr. **Ioannis ANTONIADIS**
National Technical University Of Athens – Greece

dr inż. **Roman BARCZEWSKI**
Politechnika Poznańska

prof. dr hab. inż. **Walter BARTELMUS**
Politechnika Wroclawska

prof. dr hab. inż. **Wojciech BATKO**
AGH w Krakowie

prof. dr hab. inż. **Adam CHARCHALIS**
Akademia Morska w Gdyni

prof. **Li CHENG**
The Hong Kong Polytechnic University – China

prof. dr hab. inż. **Wojciech CHOLEWA**
Politechnika Śląska

prof. dr hab. inż. **Zbigniew DĄBROWSKI**
Politechnika Warszawska

prof. **Charles FARRAR**
Los Alamos National Laboratory – USA

prof. **Wiktor FRID**
Royal Institute of Technology in Stockholm – Sweden

dr inż. **Tomasz GAŁKA**
Instytut Energetyki w Warszawie

prof. **Len GELMAN**
Cranfield University – England

prof. **Mohamed HADDAR**
National School of Engineers of Sfax – Tunisia

prof. dr hab. inż. **Jan KICIŃSKI**
IMP w Gdańsku

prof. dr hab. inż. **Daniel KUJAWSKI**
Western Michigan University – USA

prof. **Graeme MANSON**
University of Sheffield – UK

prof. dr hab. **Wojciech MOCZULSKI**
Politechnika Śląska

prof. dr hab. inż. **Stanisław RADKOWSKI**
Politechnika Warszawska

prof. **Bob RANDALL**
University of South Wales – Australia

prof. dr **Raj B. K. N. RAO**
President COMADEM International – England

prof. **Riccardo RUBINI**
University of Modena and Reggio Emilia – Italy

prof. **Massimo RUZZENE**
Georgia Institute of Technology – USA

prof. **Vasily S. SHEVCHENKO**
BSSR Academy of Sciences Mińsk – Belarus

prof. **Menad SIDAHMED**
University of Technology Compiègne – France

Prof. **Tadeusz STEPINSKI**
Uppsala University - Sweden

prof. **Wiesław TRĄMPCZYŃSKI**
Politechnika Świętokrzyska

prof. dr hab. inż. **Tadeusz UHL**
AGH w Krakowie

prof. **Vitalijus VOLKOVAS**
Kaunas University of Technology – Lithuania

prof. **Keith WORDEN**
University of Sheffield – UK

prof. dr hab. inż. **Andrzej WILK**
Politechnika Śląska

dr **Gajraj Singh YADAVA**
Indian Institute of Technology – India

prof. dr hab. inż. **Radosław ZIMOROZ**
Politechnika Wroclawska

prof. dr hab. inż. **Bogdan ŻÓLTOWSKI**
UTP w Bydgoszczy

WYDAWCA:

Polskie Towarzystwo Diagnostyki Technicznej
ul. Narbutta 84
02-524 Warszawa

REDAKTOR NACZELNY:

prof. dr hab. inż. **Wiesław STASZEWSKI**

SEKRETARZ REDAKCJI:

dr inż. **Sławomir WIERZBICKI**

CZŁONKOWIE KOMITETU REDAKCYJNEGO:

dr inż. **Krzysztof LIGIER**
dr inż. **Paweł MIKOŁAJCZAK**

ADRES REDAKCJI:

Redakcja Diagnostyki
Katedra Budowy, Eksploatacji Pojazdów i Maszyn
UWM w Olsztynie
ul. Oczapowskiego 11, 10-736 Olsztyn, Poland
tel.: 89-523-48-11, fax: 89-523-34-63
www.diagnostyka.net.pl
e-mail: redakcja@diagnostyka.net.pl

KONTO PTDT:

Bank PEKAO SA O/Warszawa
nr konta: 33 1240 5963 1111 0000 4796 8376

NAKLAD: 500 egzemplarzy

Spis treści / Contents

Paweł MARKIEWICZ, Tadeusz UHL – AGH University of Science and Technology	3
MIMO random control method for vibration testing <i>Rozwój systemów sterowania dla testów wibracyjnych MIMO</i>	
Joanna IWANIEC – AGH University of Science and Technology.....	11
Identification of car suspension system parameters on the basis of exploitative measurements <i>Eksploatacyjna identyfikacja parametrów układu zawieszenia samochodu osobowego</i>	
Rafał HEIN, Cezary ORLIKOWSKI – Gdansk University of Technology	17
Hybrid model of geared rotor system <i>Hybrydowy model układu wirników z przekładnią</i>	
Andrzej GRZĄDZIELA, Bogdan SZTUROMSKI, Marcin KLUCZYK – Polish Naval Academy.....	23
Diagnosis design of ship hull strength of treated by dynamic load <i>Diagnozowanie projektowe wytrzymałości kadłuba okrętowego poddanego oddziaływaniom dynamicznym</i>	
Tomasz BARSZCZ, Andrzej BIELECKI – AGH University of Science and Technology, Mateusz WÓJCIK – Jagiellonian University	31
Vibration signals processing by cellular automata for wind turbines intelligent monitoring <i>Przetwarzanie sygnałów drganiowych przy pomocy automatów komórkowych w celu inteligentnego monitoringu turbin wiatrowych</i>	
Mirosław PAJOR, Jacek ZAPŁATA – Zachodniopomorski Uniwersytet Technologiczny w Szczecinie	37
Supervising and compensation of thermal error of CNC feed ball screw <i>Nadzorowanie termiczne oraz kompensacja błędów odkształceń cieplnych śrub pociągowych obrabiarek CNC</i>	
Rafał HEIN, Cezary ORLIKOWSKI – Gdansk University of Technology	43
Simplified dynamic model of rotating beam <i>Uproszczony model dynamiczny wirującej belki</i>	
Bogdan BROEL-PLATER, Paweł DWORAK, Krzysztof JAROSZEWSKI – Zachodniopomorski Uniwersytet Technologiczny w Szczecinie.....	49
Chosen aspects of micro milling machine diagnostics <i>Wybrane aspekty diagnostyki mikrofrezarki</i>	
Rafał BURDZIK – The Silesian University of Technology	57
Research on structure and directional distribution of vibration generated by engine in the location where vibrations penetrate the human organism <i>Badania struktury i rozkładu kierunkowego drgań pochodzących od silnika w miejscach wnika- nia do ciała kierowcy</i>	
Łukasz KONIECZNY, Rafał BURDZIK, Jan WARCZEK – The Silesian University of Technology	63
The uncertainty of determining shock absorber damping characteristic on indicator test stand <i>Niepewność wyznaczania charakterystyki tłumienia amortyzatora na stanowisku indykatorowym</i>	
Vitalij NICHOGA, Igor STOROZH – Lviv Polytechnic National University, Liubomyr VASHCHYSHYN – Karpenko Physico-Mechanical Institute of the NAS of Ukraine	67
Model of rail crack based on a discrete set of loops with current <i>Model pęknięcia szyny kolejowej bazujący na dyskretnych pętach prądowych</i>	
Warto przeczytać / Worth to read	71

MIMO RANDOM CONTROL METHOD FOR VIBRATION TESTING

Paweł MARKIEWICZ, Tadeusz UHL

AGH University of Science and Technology, Faculty of Mechanical Engineering and Robotics,
Department of Robotics and Mechatronics
Al. Mickiewicza 30, 30-059 Kraków, fax: +48 12 634 35 05, e-mail: pmarkiew@agh.edu.pl

Summary

In following paper control algorithms used for MIMO vibration control were presented and investigated with regard to application in modal analysis. Implementation of existing control algorithms was presented for verification of its operation and development of new method combining several older methods. Objective of implementation of new method was increasing performance and quality of calculations and closer look in to development of SINE SWEEP and TIME WAVEFOR REPLICATION. Comparison of simulation and measurement data is presented in two cases of control with six degree of freedom system.

Keywords: modal analysis, vibration control, environmental testing.

ROZWÓJ SYSTEMÓW STEROWANIA DLA TESTÓW WIBRACYJNYCH MIMO

Streszczenie

W artykule opisano istniejące metody sterowania MIMO, oraz ich zastosowanie w analizie modalnej. Przedstawiono implementację istniejących algorytmów sterowania do testów wibracyjnych MIMO celem weryfikacji ich działania oraz połączenia ich w nową metodę sterowania. Celem utworzenia nowej metody sterowania było zwiększenie wydajności i jakości obliczeń a także spojrzenie w kierunku dalszego rozwoju sterowania do metod SINE SWEEP oraz TIME WAVEFORM REPLICATION. Porównanie wyników symulacji oraz danych pomiarowych zaprezentowane jest na dwóch przykładach kontroli systemu o sześciu stopniach swobody.

Słowa kluczowe: analiza modalna, sterowanie wibracjami, testy środowiskowe.

1. INTRODUCTION

1.1. Purpose and resources

Most of the research and calculations presented in following paper were performed as a part of internship project in LMS International, in Belgium. The project was related to verification and development of control algorithm used in part of software that is produced by the company. Main purpose of the research is controlling vibration environmental testing of structures requiring multiple points of excitation. The research is based on various control methods applied for vibrational testing starting from elongated structures random control through sine control and finishing on square system models.

For better understanding the principle of vibration testing that will be discussed in details, it would be roughly described on an example of structure that could be observed in everyday life, for example car dashboard. Dashboard – which in further description would be called test subject is analyzed in normal operation conditions. Multiple accelerometers are placed on the test subject and road test is conducted. Therefore stored data from

accelerometers is a target result that is desired as a response in environmental test (either spectrum of data – random control, or time signal – time waveform replication). For this purpose algorithms listed before are used in processing the data and creating drive signals for exciters that are connected to test subject. Exciters have got to be controlled in this way that response signal of accelerometers mounted on test subject match in given threshold the data from road test or other assumed form.

1.2. Description of problem

Starting with sketching up main principles of MIMO testing would be most convenient to describe what exactly is happening with the system and how it is done. As presented in previous part of introduction, test that is performed is done on some mechanical structure, which is either suspended or mounted on shaker system (TEAM Cube device). Structure is excited with vibrations. Basically exciters (electrical, hydraulic etc.) are acting on the structure with force that is variable in time. In case of MIMO analysis, the number of shakers must be higher than one. Currently tests were done with up to 6 exciters.

When structure is being excited by means described above, response of the system is measured by multiple accelerometers. In current stage the whole setup is prepared to process square systems – those consisting of same number of inputs and same number of outputs. Means used for digitalization of results are SCADAS, which front ends are also used for creating drive signals for exciters. Front end is connected to amplifiers of given type of actuation, either for electromagnetic shakers or hydraulic valves.

Data acquired from measurements is processed in computer software Test.Lab, for which algorithms are being developed. At first part of the measurement so called system identification is performed, which basically is exciting the system with band limited white noise. Usually the band of the noise is much wider than band in which test itself is performed.

2. DESCRIPTION OF MEASUREMENT SETUP

For executing operations for which calculations are performed in control algorithms, proper hardware is needed. Measurement and actuation devices along with data acquisition systems are considered to be a part of system under test. First device that would be described is double function device, used for creating time signal that is sent to amplifiers and is used also for collecting data from transducer. This device is called SCADA. In research performed in company various types of data acquisition systems were used, all of them were compliant with Test.Lab software. Devices are also produced by the LMS International Company.

For converting drive signals to force actually exciting the structure, various types of shakers were used, for electrical shakers amplification of signal was required. For creating the analog signal from values computed by the algorithm, digital to analog converter is used. In case of hydraulic shakers systems with PID controllers controlling valves that are responsible for driving actuators with given form of signal were required.

As a final piece of equipment connected back to SCADA, transducers modifying accelerations in to electrical signal which then is processed through analog to digital converter, and further processed as a digitalized value in the algorithm itself.

2.1. Measurement and signal generation

Supervisory control and data acquisition systems are devices used for gathering and processing data. Usually the devices are converting electrical values such as voltage to digital form that can be processed further by computer. Second application of SCADA systems is generation of analog signal, that could be further directed to devices that are being controlled. For processing input data, subsystems called Analog

to Digital Converters are used, principle of operation of this type of subsystem will be discussed in further parts of paper, along with devices for output signal generation, Digital to Analog Converters.

Those devices are available in various sizes and configurations, following from mobile devices with rugged construction to multiple customizable systems with interchangeable cards. Following devices are able to provide from 8 channels up to 2000 channels when connected in network. In many types of data acquisition and control systems wireless communication is embedded for various diagnostic and test applications.

2.2 Excitation system

Exciter is a device which role is to excite vibrations in the structure. Sometimes it is called shaker. Simplest way of describing this device is, to say it's actuator with very small amplitude of motion. We can diversify exciters in three main groups: electrodynamics, piezoelectric and hydraulic. Those types of exciters have various applications usually regarding size of the structure, amplitude and bandwidth of desired vibrations

Perfect example of multi axial hydraulic exciter system is device called Cube, produced by TEAM corporations. This unit is composed of six hydraulic shakers mounted inside of cubic structure which outer surface is prepared for mounting test pieces for measurements.

Each of the exciters composing this device is responsible for one degree of freedom in motion that is executed by the device. According to the manufacturer the device operating frequencies range from 0 to 250 Hz, can provide displacement of 100mm and force up to 62 kN.

TEAM cube was used for testing MIMO random algorithm mentioned in literature, results from measurements and tests were used in Matlab validation discussed in details in further parts of the paper.



Figure 1. Team CUBE in KU Leuven

2.3. Sensors

Devices that are used for gathering information about vibrations – transducers converting values of acceleration to electrical signal are called accelerometers. There are many types of accelerometers that vary regarding on the principle of operation. Currently most common type of accelerometers that are applied for research and test applications are MEMS accelerometers. MEM stands for Micro Electro Mechanical System. But the first and most groundbreaking device that was introduced was piezoelectric accelerometer. Piezoelectric accelerometers mostly find application in commercial use rather than testing. MEMS accelerometers are usually small systems, in many cases 3 accelerometers in one device – oriented along 3 axes. These type of accelerometer are called 3 axis accelerometers and provide data about motion in 3 dimensions. Principle of operation of MEMS accelerometers is based on cantilever beam with seismic mass attached to it. Due to the motion of the device, mass deflects from its original position. Deflection of the mass is measured, in most cases in analogue way, converting the deflection to capacitance – due to change of distance between two conductors. Than the capacitance has an influence on the voltage that is between two parts of the material and is further processed in SCADAS system connected via shielded cable to the accelerometer. Biggest disadvantage of using this type of devices for measurements, is introducing their mass to the system, what causes changes in the system properties.

3. THEORETICAL BASE FOR ALGORITHM DEVELOPMENT

3.1. Control method

First step that was performed during research regarding MIMO random was implementation of system identification of TEAM Cube (6 exciters - in description called “Output 1, 2, ..., 6”) equipped with 12 response channels (accelerometers) placed in corners of the cube (1, 2, 3, 4) at the top and bottom side, measuring acceleration in X, Y or Z, to old existing algorithm, that was used and developed for testing elongated structures such as pipes and elongated boxes.

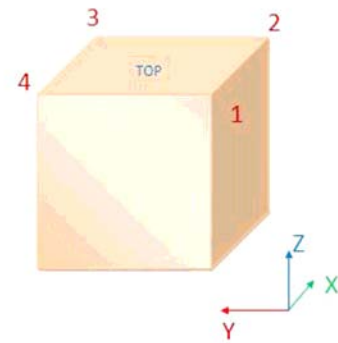


Figure 2. orientation scheme of CUBE

During data processing in this algorithm data taken from system identification is being interpolated so that FRF could be used for creating longer time domain signals that are being used for simulating drives.

Frequency response model is showing relation between inputs and outputs as Amplitude [(m/s²)/V] vs. Frequency [Hz]. System identification was performed in much wider spectrum than shown on plots, but only band from 20 to 200Hz was chosen for simulation and environmental testing, due to the characteristics of the system.

After implementation of FRF the reference model was implemented. Two tests were performed with two reference models, for which Cross Spectral Density, Power Spectral Density and Coherence was adjusted in the way giving two easily observable schemes of structure behavior. 1st example was “Zrotation”, so control algorithm had to adjust the input signals (drive signals) in such manner that the Cube would only execute vibrations as rotation around Z axis.

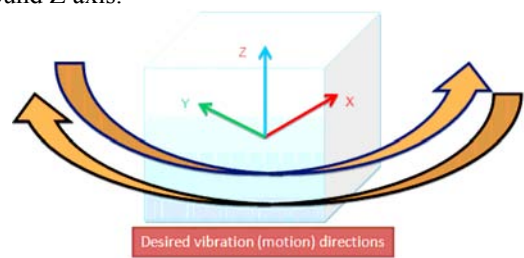


Figure 3. Z Rotation scheme

	Top3+X	Top4+X	Base3+X	Base4+X	Top2+Y	Top3+Y	Base2+Y	Base3+Y	Top1+Z	Top2+Z	Top3+Z	Top4+Z
Top3+X	0.5045	0.4994	0.4994	0.4994	0.4994	0.4994	0.4994	0.4994	0.0050	0.0050	0.0050	0.0050
Top4+X	0.0000	0.5045	0.4994	0.4994	0.4994	0.4994	0.4994	0.4994	0.0050	0.0050	0.0050	0.0050
Base3+X	0.0000	0.0000	0.5045	0.4994	0.4994	0.4994	0.4994	0.4994	0.0050	0.0050	0.0050	0.0050
Base4+X	0.0000	0.0000	0.0000	0.5045	0.4994	0.4994	0.4994	0.4994	0.0050	0.0050	0.0050	0.0050
Top2+Y	0.0000	0.0000	0.0000	0.0000	0.5045	0.4994	0.4994	0.4994	0.0050	0.0050	0.0050	0.0050
Top3+Y	0.0000	0.0000	0.0000	0.0000	0.0000	0.5045	0.4994	0.4994	0.0050	0.0050	0.0050	0.0050
Base2+Y	0.0000	0.0000	0.0000	0.0000	0.0000	0.0000	0.5045	0.4994	0.0050	0.0050	0.0050	0.0050
Base3+Y	0.0000	0.0000	0.0000	0.0000	0.0000	0.0000	0.0000	0.5045	0.0050	0.0050	0.0050	0.0050
Top1+Z	0.0000	0.0000	0.0000	0.0000	0.0000	0.0000	0.0000	0.0000	0.0050	0.0050	0.0050	0.0050
Top2+Z	0.0000	0.0000	0.0000	0.0000	0.0000	0.0000	0.0000	0.0000	0.0050	0.0050	0.0050	0.0050
Top3+Z	0.0000	0.0000	0.0000	0.0000	0.0000	0.0000	0.0000	0.0000	0.0000	0.0050	0.0050	0.0050
Top4+Z	0.0000	0.0000	0.0000	0.0000	0.0000	0.0000	0.0000	0.0000	0.0000	0.0000	0.0050	0.0050

Figure 4. CPSD of "Z rotation"

	Top3+X	Top4+X	Base3+X	Base4+X	Top2+Y	Top3+Y	Base2+Y	Base3+Y	Top1+Z	Top2+Z	Top3+Z	Top4+Z
Top3+X		0.9800	0.9800	0.9800	0.9800	0.9800	0.9800	0.9800	0.0100	0.0100	0.0100	0.0100
Top4+X			0.9800	0.9800	0.9800	0.9800	0.9800	0.9800	0.0100	0.0100	0.0100	0.0100
Base3+X				0.9800	0.9800	0.9800	0.9800	0.9800	0.0100	0.0100	0.0100	0.0100
Base4+X					0.9800	0.9800	0.9800	0.9800	0.0100	0.0100	0.0100	0.0100
Top2+Y						0.9800	0.9800	0.9800	0.0100	0.0100	0.0100	0.0100
Top3+Y							0.9800	0.9800	0.0100	0.0100	0.0100	0.0100
Base2+Y								0.9800	0.0100	0.0100	0.0100	0.0100
Base3+Y									0.0100	0.0100	0.0100	0.0100
Top1+Z										0.9800	0.9800	0.9800
Top2+Z											0.9800	0.9800
Top3+Z												0.9800

Figure 5. Coherence of "Z rotation"

Reference models presented in tables require the system to perform rotation around Z axis. Therefore value of all power spectral densities and cross power spectral densities describing channels representing accelerations along axes X and Y are set to corresponding values. Z axis cross power spectral densities and power spectral densities are set to low value, not exactly zero because such performance would be hard to obtain in control system. Regarding coherence between channels, correlation between channels X and Y are set to be almost equal 1, this means that each of the signals should be in phase. When those channels are in phase and Z channel is out of phase regarding X and Y while between Z channel coherence is almost 1 phenomenon of rotation around Z axis occurs without rotation around other axes.

2nd example was implementation of model that would perform only linear motion along Z axis – "Ztranslation".

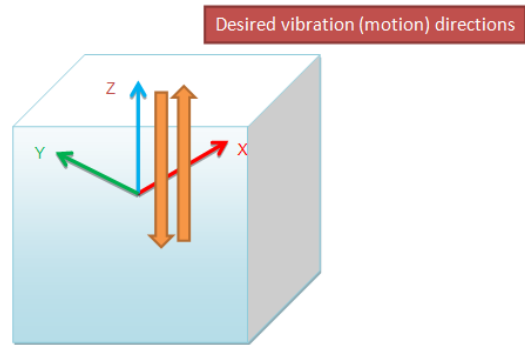


Figure 6. Z Translation scenario

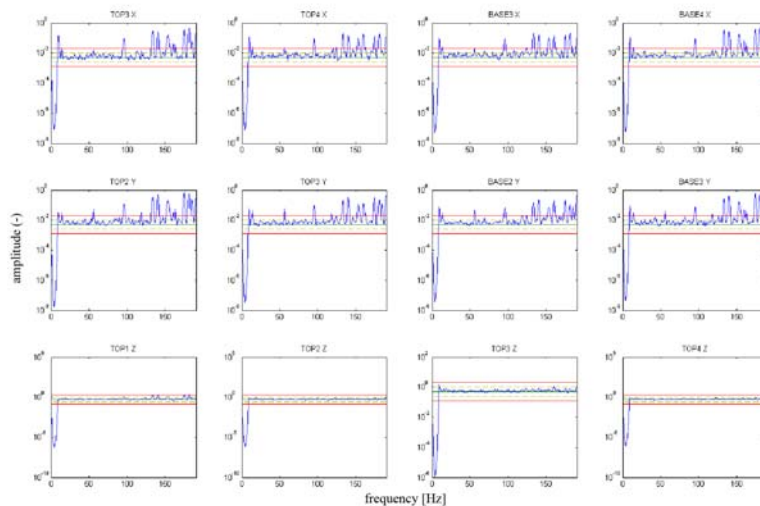


Figure 7. Simulated Response

	Top3:+X	Top4:+X	Base3:+X	Base4:+X	Top2:+Y	Top3:+Y	Base2:+Y	Base3:+Y	Top1:+Z	Top2:+Z	Top3:+Z	Top4:+Z
Top3:+X		0.9800	0.9800	0.9800	0.9800	0.9800	0.9800	0.9800	0.0100	0.0100	0.0100	0.0100
Top4:+X			0.9800	0.9800	0.9800	0.9800	0.9800	0.9800	0.0100	0.0100	0.0100	0.0100
Base3:+X				0.9800	0.9800	0.9800	0.9800	0.9800	0.0100	0.0100	0.0100	0.0100
Base4:+X					0.9800	0.9800	0.9800	0.9800	0.0100	0.0100	0.0100	0.0100
Top2:+Y						0.9800	0.9800	0.9800	0.0100	0.0100	0.0100	0.0100
Top3:+Y							0.9800	0.9800	0.0100	0.0100	0.0100	0.0100
Base2:+Y								0.9800	0.0100	0.0100	0.0100	0.0100
Base3:+Y									0.0100	0.0100	0.0100	0.0100
Top1:+Z										0.9800	0.9800	0.9800
Top2:+Z											0.9800	0.9800
Top3:+Z												0.9800

Figure 8. CPSD of "Z translation"

	Top3:+X	Top4:+X	Base3:+X	Base4:+X	Top2:+Y	Top3:+Y	Base2:+Y	Base3:+Y	Top1:+Z	Top2:+Z	Top3:+Z	Top4:+Z
Top3:+X		0.0100	0.0100	0.0100	0.0100	0.0100	0.0100	0.0100	0.0100	0.0100	0.0100	0.0100
Top4:+X			0.0100	0.0100	0.0100	0.0100	0.0100	0.0100	0.0100	0.0100	0.0100	0.0100
Base3:+X				0.0100	0.0100	0.0100	0.0100	0.0100	0.0100	0.0100	0.0100	0.0100
Base4:+X					0.0100	0.0100	0.0100	0.0100	0.0100	0.0100	0.0100	0.0100
Top2:+Y						0.0100	0.0100	0.0100	0.0100	0.0100	0.0100	0.0100
Top3:+Y							0.0100	0.0100	0.0100	0.0100	0.0100	0.0100
Base2:+Y								0.0100	0.0100	0.0100	0.0100	0.0100
Base3:+Y									0.0100	0.0100	0.0100	0.0100
Top1:+Z										0.9990	0.9990	0.9990
Top2:+Z											0.9990	0.9990
Top3:+Z												0.9990
Top4:+Z												

Figure 9. Coherence of "Z translation"

In case described above the desired motion of system was only translation along the Z axis, this setup requires only coherence between Z channels. During testing vertical motion should not be influenced by motion from other directions (X and Y) therefore cross power spectral density is set to 1 between Z channels.

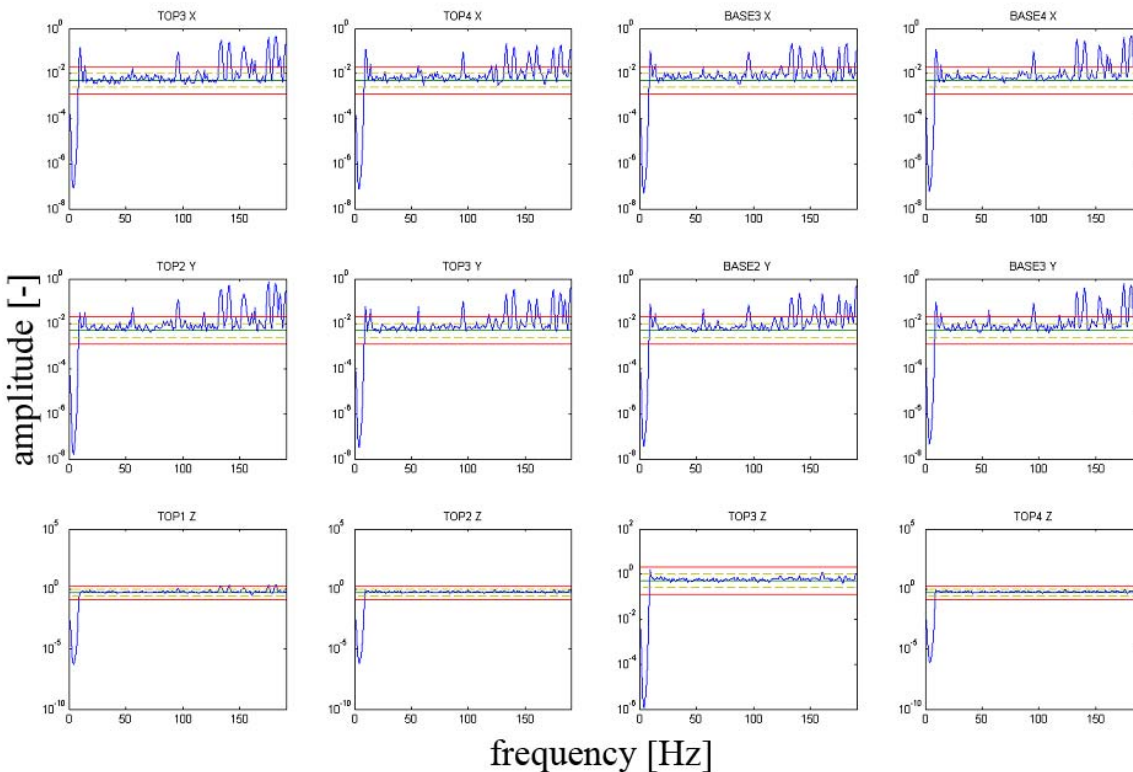


Figure 10. Simulated Response Z Translation

4. SIMULATION AND EXPERIMENT RESULTS COMPARISON

As in case of first discussed control method (3.1.) same procedures and same virtual model will be applied. The system will be tested as in previous example in frequency range from 0 to 200Hz, this time the simulation results will be compared with measurements performed on Team CUBE device in a setup described in first algorithm. The test which was performed on the real structure used algorithm from (3.2.)

4.1. Z-Rotation case

During “Z-Rotation” case the system needs to be excited in a way that motion of the structure is performed only as a rotation around Z-axis, same reference profiles were used as in case of previous implementations.

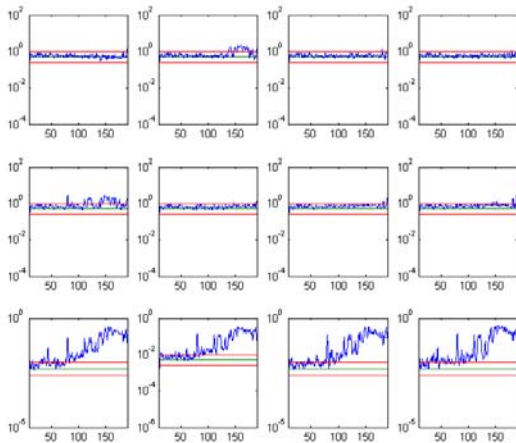


Figure 11. new control results - z-rotation

Control results obtained after performing 36 iterations are satisfactory, even though in case of Z signals we can see big offset from desired values, exciding +/-3db range, but in case of this test it still value that could be neglected because target value is zero and results are of order so could be called acceptable, comparing this results to measurement results it could be said that control in case of real measurements works better.

4.2. Z-Translation case

During “Z-Translation” case the system needs to be excited in a way that motion of the structure is performed only as a translation along Z-axis, same reference profiles were used as in case of previous implementations.

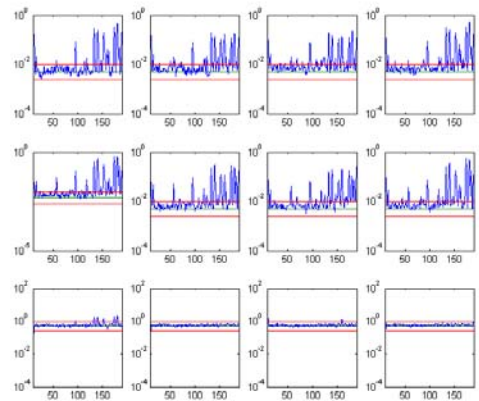


Figure 12. new control results - z-translation

In the same manner as in case of previous simulation, signal which is set as reference do be equal zero, exceeds the limits. Regardless of this fact the result is satisfying as the output signal does not have big value that could influence the test overall.,

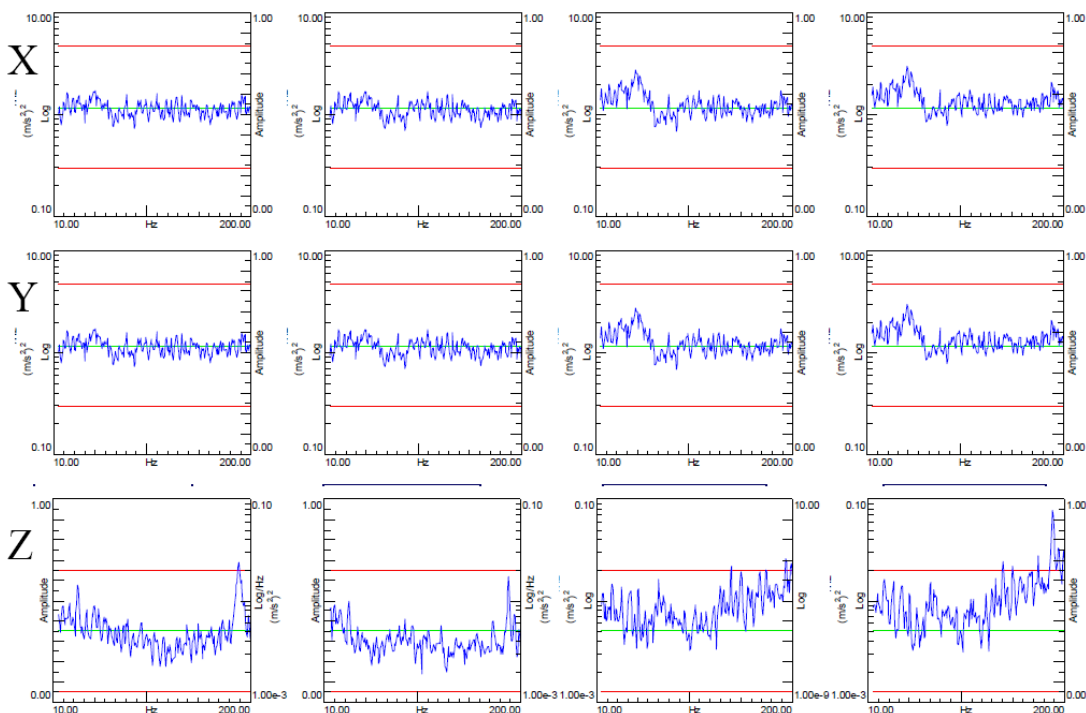


Figure 13. Measurement Results, Z Rotation

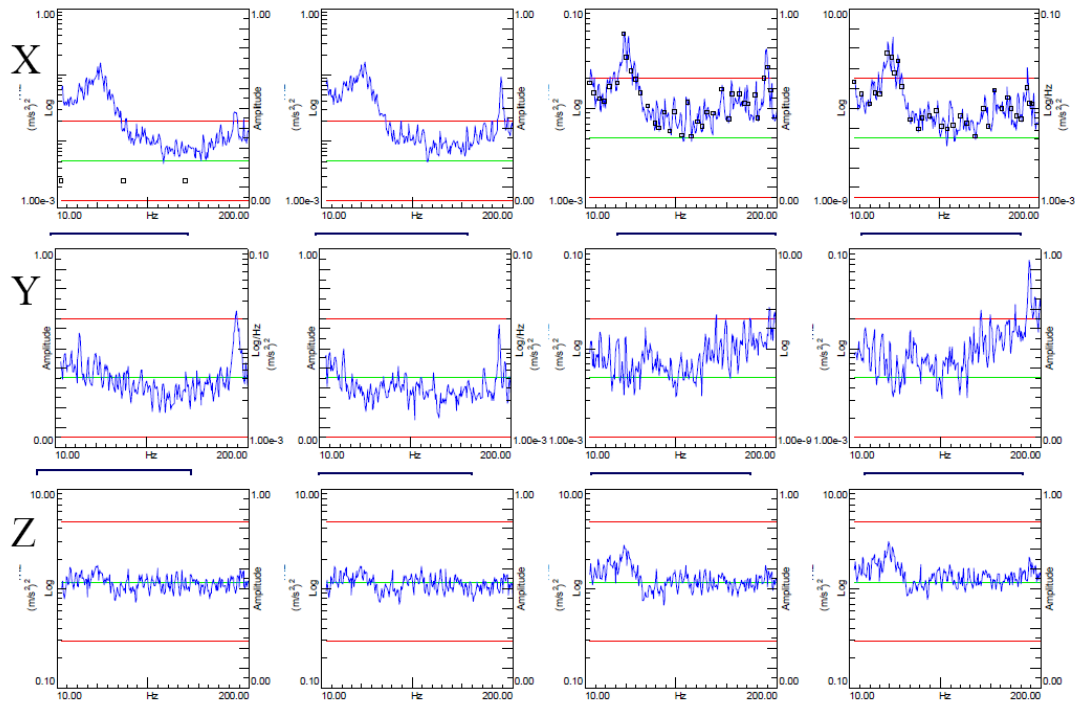


Figure 14. Measurement Results, Z Translation

similar behavior could be observed in measurements performed on real structure.

Comparing the results we can state, that the values of coherence from simulation and measurements are correct, in every case values of coherence are directed in the way that reference model is set up, therefore proper operation of excitation system is obtained.

5. CONCLUSIONS

Summing up the whole research with base of results, a lot of questions rise up. Even though merging presented algorithms resulted in obtaining method which is more efficient in calculations, uses much less control loop iterations for performing calculations the system is not perfect, in many cases it was not able to control spectra at lower frequencies and had problems with controlling systems with higher number of sensors. Yet it could

be used as a base for developing next methods of control, such as MIMO sine sweep, and MIMO time waveform replication, which is the most complex from control point of view from all vibrational MIMO testing schemes.

The algorithm operation was only verified with simulation methods in Matlab, therefore its comparison with real measurements is presented to be a visualization of its capabilities. Real verification of its operation would be confirmed by performing environmental test and investigating the results, which may be coherent with simulation as the new method is solely based on previously existing and functional control methodologies.

If such tests would prove proper operation of this new control methodology, next step in development could be undertaken.

REFERENCES

- [1] Underwood, M. A., *Multi-exciter Testing Applications: Theory and Practice*, Proceedings of the institute of Environmental Sciences and Technology, April 2002.
- [2] Underwood, M. A. and Keller, T., *Rectangular Control of Multi-Shaker Systems; Theory and some Practical results*, Proceedings of the Institute of Environmental Sciences and Technology, April 2003.
- [3] Underwood, M.A., *Adaptive Control Method for Multiexciter Sine Tests*, United States Patent No. 5,299,459, April 1994.
- [4] Underwood, M. A., *Apparatus and Method for Adaptive Closed Loop Control of Shock Testing Systems*, United States Patent No. 5,517,426, May 1996.
- [5] Underwood, M. A. and Keller, T., *Understanding and Using the Spectral Density Matrix*, Proceedings of the 76th Shock & Vibration Symposium, Destin, Florida, October 2005.
- [6] Smallwood, D. O. and Gregory, D., *Evaluation of a Six-DOF Electrodynamic Shaker System*.
- [7] Underwood, M.A., and Hale, M., "MIMO Testing Methodologies"
- [8] Matlab help, Matlab version 7.9.0 (R2009b).
- [9] SCADA available at: <http://pl.wikipedia.org/wiki/SCADA>
- [10] CUBE specification available at: <http://www.teamcorporation.com/cube.php>
- [11] Accelerometer available at: <http://en.wikipedia.org/wiki/Accelerometer>



destructive testing and satellite technology.

Pawel MARKIEWICZ

received a M.Sc. degree in Mechatronics from the Faculty of Mechanical Engineering and Robotics, AGH University of Science and Technology in 2012. He is a Ph.D. Student in the Department of Mechatronics and Robotics. His main research interest is non-



analysis. His field of scientific interest concerns control systems and mechatronic systems.

Tadeusz UHL

received a M.Sc. degree in 1979 at AGH University of Science and Technology, the Ph.D. in 1983. He is currently employed at AGH University as a professor and Head of Department of Robotics and Mechatronics. His main area of research is construction dynamics, especially modal

IDENTIFICATION OF CAR SUSPENSION SYSTEM PARAMETERS ON THE BASIS OF EXPLOITATIONAL MEASUREMENTS

Joanna IWANIEC

AGH University of Science and Technology, Faculty of Mechanical Engineering and Robotics,
Department of Robotics and Mechatronics
Mickiewicz Alley 30, 30-059 Krakow, fax: (012) 634-35-05, email: jiwaniec@agh.edu.pl

Summary

The paper concerns exploitation identification of structural parameters of the Toyota Camry suspension system. Analysis was carried out by means of the output-only nonlinear system identification method for vibration accelerations recorded along the centre line of absorber while driving over a bumpy road profile. As the measure of accuracy of estimated suspension parameters the percentage relative error of car body mass estimation was assumed. Presented methodology can be used for the purposes of model based diagnostics and maintenance planning.

Keywords: exploitation (output-only) identification, nonlinear system, car suspension system.

EKSPLOATACYJNA IDENTYFIKACJA PARAMETRÓW UKŁADU ZAWIESZENIA SAMOCHODU OSOBOWEGO

Streszczenie

W pracy przedstawiono rezultaty eksploatacyjnej identyfikacji parametrów układu zawieszenia samochodu osobowego Toyota Camry. Badania przeprowadzono z zastosowaniem eksploatacyjnej metody identyfikacji układów nieliniowych na podstawie charakterystyk czasowych przyspieszeń drgań zmierzonych wzdłuż osi amortyzatora podczas jazdy po wyboistej nawierzchni. Jako miarę dokładności estymacji parametrów rozpatrywanego układu zawieszenia przyjęto procentowy błąd względny estymacji masy karoserii. Zaprezentowana w pracy metoda badawcza znajduje zastosowanie w diagnostyce realizowanej w oparciu o model układu nieuszkodzonego oraz w planowaniu przeglądów.

Słowa kluczowe: identyfikacja w warunkach eksploatacyjnych, układ nieliniowy, układ zawieszenia samochodu osobowego.

1. INTRODUCTION

Vast majority of real mechanical systems is nonlinear to a certain degree. Nonlinear industrial systems can be classified as systems designed for work in nonlinear ranges of dynamic characteristics and systems of nonlinear properties resulting from fault appearance. Although the sources of nonlinear properties can vary [1, 2, 3, 4], all the nonlinear systems exhibit some common properties. In general, they do not follow the superposition principle and exhibit complex phenomena unusual for linear systems, such as jumps, self-induced and chaotic vibrations, changes in natural frequencies resulting from changes in excitation amplitudes and coexistence of many stable equilibrium positions. In view of these properties, classical identification methods can not be used for the purposes of nonlinear system identification.

For many years linearization methods [5, 6] were the only methods used for the purposes of nonlinear system identification. In the following years the concept of nonlinear normal modes was introduced

[7, 8] while for weakly nonlinear systems perturbation theory was developed [9, 10]. Recently, mechanical systems are designed for work in nonlinear ranges of dynamic characteristics taking advantage of phenomena characteristic for nonlinear systems [11, 12].

The first research into nonlinear system identification methods goes back to the seventies [13, 14]. Then identification of single degree-of-freedom systems with various types of nonlinearities was considered. Multiple degree-of-freedom identification methods have been elaborated over last 15 years.

The methods considered above are called 'classical' nonlinear system identification methods and are usually classified into a few basic groups: linearization methods, time domain methods, frequency domain methods, modal methods, time-frequency analysis methods, methods based on neural networks, wavelet transform methods, structural model updating. Unfortunately, the range of practical applications of these methods is limited due to strong requirements concerning linear system

behaviour around any operating point and necessity of performing input (excitation) measurement.

In the paper, for the purposes of identification of car suspension parameters, application of the exploitational nonlinear system identification method was proposed. Selection of such a method is motivated by the fact that, on the contrary to the classical nonlinear system identification methods, it requires neither the knowledge of excitations acting on the system of interest nor linear system dynamic behaviour in a broad frequency range around any operating point [15, 16]. The possibility of system identification in the exploitational conditions is of key importance since the measurement of operational exciting forces (e.g. tire – road contact forces) is difficult or impossible to carry out and diagnostics of many industrial systems, for the economical or technological reasons, should be carried out during the normal work.

2. ASSUMED IDENTIFICATION METHOD

Identification of the considered suspension system parameters was performed by means of the nonlinear system identification method [15, 17], the algorithm of which combines restoring force, boundary perturbation and direct parameter estimation techniques (Fig. 1). Since the method requires neither input measurement nor linear system behaviour around an operating point, it can be used for both nonlinearity detection and parameter identification of nonlinear systems working under operational loads, the measurement of which is difficult or impossible to carry out.

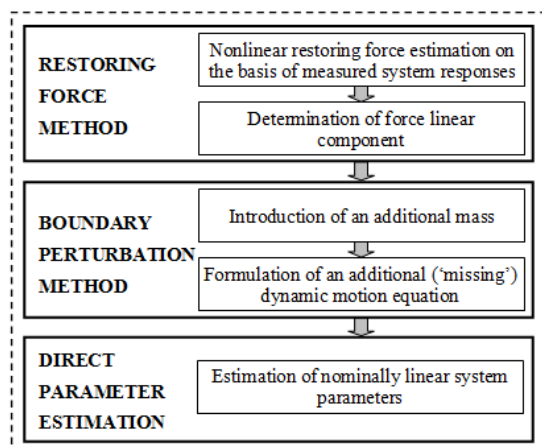


Fig. 1. Algorithm of the applied exploitational nonlinear system identification method

In the first step of the considered algorithm, system dynamic motion equations are formulated and nonlinear restoring forces are reconstructed on the basis of measured system responses. In the following step, identified nonlinear restoring forces are eliminated from the formulated dynamic motion equations that describe balance of forces acting on

the considered system. Since the excitation remains unknown, the number of unknown parameters is greater than the number of system dynamic motion equations that can be formulated. In order to provide an additional dynamic motion equation and determine absolute values of system parameters the boundary perturbation method is used. The method consists in introducing an additional mass altering dynamic behaviour of the considered system and retaking measurements of modified system masses accelerations. In the final step values of system parameters are estimated.

3. IDENTIFICATION OF CAR SUSPENSION PARAMETERS

The research was carried out for the rear left suspension system of Toyota Camry, version 2.2 LE, 2001 (Fig. 2).

In the course of the identification experiment, the measurements of acceleration time histories were taken by means of two single-axial piezoelectric sensors placed on the spindle (sensor 1, 'lower', Fig. 3a) and the upper strut connection with the body (sensor 2, 'upper', Fig. 3b). Vibration acceleration time histories measured along the centre line of the absorber were registered with the use of the NI USB-6009 Multifunction Data Acquisition Device (14-bit, 48 kS/s).



Fig. 2. Considered car: Toyota Camry 2.2 LE (2001)

Measurements were taken in two sessions. In the second session, in order to alter system dynamic behaviour, back of the car was loaded with an additional mass $\Delta M_2 \approx 56,25$ [kg] by filling up 35 litres of petrol and 30 litres of LPG. Value of ΔM_2 was calculated under assumption that 1 litre of petrol weights about 0,75 [kg] while 1 litre of LPG about 1 [kg]. Example acceleration time histories measured in the considered measurement points are presented in the Fig. 4.

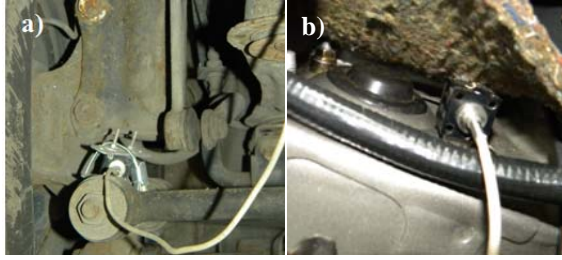


Fig. 3. Location of a) sensor 1 ('lower'), b) sensor 2 ('upper')

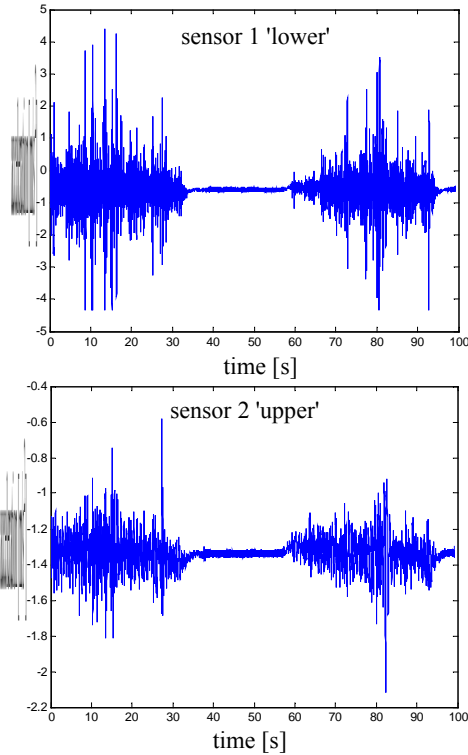


Fig. 4. Example acceleration time histories measured during the second session (for the body mass $M_2 + \Delta M_2$)

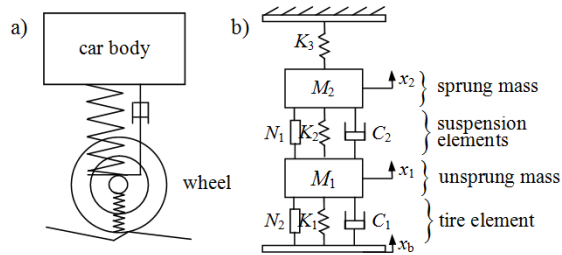


Fig. 5. Assumed quarter car model [17, 18], M_1 : sprung mass, M_2 : unsprung mass, K_1, K_2 : stiffness coefficient of tire and suspension, C_1, C_2 : damping coefficient of tire and suspension, x_1, x_2, x_b : displacements of M_1, M_2 and tire patch, N_1, N_2 : nonlinear forces

For the purposes of the considered suspension system identification, the quarter car model presented in the Fig. 5 was assumed [17, 18].

Dynamic motion equations formulated for the M_1 and M_2 masses are as follows:

$$\begin{cases} M_1 \{\ddot{x}_1\} + (C_1 + C_2)\{\dot{x}_1\} + (K_1 + K_2)\{x_1\} - \\ - C_2\{\dot{x}_2\} - K_2\{x_2\} + N_1 + N_2 = C_1\{\dot{x}_b\} + K_1\{x_b\} \\ M_2 \{\ddot{x}_2\} - C_2\{\dot{x}_1\} + C_2\{\dot{x}_2\} - K_2\{x_1\} + \\ + (K_2 + K_3)\{x_2\} = N_1 \\ N_1 = N_1(\{x_1(t)\}, \{x_2(t)\}, \{\dot{x}_1(t)\}, \{\dot{x}_2(t)\}) \\ N_2 = N_2(\{x_1(t)\}, \{x_b(t)\}, \{\dot{x}_1(t)\}, \{\dot{x}_b(t)\}) \end{cases} \quad (1)$$

For the considered suspension system, with the application of the direct parameter estimation technique, the following equations were formulated:

$$K_2 \left(1 - \frac{1}{T_{21}(\omega_k)} \right) + K_3 = \omega_k^2 M_2 \quad (2)$$

and:

$$T_{21}(0) = \frac{K_2}{K_2 + K_3} \quad (3)$$

where: $\{T_{21}(j\omega)\} = X_2(j\omega) / X_1(j\omega)$: transmissibility function between the sprung mass M_2 and unsprung mass M_1 (with nonlinear restoring forces subtracted), $X_1(j\omega), X_2(j\omega)$: Fourier transforms of signals $x_1(t)$ and $x_2(t)$, $k = 1, 2, \dots, N_f, N_f$: number of spectral lines of useful data, $T_{21}(0)$: transmissibility function evaluated at zero frequency.

Since in practice the exact value of mass M_2 remains unknown, direct parameter estimation method provides two equations with three unknowns - M_2, K_2 and K_3 . Therefore, at this stage of the analysis, only ratios of parameters (with respect to the mass M_2) are available.

In order to provide an additional dynamic motion equation, boundary perturbation method was used. The method consists in introducing an additional mass ΔM_2 altering dynamic behaviour of the considered system (linear system natural frequencies) and retaking measurements for such a modified system. An additional equation is as follows:

$$K_2 \left(1 - \frac{1}{T_{21}'(\omega_p)} \right) + K_3 = \omega_p^2 M_2 \quad (4)$$

where: $\{T_{21}'(j\omega)\} = X_2'(j\omega) / X_1'(j\omega)$: transmissibility function between the sprung mass ($M_2 + \Delta M_2$) and unsprung mass M_1 , $p = 1, 2, \dots, N_f', N_f'$: number of spectral lines of useful data.

Since at this stage three equations with three unknowns can be formulated, it is possible to estimate the absolute values of demanded parameters.

In the next step of analysis, on the basis of carried out measurements of system responses to exploitational excitation, transmissibility functions of the initial and modified system were estimated ($\{T_{21}\}$ and $\{T_{21}'\}$, respectively). Comparison of estimated functions $\{T_{21}\}$ and $\{T_{21}'\}$ is presented in the Fig. 6. As the result of system modification, resonant frequencies of transmissibility function were shifted towards lower values.

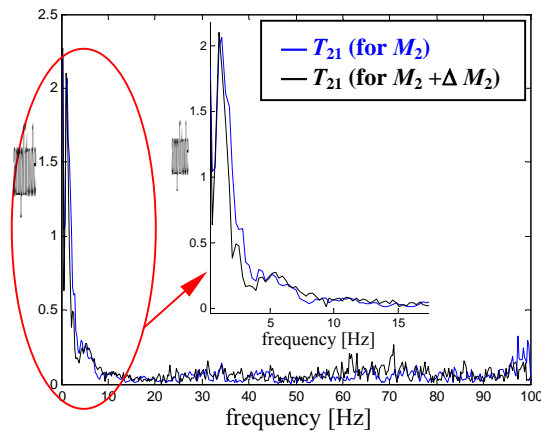


Fig. 6. Comparison of estimated transmissibility functions $\{T_{21}\}$ (for M_2) and $\{T_{21}'\}$ (for $M_2 + \Delta M_2$)

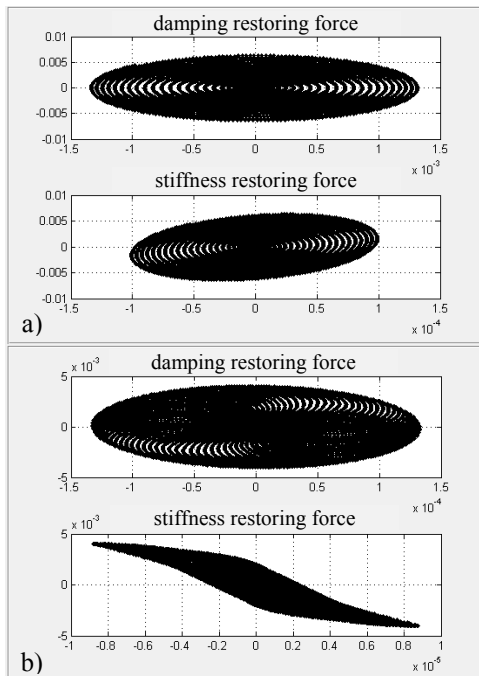


Fig. 7. Damping and stiffness restoring forces identified for frequencies a) $f = 0,7813$ [Hz], b) $f = 4,6875$ [Hz]

In order to verify linearity of the considered system, dynamic motion equation formulated for the sprung mass M_2 was written in the form:

$$M_2 \{\ddot{x}_2\} = -C_2 (\{\dot{x}_2\} - \{\dot{x}_1\}) - K_2 (\{x_2\} - \{x_1\}) - K_3 \{x_2\} + N_1 (\{x_1(t)\}, \{x_2(t)\}, \{\dot{x}_1(t)\}, \{\dot{x}_2(t)\}) \quad (5)$$

expressing relation between acceleration of the sprung mass M_2 and relative velocity or relative displacement between masses M_1 and M_2 . On the basis of measured vibration accelerations time histories, by means of time-domain integration, vibration velocities and displacements in the considered measurement points were determined. Before each integration, constant components were removed from the analyzed signals. Selected

characteristics of estimated stiffness and damping restoring forces are presented in the Fig. 7.

In the considered frequency bandy, reconstructed damping restoring forces are linear while the vast majority of stiffness restoring forces reconstructed for resonant areas of $\{T_{21}\}$ function display hysteretic properties.

Estimation of the considered suspension system parameters was carried out for frequencies and magnitudes of identified 'peaks' of transmissibility functions $\{T_{21}\}$ and $\{T_{21}'\}$ (Table 1) with the application of the created software [19].

Table 1. Parameters of estimated transmissibility functions

	Transmissibility function parameters			
	ω [Hz]	$T_{21}(\omega)$	ω' [Hz]	$T_{21}'(\omega)$
1.	1,3021	2,0654	1,0417	2,0991
2.	2,8646	0,6101	2,3437	0,4953
3.	4,1667	0,2936	3,3854	0,1758
4.	5,2083	0,2629	4,4271	0,2415
5.	-	-	5,4688	0,2778
6.	6,5104	0,1798	5,9896	0,2432
7.	8,5937	0,0718	7,0313	0,1687
8.	9,3750	0,0776	8,0729	0,1163
9.	10,1562	0,0663	9,6354	0,0820
10.	10,6770	0,0807	10,4166	0,0794
11.	11,1979	0,0775	10,9375	0,0834
12.	-	-	11,7187	0,0765
13.	13,0208	0,0429	12,2395	0,0705
14.	-	-	13,2812	0,0744
15.	14,8437	0,0433	14,0625	0,0589

Since the magnitude of the estimated transmissibility function $\{T_{21}\}$ approaches 2,25 as the frequency approaches 0 [Hz], on the basis of the equation (3), the following relation between K_2 and K_3 is obtained:

$$K_3 = -0,6 \cdot K_2 \quad (6)$$

According to the owners manual [20], mass of the considered car body:

$$M_{car\ body}^{theoretical} = 1380 [kg] \quad (7)$$

In the course of the carried out identification experiments, the car was loaded with an additional mass of equipment, fuel and passengers of overall value 230 [kg]. Therefore it was assumed that total mass of the considered car body during measurements amounted to:

$$M_{car\ body}^{total(real)} = 1610 [kg] \quad (8)$$

Taking into account mass distribution (0,59 front axle and 0,41 rear axle), it was assumed that mass concentrated on the considered rare left suspension system [19]:

$$M_2^r = 0,5 \cdot 0,41 \cdot M_{car\ body}^{total(real)} [kg] \quad (9)$$

therefore:

$$M_2^r = \frac{0,41}{2} \cdot 1610 = 330 [kg] \quad (10)$$

Mass value estimated with the application of the exploitational nonlinear system identification method equals:

$$M_2^e = 326 [kg] \quad (11)$$

As the measure of parameter estimation accuracy, the relative percentage errors of M_2 estimation was assumed:

$$Err = \frac{|M_2^r - M_2^e|}{M_2^r} \cdot 100 \cdot [\%] \quad (12)$$

where M_2^e denotes estimated mass, M_2^r real mass value.

Therefore, on the basis of relation (12), it can be stated that estimated value of mass M_2^e is burdened with the percentage relative error:

$$Err = \frac{|330 - 326|}{330} \cdot 100 \cdot [\%] = 1,21 [\%] \quad (13)$$

Estimated value of the considered suspension system stiffness coefficient equals:

$$K_2^e = 2610 [N/m] \quad (14)$$

while the value of stiffness coefficient K_2^z recommended by the producer of spare parts amounts to:

$$K_2^z = 3700 [N/m] \quad (15)$$

Estimated value K_2^e of stiffness coefficient is significantly lower than the recommend value K_2^z .

4. CONCLUSIONS AND FINAL REMARKS

The paper concerns identification of structural parameters of car suspension system carried out on the basis of vibration accelerations recorded along the centre line of absorber while driving over the bumpy road profile. Analysis was carried out with the application of the output-only nonlinear system identification method. Accuracy of the estimated suspension parameters was assessed on the basis of the relative percentage errors of the considered car body mass estimation. Obtained results can be influenced by:

- serial connection of shock absorber with elastic elements,
- application of the original part of stiffness coefficient lower than in case of the equivalent (3700 [N/m]) used for tuning up,
- wear of elements,
- clearances, elasticity of connections (e.g. rubber rings),

- estimation of dynamic stiffness coefficient in the whole system operating point instead of static stiffness coefficient,
- higher load (filled trunk),
- inaccurate mounting of sensors (deviation of measurement direction from vertical line, usage of magnet for the 'upper' sensor mounting).

Accuracy of the considered suspension system parameters estimation is influenced by the accuracy of transmissibility function (and parameters of its extrema) estimation. Therefore it is necessary to guarantee high accuracy of sensors fastening (directions of sensor measurement axis and orientation of the coordinate axis should be consistent) while the value of an additional mass ΔM_2 should be reasonably high.

ACKNOWLEDGEMENTS

The research was financed from Polish means for science (from 2010 till 2012) as the research project N N504 493439.

REFERENCES

- [1] Al-Bender F., Symens W., Swevers J., Van Brussel, 2004, *Analysis of dynamic behavior of hysteresis elements in mechanical systems*, Int. Journal of Nonlinear Mechanics, 39, 1721-1735.
- [2] Babitsky V., Krupenin V. L., 2001, *Vibrations of strong nonlinear discontinuous systems*, Springer, Berlin.
- [3] Kerschen G., Worden K., Vakakis A.F., Golinval J.C., 2006, *Past, present and future of nonlinear system identification in structural dynamics*, Mech. Systems and Signal Processing, 20, 505-592.
- [4] Nayfeh A. H., Pai L., 2004, *Linear and nonlinear structural Mechanics*, Wiley Interscience, New York.
- [5] Rice H. J., 1995, *Identification of weakly nonlinear systems using equivalent linearization*, Journal of Sound and Vibration, 185, 473-481.
- [6] Soize C., Le Fur O., 1997, *Modal identification of weakly non-linear system using a stochastic linearization method*, Mechanical Systems and Signal Processing, 11, 37-49.
- [7] Rand R., 1974, *A direct method for nonlinear normal modes*, International Journal of Non-Linear Mechanics, 9, 363-368.
- [8] Rosenberg R. M., 1962, *The normal modes of nonlinear n-degree-of-freedom systems*, Journal of Applied Mechanics, 29, 7-14.
- [9] Kevorkian J., Cole J. D., 1996, *Multiple Scales and Singular Perturbation Methods*, Springer, New York.

- [10] Nayfeh A. H., 1981, *Introduction to Perturbation Techniques*, Wiley Interscience, New York.
- [11] Rhoads J. F., Shaw S. W., Turner K. L., Baskaran R., 2005, *Tunable MEMS filters that exploit parametric resonance*, Journal of Vibration and Acoustics.
- [12] Vakakis A. F., Gendelman O., 2001, *Energy pumping in nonlinear mechanical oscillators: Part II – resonance capture*, Journal of Applied Mechanics, 68, 42-48.
- [13] Ibanez P., 1973, *Identification of dynamic parameters of linear and nonlinear structural models from experimental data*, Nuclear Engineering and Design, 25, 30-41.
- [14] Masri S. F., Caughey T. K., 1979, *A nonparametric identification technique for nonlinear dynamic problems*, Journal of Applied Mechanics, 46, 433-447.
- [15] Haroon M., Adams D. E., Luk Y. W.: *A Technique for Estimating Linear Parameters Using Nonlinear Restoring Force Extraction in the Absence of an Input Measurement*, ASME Journal of Vibration and Acoustics, vol. 127, 2005, 483–492.
- [16] Iwaniec J.: *Output-Only Technique for Parameter Identification of Nonlinear Systems Working Under Operational Loads*, Key Engineering Materials, Vol. 347, 2007, 467-472.
- [17] Iwaniec J.: *Selected issues of exploitation identification of nonlinear systems* (in Polish), AGH University of Science and Technology Press, Krakow, 2011.
- [18] Iwaniec J.: *Sensitivity analysis of identification method dedicated to nonlinear systems working under operational loads*, Journal of Theoretical and Applied Mechanics, Vol. 49, No. 2, 2011.
- [19] Iwaniec J.: Report from the MNiSW research project N N504 493439 'Method dedicated to identification of models of mechanical systems working under exploitation conditions and its applications', Krakow, 2013.
- [20] <http://www.toyota.com/owners/web/pages/resources/owners-manuals>
- DSc. Eng. (dr. hab. inż.) **Joanna IWANIEC**, since 2005, has been working in the Department of Robotics and Mechatronics, Faculty of Mechanical Engineering and Robotics, AGH University of Science and Technology in Krakow. Her scientific interests concern modal analysis, regularization, signal processing and identification of nonlinear systems.

HYBRID MODEL OF GEARED ROTOR SYSTEM

Rafał HEIN, Cezary ORLIKOWSKI

Faculty of Mechanical Engineering, Department of Mechanics and Mechatronics
Gdansk University of Technology, Narutowicza Street 11/12, 80-233 Gdansk
fax: (+48) 58 347 21 51, email: rahe@pg.gda.pl

Summary

In the paper a hybrid model of a geared multirotor system has been developed. The model is obtained by application of both the modal decomposition methodology and the spatial discretization method. Reduced modal model was constructed for the system without gyroscopic and damping effects. The gyroscopic interaction, damping and other phenomena which are difficult to include in the modal approach were modeled by application of simply lumping technique. Such approach enables to obtain accurate, low order model of geared rotor system with coupled bending and torsional vibrations. In the model it is possible to include nonproportional or nonlinear damping. Obtained hybrid model has been compared with high order FEM model. Simulation results prove that proposed method of modeling is efficient and relatively easy to use.

Keywords: mechanical system, modelling, vibration, modal analysis, model reduction.

HYBRYDOWY MODEL UKŁADU WIRNIKÓW Z PRZEKŁADNIĄ

Streszczenie

W artykule przedstawiono hybrydowy model układu wielowirnikowego z przekładnią. Otrzymano go stosując dwie metody: dekompozycji modalnej oraz dyskretyzacji przestrzennej. Zredukowany model modalny zbudowano dla układu bez efektu żyroskopowego i tłumienia. Oddziaływania żyroskopowe, tłumienie oraz inne zjawiska, które są trudne do uwzględnienia w modelu modalnym modelowano stosując metodę elementów skończonych. Takie podejście umożliwia otrzymanie dokładnego modelu niskiego rzędu uwzględniającego sprzężone drgania giętno-skrętne. W modelu można uwzględnić nieproporcjonalne lub nieliniowe tłumienie. Skonstruowany model hybrydowy został porównany z modelem referencyjnym wysokiego rzędu otrzymanym metodą sztywnych elementów skończonych. Wyniki symulacji potwierdzają skuteczność zastosowanej metody.

Słowa kluczowe: układy mechaniczne, modelowanie, drgania, analiza modalna, redukcja modeli.

1. INTRODUCTION

Rotor systems are constructed from components, some of them are lumped parameter elements and others distributed ones. Such systems are composed of rigid disks mounted on a flexible shafts [3]. Avoiding the mathematical difficulties arising from the manipulation of sets of mixed ordinary and partial differential equations, different approximate lumped models of distributed-lumped systems are usually applied. By using the finite-element method it is possible to obtain an accurate model and final results. However, obtaining a sufficiently accurate result requires a very fine mesh size and therefore a high order model.

For the response analysis of large systems, the use of a high order model requires considerable computer run time and memory. Additionally, in many cases a high order model is not very useful, e.g. in control systems analysis and design. In such cases designers greatly benefit from the availability

of very small, low order models that capture the behaviour of a complex system with appropriate accuracy. However a simple but adequate model of a complex distributed-lumped parameter system should reflect the basic properties and provides good insight into the modelled process.

In this paper the method of modelling a geared-rotor system is presented. The proposed approach enables to obtain an accurate, low-order, lumped parameter representation of the investigated system. The final model consists of: 1- reduced modal model of an undamped, linear beam subsystem without gyroscopic phenomena and 2 - spatially lumped model of the gyroscopic effect and non-proportional and/or nonlinear damping. The gear mesh is modelled using a spring (spring – damper) element along the pressure line [10]. A gear transmission error can be introduced as a displacement excitation. Nonlinearity of the gear mesh (backlash) can be also easily introduced in such model.

2. RFEM MODEL OF GEARED ROTOR SYSTEM

Let us consider the rotor system presented in Fig. 1.

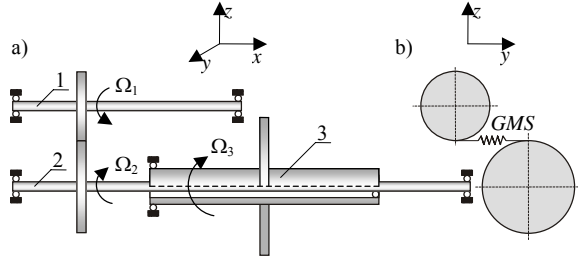


Fig. 1. General view of the considered rotor system

The considered geared rotor system consists of three shafts rotating with angular velocities: $\Omega_1 \neq 0$, $\Omega_2 \neq 0$, $\Omega_3 = 0$. Two of them 1 and 2 (Fig. 1) are coupled by a gear. Another pair of rotors 2 and 3 are coupled by bearing.

In the case of a geared rotor system a coupled phenomenon of torsional and lateral vibrations can appear as the result of the gear meshing effect. There is a large number of modelling methods related to geared rotor system coupled vibrations [1,10]. The purpose of this paper is to present a simplified hybrid model of a geared rotor system obtained by application of both: modal decomposition and spatial discretization methods.

Assuming that the axial motion of the shafts are negligible, each shaft can be considered as a simply supported beam vibrating in two perpendicular planes: xy , xz and as a torsional shaft vibrating around x axis. Torsional and transverse vibrations are coupled by the gear mesh spring (GMS-Fig. 1), which represents the gear mesh stiffness.

The model of presented structure was built based on the Timoshenko beam model. It includes: rotary inertia, shear deformation, the gyroscopic effect as well as internal and/or external damping.

By applying the rigid finite-element method (RFEM) [2,4] one can obtain the following equations for the rotor system:

$$M\ddot{q} + B\dot{q} + Kq + G\dot{q} = f, \quad (1)$$

where:

q – vector of generalized displacement, f – vector of generalized forces, M, B, K, G – matrices of inertia, damping, stiffness and gyroscopic respectively,

$$M = \text{diag}(M_y, M_z, M_{xz}, M_{xy}, M_{yz}),$$

$$M_y = \text{diag}(M_{y1}, M_{y2}, M_{y3}),$$

$$M_z = \text{diag}(M_{z1}, M_{z2}, M_{z3}),$$

$$M_{xz} = \text{diag}(M_{xz1}, M_{xz2}, M_{xz3}),$$

$$M_{xy} = \text{diag}(M_{xy1}, M_{xy2}, M_{xy3}),$$

$$M_{yz} = \text{diag}(M_{yz1}, M_{yz2}, M_{yz3}),$$

$$B = \begin{bmatrix} B_y & 0 & 0 & 0 & B_0 \\ 0 & B_z & 0 & 0 & 0 \\ 0 & 0 & B_{xz} & 0 & 0 \\ 0 & 0 & 0 & B_{xy} & 0 \\ B_0 & 0 & 0 & 0 & B_{yz} \end{bmatrix},$$

$$B_y = \begin{bmatrix} B_{y11} & 0 & 0 \\ 0 & B_{y22} & B_{y23} \\ 0 & B_{y32} & B_{y33} \end{bmatrix}, B_z = \begin{bmatrix} B_{z11} & B_{z12} & 0 \\ B_{z21} & B_{z22} & B_{z23} \\ 0 & B_{z32} & B_{z33} \end{bmatrix}$$

$$B_{yz} = \begin{bmatrix} B_{yz11} & B_{yz12} & 0 \\ B_{yz12} & B_{yz22} & 0 \\ 0 & 0 & B_{yz33} \end{bmatrix}, B_0 = \begin{bmatrix} B_{011} & B_{012} & 0 \\ B_{021} & B_{022} & 0 \\ 0 & 0 & 0 \end{bmatrix},$$

$$B_{xz} = \text{diag}(B_{xz1}, B_{xz2}, B_{xz3}),$$

$$B_{xy} = \text{diag}(B_{xy1}, B_{xy2}, B_{xy3}),$$

$$K = \begin{bmatrix} K_y & 0 & 0 & 0 & K_0 \\ 0 & K_z & 0 & 0 & 0 \\ 0 & 0 & K_{xz} & 0 & 0 \\ 0 & 0 & 0 & K_{xy} & 0 \\ K_0 & 0 & 0 & 0 & K_{yz} \end{bmatrix},$$

$$K_0 = \begin{bmatrix} K_{011} & K_{012} & 0 \\ K_{021} & K_{022} & 0 \\ 0 & 0 & 0 \end{bmatrix}, K_y = \begin{bmatrix} K_{y11} & 0 & 0 \\ 0 & K_{y22} & K_{y23} \\ 0 & K_{y32} & K_{y33} \end{bmatrix},$$

$$K_z = \begin{bmatrix} K_{z11} & K_{z12} & 0 \\ K_{z21} & K_{z22} & K_{z23} \\ 0 & K_{z32} & K_{z33} \end{bmatrix},$$

$$K_{yz} = \begin{bmatrix} K_{yz11} & K_{yz12} & 0 \\ K_{yz21} & K_{yz22} & 0 \\ 0 & 0 & K_{yz33} \end{bmatrix},$$

$$K_{xz} = \text{diag}(K_{xz1}, K_{xz2}, K_{xz3}),$$

$$K_{xy} = \text{diag}(K_{xy1}, K_{xy2}, K_{xy3}),$$

$$G = \begin{bmatrix} 0 & 0 & 0 & 0 & 0 \\ 0 & 0 & 0 & 0 & 0 \\ 0 & 0 & 0 & G_0 & 0 \\ 0 & 0 & -G_0 & 0 & 0 \\ 0 & 0 & 0 & 0 & 0 \end{bmatrix}, G_0 = \begin{bmatrix} G_{01} & 0 & 0 \\ 0 & G_{02} & 0 \\ 0 & 0 & G_{03} \end{bmatrix},$$

$$G_{01} = G_1^* \Omega_1, G_{02} = G_2^* \Omega_2, G_{03} = G_3^* \Omega_3,$$

G_1^*, G_2^*, G_3^* – diagonal, gyroscopic matrices of FE-s moment of inertia (bending),

$$q = \text{col}(q_y, q_z, q_{xz}, q_{xy}, q_{yz}),$$

$$q_y = \text{col}(q_{y1}, q_{y2}, q_{y3}), q_z = \text{col}(q_{z1}, q_{z2}, q_{z3}),$$

$$q_{xz} = \text{col}(q_{xz1}, q_{xz2}, q_{xz3}), q_{xy} = \text{col}(q_{xy1}, q_{xy2}, q_{xy3}),$$

$$q_{yz} = \text{col}(q_{yz1}, q_{yz2}, q_{yz3}),$$

following applied subscripts are related to the generalized displacements:

y – transverse displacement along y axis,

z – transverse displacement along z axis,

xy – angular bending displacement in xy plane,

xz – angular bending displacement in xz plane,
 yz – torsional displacement,
subscripts 1, 2, 3 denote subsystems (rotors).

Submatrices in: $B_y, B_z, B_{yz}, B_{xz}, B_{xy}, B_0$ and in $K_y, K_z, K_{yz}, K_{xz}, K_{xy}, K_0, G_0$ have dimensions related to number of finite elements applied in the RFEM model.

All matrices were obtained from RFE model [3,4] by rearrangement according to general displacement q .

In general, f can be a function of Ω_1, Ω_2 and Ω_3 (e.g. centrifugal forces).

By substituting:

$$f_B = B\dot{q}, f_G = G\dot{q}, \quad (2)$$

we can present equation (1) in the form

$$M\ddot{q} + Kq = f + f_B + f_G \quad (3)$$

or

$$M\ddot{q} + Kq = f_\Sigma, \quad (4)$$

where

$$f_\Sigma = f + f_B + f_G. \quad (5)$$

3. MODAL DECOMPOSITION

The model described by equation (4) can be written in modal representation as:

$$M_m\ddot{q}_m + K_m q_m = f_m, \quad (6)$$

where:

$$M_m = \Phi^T M \Phi = \text{diag}(m_1, \dots, m_r, \dots, m_n),$$

$$K_m = \Phi^T K \Phi = \text{diag}(k_1, \dots, k_r, \dots, k_n),$$

$$q_m = \text{col}(q_{m1} \dots q_{mr} \dots q_{mn}), f_m = \Phi^T f_\Sigma,$$

$$\Phi = \text{col}(\varphi_1, \dots, \varphi_r, \dots, \varphi_n),$$

in which:

m_i – modal coefficients of inertia, k_i – modal coefficients of stiffness φ_i – eigenvectors of matrix $M^{-1}K$.

By solving (6) we can next obtain the solution of (1) in the following form:

$$q = \Phi q_m, \dot{q} = \Phi \dot{q}_m. \quad (7)$$

4. REDUCED MODAL MODEL

Modal model (6) can be reduced by removing those rows and columns in M_m, K_m which are insignificant to the system's dynamics. Thus, in such approach we obtain:

$$M_{mr}\ddot{q}_{mr} + K_{mr}q_{mr} = f_{mr}, \quad (8)$$

where:

$$\left. \begin{aligned} M_{mr} &= \text{diag}(m_1, \dots, m_r), K_{mr} = \text{diag}(k_1, \dots, k_r), \\ q_{mr} &= \text{col}(q_{m1}, \dots, q_{mr}), f_{mr} = \Phi_r^T f_\Sigma, \\ \Phi_r &= \text{col}(\varphi_1, \dots, \varphi_r). \end{aligned} \right\} (9)$$

An approximate solution of (1) by the application of reduced order model (8) can be obtained from the formulas:

$$q = \Phi_r q_{mr}, \dot{q} = \Phi_r \dot{q}_{mr}. \quad (10)$$

However, in order to obtain better static accuracy of reduced model (see chapter 6) one can apply also modal stiffness coefficients of modes $r+1, \dots, n$ (static correction). In such case instead of (9) we have:

$$\left. \begin{aligned} M_{mr} &= \text{diag}(m_1, \dots, m_r, 0, \dots, 0), K_{mr} = K_m, \\ q_{mr} &= q_m, f_{mr} = f_{mr}, \Phi_r = \Phi_r. \end{aligned} \right\} (11)$$

It should be mentioned that applying formulas (11) the order of the model is the same as by application (9).

5. HYBRID REDUCED MODEL

By taking into account (2) and (5) we can transform (8) into the following form:

$$M_{mr}\ddot{q}_{mr} + K_{mr}q_{mr} = \Phi_r^T f - \Phi_r^T B \Phi_r \dot{q}_{mr} - \Phi_r^T G \Phi_r \dot{q}_{mr} \quad (12)$$

Equations (12) and (10) present the final hybrid model, in which f is the input data and q is the response of the system. A block diagram describing the above hybrid model is presented in Fig. 2. This shows that in the hybrid model matrices M_{mr}, K_{mr} are taken from modal reduced models (8) and matrices B, G origin from the initial FEM model (1).

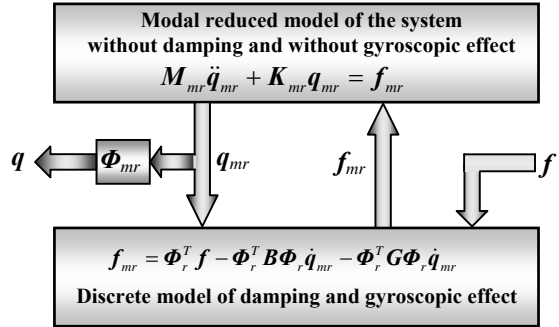


Fig. 2. Block diagram of the hybrid model

Proposed method of hybrid modelling of geared rotor system was previously applied by authors for successful modelling of other (non geared) rotor systems [5-9].

6. NUMERICAL CALCULATIONS AND RESULTS

The continuous structure (Fig. 1) is divided into 203 rigid finite elements (RFE) and 209 spring damping elements (SDE). Discrete model obtained by using the RFE method is shown in Fig. 3b. Each RFE has five degrees of freedom, i.e. transverse displacement

along axes y and z and angular displacement around all three axes.

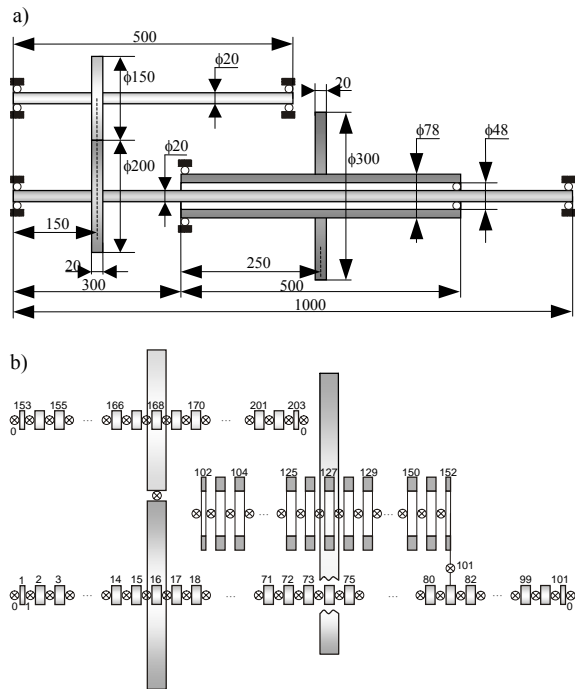


Fig. 3. Investigated continuous structure – a) and its discrete model – b)

Parameters of RFEs are presented in Tabs. 1÷4. They are calculated for the following physical data: modulus of elasticity (Young) $E=2 \cdot 10^{11}$ [Pa], shear modulus (Kirchhoff) $G=7.8 \cdot 10^{10}$ [Pa], mass density $\rho=8000$ [kg/m³]. Denotation of the RFEs parameters one can find in [3,4].

Tab. 1. The inertia coefficients of RFE no. i

i	m_i [kg]	$J_{y>i}$ [kgm ²]	$J_{z>i}$ [kgm ²]
1, 101, 153, 203	0.01256	$3.4033 \cdot 10^{-7}$	$6.2831 \cdot 10^{-7}$
2÷15, 17÷100, 154-167, 169-202	0.02513	$8.3775 \cdot 10^{-7}$	$1.2566 \cdot 10^{-6}$
16	5.02654	0.0127339	0.0253840
168	2.77716	0.0040673	0.0079496
102, 152	0.11875	$6.2503 \cdot 10^{-5}$	$1.2451 \cdot 10^{-4}$
103÷126, 128÷151	0.23750	$1.2649 \cdot 10^{-4}$	$2.4902 \cdot 10^{-4}$
127	10.54519	0.06341441	0.12665307

Tab. 2. The stiffness coefficients of SDE no. k

i	j	k	$c_{k,z}$ [Nm ⁻¹]	$c_{k,x}=c_{k,y}$ [Nm ⁻¹]	$c_{k,xz}$ [Nm]
1	2	1	6283185307.179	2067560665.144	157079.633
...			
100	101	100			
102	103	102			
...	59376101152.847	19538448285.609	31127921.029
151	152	151			
153	154	153			
...			
202	203	202	6283185307.179	2067560665.144	157079.633
81	152	101			
0	1	0			
101	0	0			
0	102	0			
0	153	0			
203	0	0			
...			
...	$2 \cdot 10^{15}$	$2 \cdot 10^{15}$	0

The full RFEM model was used as the reference model for validation of simplified hybrid model of

considered system. In this model the gyroscopic effect was included. Fig. 6 presents the influence of the gyroscopic effect on the frequency characteristics, in the case when the angular velocities $\Omega_1=\Omega_2=1000$ [rad/s] were assumed.

Tab. 3. The damping coefficients of SDE no. k

i	j	k	$b_{k,z}$ [Nsm ⁻¹]	$b_{k,x}=b_{k,y}$ [Nsm ⁻¹]	$b_{k,xz}$ [Nsm]
1	2	1	2617993.878	861483.61	65.45
...			
100	101	100			
102	103	102			
...	24740042.147	8141020.119	12969.967
151	152	151			
153	154	153			
...			
202	203	202	2617993.878	861483.61	65.45
81	152	101			
0	1	0			
101	0	0			
0	102	0			
0	153	0			
203	0	0			
...			
...	0	0	0

Tab. 4. The connection coordinates of SDE no. k to RFE no. i

i	j	k	$s_{r,k,z}$ [m]	$s_{r,k,x}$ [m]	$s_{p,k,z}$ [m]	$s_{r,k,y}$ [m]
1	2	1	0.0025	0	-0.005	0
...	0.005	0	-0.005	0
100	101	100	0.005	0	-0.0025	0
102	103	102	0.0025	0	-0.005	0
...	0.005	0	-0.005	0
151	152	151	0.005	0	-0.0025	0
153	154	153	0.0025	0	-0.005	0
...	0.005	0	-0.005	0
202	203	202	0.005	0	-0.0025	0
81	152	101	0.0025	0	0	0
0	1	0	0	0	-0.0025	0
101	0	0	0.0025	0	0	0
0	102	0	0	0	-0.0025	0

Taking into account the RFEM model without damping and gyroscopic effect the modal reduced model was built. Fig. 4 presents eigenfunctions corresponding to too selected eigenvalues: $\omega_1=122.62$, $\omega_3=322.81$ of the system (without damping and gyroscopic interactions).

Modal reduced model (9, 11) was built for 8 retained modes. Comparison of frequency characteristics related to full undamped model and reduced model are presented in Fig. 5.

The modal reduced model was next combined with discrete model of gyroscopic interaction and damping. In this way a hybrid model of considered system was obtained.

To verify the obtained reduced hybrid model, its frequency response was compared to that of the full FEM model (reference model). The results are presented in Fig. 7 and 8.

The simulation results prove that obtained hybrid, reduced model presents very nice accuracy in the frequency range related to the number of retained modes.

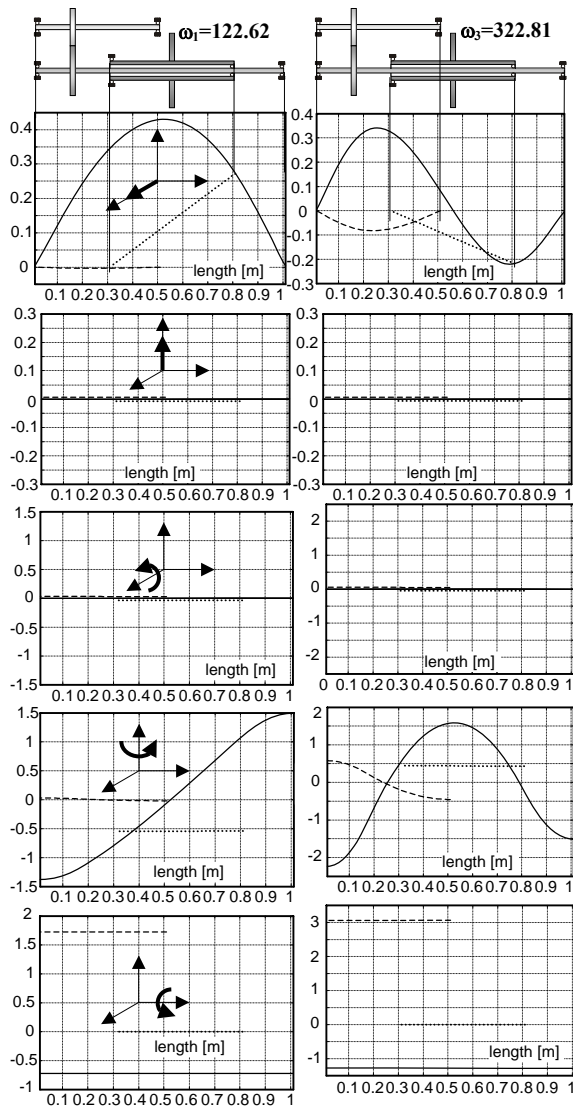


Fig. 4. Examples of eigenfunctions of investigated rotor system

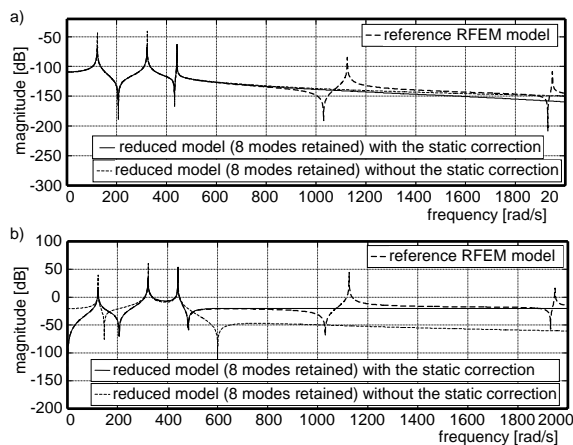


Fig. 5. Modal models validation in frequency domain: a) input – force acting along z axis and applied at the 16 RFE, output – transverse displacement at the same point and along the same axis; b) input – kinematic excitation (displacement) along gear pressure line, output – the same as in the case a)

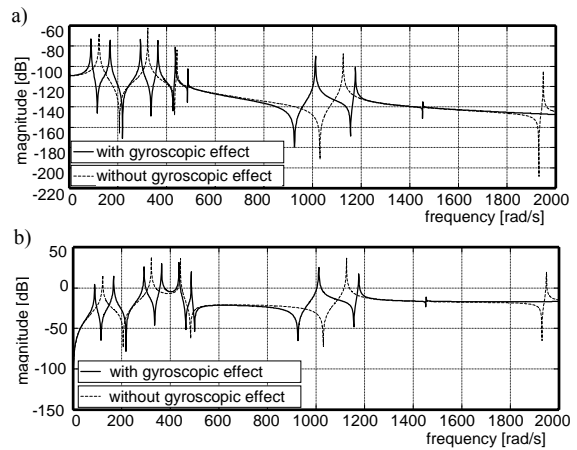


Fig. 6. Influence of the gyroscopic effect on frequency characteristics. Inputs and outputs in a) and b) are the same as in Fig. 5

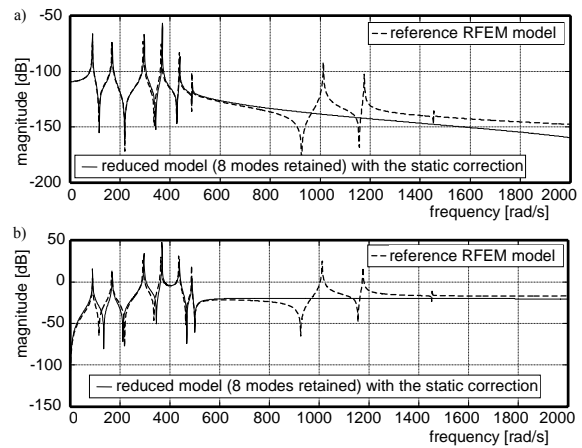


Fig. 7. The frequency characteristics of models with gyroscopic effect and without damping: a) force excitation, b) kinematic excitation. Inputs and outputs are the same as in Fig. 5

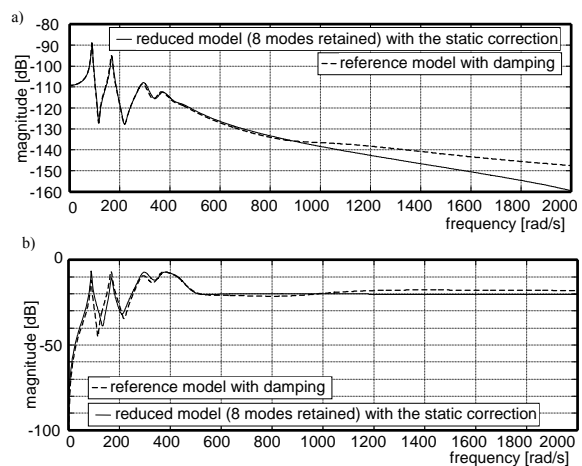


Fig. 8. The frequency characteristics of models with gyroscopic effect and non proportional damping: a) force excitation. Inputs and outputs are the same as in Fig. 5, b) kinematic excitation

7. CONCLUSIONS

In this paper the method of modelling a geared rotor system is presented. The proposed approach enables to obtain an accurate low-order lumped parameter representation of the investigated system. The final model consists of reduced modal models of undamped beam/shaft systems and spatially lumped model of the gyroscopic effect and a non-proportional damping model. The gear mesh was modelled using a spring element along the gear pressure line. The transmission error can be introduced as a displacement excitation. The obtained simulation results, in the form of corresponding frequency characteristics, prove that the proposed method is efficient and can be applied in the case of more complex geared rotor systems. For example, nonlinear damping or nonlinearity of gear mesh can be included. Also unbalanced and speed varying rotors can be considered. In such cases the time domain investigations must be performed. It will be the authors future work in the rotor dynamics modelling area.

References

- [1] An Sung L., Jin Woong H., Dong-Hoon C.: *Coupled lateral and torsional vibration characteristics of a speed increasing geared rotor-bearing system*, Journal of Sound and Vibration, 2003, Vol. 263, p. 725-742
- [2] Gawroński W., Kruszewski J., Ostachowicz W., Tarnowski J., Wittbrodt E.: *The finite element method in the dynamics of structures* [in Polish], Arkady, Warsaw 1984
- [3] Krämer E.: *Dynamics of Rotors and Foundations*, Springer-Verlag, 1993
- [4] Kruszewski J., Gawroński W., Wittbrodt E., Najbar F., Grabowski S.: *The rigid finite element method* [in Polish], Arkady, Warsaw 1975
- [5] Orlikowski C.: *Modelling, analysis and synthesis of dynamic systems by application of bond graphs*. Gdańsk University of Technology Press, Gdańsk, 2005 [in Polish]
- [6] Orlikowski C., Hein R.: *Modal reduction and analysis of gyroscopic systems*. Solid State Phenomena, 2010, Vol. 164 p. 189-194
- [7] Orlikowski C., Hein R.: *Hybrid, approximate models of distributed-parameter systems*. The 12th Mechatronics Forum Biennial International Conference. Part 2/2, Zurich, June 28-30, 2010 / H. Wild, K. Wegner. - Swiss Federal Institute of Technology, 2010, p. 163-170
- [8] Orlikowski C., Hein R.: *Reduced model of gyroscopic system, Selected Problems of Modal Analysis of Mechanical Systems*, Editor T. Uhl, Radom: Publishing House of the Institute for Sustainable Technologies National Research Institute, 2009, AGH, Kraków 2007
- [9] Orlikowski C., Hein R.: *Modelling and analysis of rotor with magnetic bearing system, Developments in mechanical engineering*, Editor J. T. Cieśliński, GUTP, Gdansk 2008
- [10] [10] Özgüven, H.N. and D.R. Houser: *Mathematical Models Used in Gear Dynamics - A Review*, Journal of Sound and Vibration, 1988. 121: p. 383-411

The research is supported from the science budget resources in 2011-2014 as the research project (N N501 120240)



Rafal HEIN, D.Sc. Eng. is an assistant professor at the Faculty of Mechanical Engineering, Gdańsk University of Technology. His research interests focus on the modelling of dynamic mechanical and mechatronic systems



Cezary ORLIKOWSKI, D.Sc. Ph.D. Eng. is an assistant professor at the Faculty of Ocean Engineering and Ship Technology, Gdańsk University of Technology. In addition, he is also working as professor and he is a Deputy Rector in The State School of Higher Professional Education in Elbląg. His current research interest include mechatronics and dynamic systems modelling.

DIAGNOSIS DESIGN OF SHIP HULL STRENGTH OF TREATED BY DYNAMIC LOAD

Andrzej GRZĄDZIELA¹, Bogdan SZTUROMSKI², Marcin KLUCZYK³

Polish Naval Academy, Mechanical Department, 81-103 Gdynia, Śmidowicza St. 69, Poland
¹a.grzadzela@amw.gdynia.pl, ²B.Szturomski@amw.gdynia.pl, ³M.Kluczyk@amw.gdynia.pl

Summary

Ship shock tests have been conducted for shock qualification of hull integrity and proper operation systems and subsystems. The ship shock trial identifies design and construction and it also validates shock hardening criteria. The main problem is that ship shock trials are costly. Numerical modeling and simulation, using FEM, may provide information to look into the details of fluid model, dynamic characteristics of ship hull and its internal component. The ship shock modeling and simulation has been performed and the predicted results were compared with ship shock test data made into sea trials. The preliminary studies of shock analysis approach are presented and the important parameters are discussed.

Keywords: simulation, underwater explosion, minehunter, hull

DIAGNOZOWANIE PROJEKTOWE WYTRZYMAŁOŚCI KADŁUBA OKRĘTOWEGO Poddanego Oddziaływaniom Dynamicznym

Streszczenie

Testy udarowościowe kadłubów prowadzone są w celu oceny ich integralności oraz poprawności działania wszystkich zamontowanych systemów. Testy udarowościowe pozwalają na identyfikację i ocenę konstrukcji oraz weryfikują odporność kadłuba. Głównym problemem jest ich wysoka cena z racji konieczności realizacji na prototypach. Modelowanie i symulacja za użyciem MES, może dostarczyć informacji do oceny bryły wody towarzyszącej, dynamicznych właściwości kadłuba i elementów wyposażenia. W artykule przedstawiono modelowanie i symulację uderzenia w fali uderzeniowej w kadłub a uzyskane wyniki porównano z wynikami poligonowymi.

Słowa kluczowe: symulacja, wybuchy podwodne, niszczyciele min, kadłub

1. INTRODUCTION

Large capacity of the calculating hardware help to make assessments of short-term (fast changing) processes, such as the impact of the pressure wave from a no-contact underwater explosion near the hull of the ship. These are issues of great complexity and indirection, each should be treated individually. It is necessary to simplify the task in many areas, because too accurate descriptions of the phenomenon may give results far from the actual one. The task becomes much more complicated in case of including the interaction between the environment and the contemplated construction. The ship is located in two mediums: water and air. Taking into account the impact of these requires solving the double-linked task using for example the finite element and boundary element method. Then the solution, at the edge of a particular medium, eg. liquid, forms the input data for the load of the deformed structure impacting on the surrounding medium. Such mutual linkage is repeated n times and at every step of the data exchange it is necessary to obtain adequate convergence. The problem becomes more complicated due to numerous non-

linearity. In the case of the impact loads by pressure wave it is not possible to disregard large displacement structures, nonlinearity of materials, failure criteria, etc. In the case of complex structures there will be contact. All these factors determine the complexity of the task and the processing power needed to obtain solutions in a reasonable time, with the possibility of assessing its results, making any corrections and repeating the calculations.

2. THE DYNAMIC EQUATION OF MOTION IN TERMS OF MES – EXPLICITE

To determine the motion parameters of the discrete model consisting of a finite number of elements in the MES the differential equation of the form [1] must be solved:

$$M\ddot{U} + C\dot{U} + KU = F \quad (1)$$

where:

K - the stiffness matrix of the structure;

M - matrix of inertia;

C - matrix of damping;

U, \dot{U}, \ddot{U} - the vector of displacement, velocity and acceleration;

F - the vector of loads.

Stiffness matrix \mathbf{K} reflects the material properties of the element and geometry. In MES stiffness matrix \mathbf{K}^e for the element is defined as the product of the elasticity and deformation matrices in the form [2]:

$$\mathbf{K}^e = \int_V \mathbf{B}^T \mathbf{D} \mathbf{B} dV \quad (2)$$

where:

\mathbf{B} - matrix deformation element;

\mathbf{D} - matrix element of elasticity;

V - volume element.

Inertia matrix \mathbf{M} - reflects the mass and the mass moments of inertia, is created the same way for the entire structure as the structure stiffness matrix \mathbf{K} . The MES inertia matrix \mathbf{M}^e for the item is defined as a square shape functions [2]:

$$\mathbf{M}^e = \rho \int_V \mathbf{N}^T \mathbf{N} dV \quad (3)$$

where:

\mathbf{N} - matrix of shape functions;

ρ - density of the element;

V - volume element.

\mathbf{C} is the damping matrix. Most define it as a linear combination of the inertia matrix and stiffness matrix [2]:

$$\mathbf{C} = \alpha \mathbf{M} + \beta \mathbf{K} \quad (4)$$

Where α and β are constant coefficients, which determine the manner specified in [3]. U represents the vector of generalized displacement of the nodes, whereas their derivatives over time represent velocity and acceleration of nodes, F is the vector of external nodal forces. These matrices and vectors in a given task depend on the type of finite elements used to describe the area in question, which translates into the size of the task. In these types of issues, reflecting the geometry of the study area and its discretization acquire a completely different dimension, as their depend on the size of the task, the computation time and the results obtained. The equation of motion with specified initial conditions at time t_0 is the basic system of equations:

$$U(t_0) = U_0 \quad \dot{U}(t_0) = \dot{U}_0 \quad (5)$$

The CAE program includes a number of ways of integration of equations of motion [1, 3, 4, 5]. The most popular are the so-called direct methods, also called step-by-step methods, or simply dynamic explicit. They are applied to any equations untreated by transformation. They are based on the assumption that the equation is satisfied in certain moments of time $t_0, t_0+\Delta t, t_0+2\Delta t, \dots, t_1$, and not the entire time interval $\langle t_0, t_1 \rangle$. The nature of variation, displacement, velocity and acceleration are assumed during the relevant time period $\langle t, t+\Delta t \rangle$. With these assumptions, the integration algorithm is reduced to finding a solution at time $t_0+i\Delta t$ by using the known

values of the function in the moments preceding $t_0, t_0+\Delta t, t_0+2\Delta t, t_0+(i-1)\Delta t$. The most common methods of numerical integration of equations of motion are: Euler's, Newmark's and Wilson's [1, 2, 3, 4]. In Newmark's numerical integration method, the basic formulas are given by [1]:

$$U_{t+\Delta t} = U_t + \dot{U}_t \Delta t + \left[\left(\frac{1}{2} - \beta \right) \ddot{U}_t + \beta \ddot{U}_{t+\Delta t} \right] (\Delta t)^2$$

$$\dot{U}_{t+\Delta t} = \dot{U}_t + \left[(1 + \gamma) \ddot{U}_t + \gamma \ddot{U}_{t+\Delta t} \right] \Delta t \quad (6)$$

where β, γ are constant factors affecting the stability and accuracy of the method. It was shown that for the values $\beta = 0,25$ and $\gamma = 0,5$ the method is unconditionally stable in papers [1,3]. Solving equations (1 and 5) with respect to $\dot{U}_{t+\Delta t}$ and $\ddot{U}_{t+\Delta t}$ we obtain:

$$\ddot{U}_{t+\Delta t} = \frac{1}{\beta (\Delta t)^2} \left[U_{t+\Delta t} - U_t - \dot{U}_t \Delta t + (\Delta t)^2 \left(\beta - \frac{1}{2} \right) \ddot{U}_t \right] \quad (7)$$

$$\dot{U}_{t+\Delta t} = \frac{\gamma}{\beta \Delta t} (U_{t+\Delta t} - U_t) + \left(1 - \frac{\gamma}{\beta} \right) \dot{U}_t + \left(1 - \frac{\gamma}{2\beta} \right) \Delta t \ddot{U}_t$$

Substituting vectors (7) to the equations of motion (1) gives the algebraic equation in the form:

$$\left[\frac{1}{\beta (\Delta t)^2} \mathbf{M} + \frac{\gamma}{\beta \Delta t} \mathbf{C} + \mathbf{K} \right] U_{t+\Delta t} =$$

$$= F_{t+\Delta t} + \mathbf{M} \left[\frac{1}{\beta (\Delta t)^2} U_t + \frac{1}{\beta \Delta t} \dot{U}_t + \left(\frac{1}{2\beta} - 1 \right) \ddot{U}_t \right] +$$

$$+ \mathbf{C} \left[\frac{\gamma}{\beta \Delta t} U_t + \left(\frac{\gamma}{\beta} - 1 \right) \dot{U}_t + \Delta t \left(\frac{\gamma}{2\beta} - 1 \right) \ddot{U}_t \right] \quad (8)$$

From the above equation displacement vector $U_{t+\Delta t}$ can be calculated. Then, from equations (7) the velocity and acceleration vectors $\dot{U}_{t+\Delta t}$ and $\ddot{U}_{t+\Delta t}$ can be obtained. Repeating this procedure for successive moments we obtain a solution in the considered time interval $\langle t_0, t_1 \rangle$.

Substituting $\beta=1/4$ and $\gamma=1/2$ we get the equation:

$$\left[\frac{4}{(\Delta t)^2} \mathbf{M} + \frac{2}{\Delta t} \mathbf{C} + \mathbf{K} \right] U_{t+\Delta t} =$$

$$= F_{t+\Delta t} + \mathbf{M} \left[\frac{4}{(\Delta t)^2} U_t + \frac{4}{\Delta t} \dot{U}_t + \ddot{U}_t \right] +$$

$$+ \mathbf{C} \left[\frac{2}{\Delta t} U_t + \dot{U}_t \right] \quad (9)$$

and

$$\ddot{U}_{t+\Delta t} = \frac{4}{(\Delta t)^2} \left[U_{t+\Delta t} - U_t - \dot{U}_t \Delta t - \frac{1}{4} (\Delta t)^2 \ddot{U}_t \right] \quad (10)$$

$$\dot{U}_{t+\Delta t} = \frac{2}{\Delta t} (U_{t+\Delta t} - U_t) - \dot{U}_t$$

The above procedure is implemented in a number of commercial applications. 'Dynamic explicit' gives a fairly stable solution, even for highly nonlinear problems. When the nonlinear static analysis obtaining a solution fails, it is recommended to repeat the task in terms of 'dynamic explicit'.

3. SELECTION OF TIME STEP IN A FAST-CHANGING ISSUES

The problem in dynamic analysis is the time step size [6]. The smaller its size, the smaller the size of the used finite elements. This relationship is very unfavorable, because the grid density is associated with a reduction in the time step. For example, doubling the number of items and selecting the appropriate time step to the new dimensions of elements may longer the computation time 10-20 times. For a dense grid time step values are of the order 10^{-6} s, and even smaller. In the fast-changing processes such as loading the construction with a pressure wave from the explosion, where the duration of load is a fraction of a millisecond in a row, time step is determined by the history of the load.

Experiments show that the solution of the dynamic task is stable when the initial time step value is less than 1/10 of the first period frequency. Good results are obtained through adoption of the time step, as the ratio of the smallest dimension of the grid elements to the speed of propagation of elastic waves (acoustic) in the material element, that is:

$$\Delta t = \frac{h}{a} \quad (11)$$

where:

h - the smallest dimension of the grid elements;

$a = \sqrt{E/\rho}$ - elastic wave velocity (acoustic).

After determining the value of time step, due to the size of the elements, one has to make sure it reflects the entire history of the load, if it should not be reduced by subsequent orders, which can lead to the range of 10^{-7} , 10^{-8} s.

4. REFLECTION OF THE GEOMETRY AND DISCRETIZATION OF THE RESEARCH

In formulating the task in terms of MES at the stage of reflecting the geometry the size of the task in relation to the computational capabilities must be taken into the account. Usually, we intend to faithfully reflect the geometry of the object. Unfortunately, the increase in accuracy will mainly increase the number of elements in the future discretization, reducing their size and the need for using solid elements of higher order. Experiments show that one should use the simplest elements possible to describe the structure. To describe the

geometry of objects such as ships it is proposed to use the shell and beam elements, and equipment constituting interior modeled as concentrated masses of the respective nodes (Fig. 1).

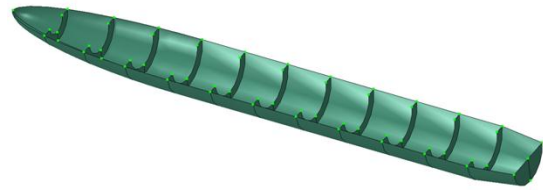


Figure 1. The geometry of the hull with the centered masses

The possibility of applying the masses gathered in the MES software algorithms can significantly reduce the size of the task, by reducing the number of elements to describe the geometry. In the nodes of the elements the mass moments of inertia can be attributed [7]. Thus, to include in the calculation model of the equipment, for example, the generator, it is not necessarily a reflection of its geometry, it is sufficient to determine its mass and calculate the mass inertia moments given the point of the ship structure and assign these values to that point. It is recommended to "distribute" such data on a few points. To present the problem, the shape functions for linear (4-node) shell element and linear (8-node) solid element are summarised below. Shape function for the linear 4-node element [7]:

$$\begin{aligned} u(g, h) = & \frac{1}{4}(1-g)(1-h)u_1 + \\ & + \frac{1}{4}(1+g)(1-h)u_2 + \\ & + \frac{1}{4}(1+g)(1+h)u_3 + \\ & + \frac{1}{4}(1-g)(1+h)u_4 \end{aligned} \quad (12)$$

Shape function for the linear hexagonal 8-node element [7]:

$$\begin{aligned} u(g, h, r) = & \frac{1}{8}(1-g)(1-h)(1-r)u_1 + \\ & + \frac{1}{8}(1+g)(1-h)(1-r)u_2 + \\ & + \frac{1}{8}(1+g)(1+h)(1-r)u_3 + \\ & + \frac{1}{8}(1-g)(1+h)(1-r)u_4 + \\ & + \frac{1}{8}(1-g)(1-h)(1+r)u_5 + \\ & + \frac{1}{8}(1+g)(1-h)(1+r)u_6 + \\ & + \frac{1}{8}(1+g)(1+h)(1+r)u_7 + \\ & + \frac{1}{8}(1-g)(1+h)(1+r)u_8 \end{aligned} \quad (13)$$

The geometry of the mine hunter 206FM - Fig. 2, is presented below by 14 475 square coating components, coating 76 triangular elements, set in space by 11 753 nodes, which at the 6 degrees of freedom at each node gives 70 518 degrees of freedom of the whole structure. It is also the size of the matrix \mathbf{K} , \mathbf{M} and \mathbf{C} .

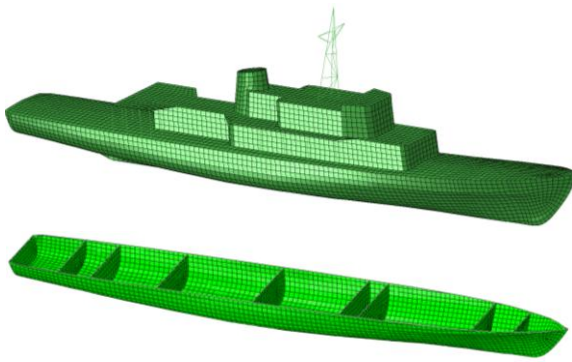


Figure 2. Polish mine hunter 206FM's
- discrete model and its cross-section

5. CONSTRUCTION LOAD – PRESSURE WAVE AFFECTING THE SHIP

Simplified descriptions of the pressure distribution as a function of time and distance from the explosion of pyrotechnic substance both in water and air are given in the literature of the twentieth century, and they can be implemented into computer programs. The explosion is the process of deflagration pressure increase that occurs in a very short time (milliseconds). The nature of this process is determined by the dynamic conditions in which the combustible mixture and, in particular turbulence medium is located. Pressure waves, called shock waves, formed during the explosion in air travel at the speed of 1000 3000 m/s and in liquid (explosion under water) or in solids reach up to 8000 m/s. Typical detonation velocity in the air range from 1500 to 3000 m/s, while the pressure reaches a value of 1 to 100 MPa. Before the arrival of the shock wave front the pressure is equal to atmospheric pressure. With the advent of the front, the pressure is rising rapidly up to a maximum value called the peak positive overpressure. Then the pressure drops to atmospheric pressure. The period of a further drop in pressure and the return to atmospheric pressure is called the period of negative phase. Important parameters of the process are: the maximum value of pressure and the area under the function describing the pressure dependence of time during the positive phase. The nature and mechanism of the explosion is determined by numerous parameters, which include:

- material properties (physical, chemical stability, heat of combustion, etc..)
- space in which combustion occurs (size, open, closed, barriers, etc.);
- properties of explosive mixtures (concentration, pressure and temperature);
- way of ignition (energy, temperature).

Here are the results of pressure measurements made on the range during the detonation of an equal mass of explosives such as hexogen (RDX), trinitrotoluene (TNT), metanite (2H), dynamite (20G5H) ammonite (54H), measured at a distance of 2 m from the burst's centre (Fig. 3). The experiment

was carried out by employees of the Department of Mining and Geo-engineering, AGH University in Krakow [9].

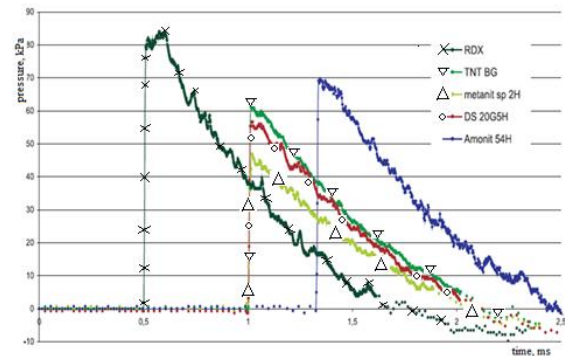


Figure 3. Pressure values at a distance of 2 m from the centre of detonation for various explosives (source: WGiG AGH in Cracow) [9]

For the strength calculations simplified models of the detonation wave are assumed [8], which usually does not take into the account the vacuum phase (Fig. 4). It is important that the time step used for the calculations included the entire history of the load, because in case of a bad choice, the phase of hypertension may be extended or completely omitted.

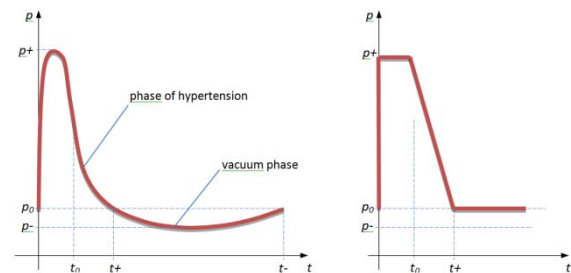


Figure 4. The structure of the shock wave and its simplification

The TNT explosion is very well described by a perfect shock wave structure, with a rapid pressure rise, a short period of positive phase from 1 to 10 ms and hypertension to 100 MPa. In case of the closed or partially closed volume, there exist other phases of the shock wave associated with the reflection from the surrounding structures. In [9] quoted several ways to determine pressure and pulse of the pressure wave depending on the distance from the explosion and the mass of the detonated load. The type of explosive is also taken into an account. For the purposes of calculations and numerical simulations to determine the intensity of pressure on the front of the wave $p(t)$ the historical, but still current dependencies are commonly used, known as Cole's model [10] of the form:

$$p_m(t) = 52.3 \left(\frac{\sqrt[3]{m}}{R} \right)^{1.13} \cdot e^C \quad (14)$$

$$C = \frac{-t \cdot 1000}{0.093 \cdot \sqrt[3]{m} \left(\frac{\sqrt[3]{m}}{R} \right)^{-0.22}} \quad (15)$$

where:

p_m - the pressure on the front of the wave, MPa,

t - time, s,

R - distance from the load, m,

m - mass of the load, kg.

These patterns allow the determination of the pressure at the front of the shock wave in water and in function of distance from the epicenter of detonation, the payload and the time period from the time of the wave at a given point in space (and not from the moment of detonation). Thus, to apply the above description in MES, a procedure should be prepared (including the above formulas) developed to describe the pressure distribution in space as a function of time from the moment of detonation, and taking into account the angle of incidence of waves on an item as it has a particular direction and vector features (Fig. 5) [8].

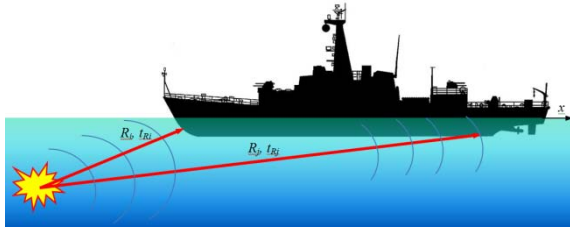


Figure 5. The distance of the element from the epicenter and the wave transit time

In this procedure, the wave transit time from the moment of explosion until you reach the first point of the structure should be omitted. This procedure was repeated for each element in a given time step. Pressure wave velocity to be used in a given medium might be a problem as it is not constant. As mentioned above, in water in the first phase of the outbreak it reaches a speed of up to 8000 m/s, then moving on, the speed drops to the speed of sound in a given medium, i.e. for water to approximately 1500 m/s. Therefore, if the epicentre of the outbreak is far enough away from the structure (over 10 m), for the calculation, it can be assumed that speed of propagation of the pressure wave is constant - equal to the speed of sound. For smaller distances it should be a description of the wave velocity as a function of distance. Ultimately, this procedure gives states the load structure at discrete moments in time. This approach can be directly implemented in CAE.

Summing up, setting the load for a particular element of construction, the time in formulas (14), must move by the value of t_R which is:

$$t_R = R/v_c \quad (16)$$

where:

t_R - time for the pressure wave to reach the component, s

R - distance from the load to the center of the element, m

v_c - sound velocity in the medium surrounding the structure, m/s

The time interval from 0 to t_R element under consideration is not influenced. The speed of sound for sea water is 1500 m/s.

To take into account the angle of the wave for a given element (Fig. 6) it is necessary to appoint two vectors, the vector normal to the element n and the pressure wave vector R whose origin is at the epicenter of the outbreak K and which ends at the center of S .

If the shell element is determined, in space, by four nodes with coordinates:

$$\begin{aligned} A(x_a; y_a; z_a) \\ B(x_b; y_b; z_b) \\ C(x_c; y_c; z_c) \\ D(x_d; y_d; z_d) \end{aligned} \quad (17)$$

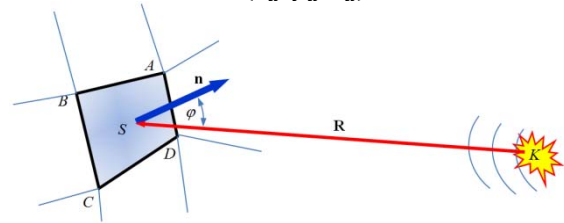


Figure 6. Element influenced by the pressure wave.

The coordinates of the centre element of $S(x_s; y_s; z_s)$ is calculated as the mean of these coordinates:

$$\begin{aligned} x_s &= \frac{x_a + x_b + x_c + x_d}{4} \\ y_s &= \frac{y_a + y_b + y_c + y_d}{4} \\ z_s &= \frac{z_a + z_b + z_c + z_d}{4} \end{aligned} \quad (18)$$

Assuming that the epicenter of the outbreak is at the point $K(x_k; y_k; z_k)$, the components of the vector R are:

$$\begin{aligned} R_x &= x_s - x_k \\ R_y &= y_s - y_k \\ R_z &= z_s - z_k \end{aligned} \quad (19)$$

The coordinates of the normal vector n to the element in question is obtained by multiplying two vectors such as AB and CB built on the sides of elements whose components are:

$$\begin{aligned} AB_x &= x_a - x_b & CB_x &= x_c - x_b \\ AB_y &= y_a - y_b & CB_y &= y_c - y_b \\ AB_z &= z_a - z_b & CB_z &= z_c - z_b \end{aligned} \quad (20)$$

Then $n = AB \times CB$:

$$\begin{aligned} n_x &= AB_y \cdot CB_z - AB_z \cdot CB_y \\ n_y &= AB_z \cdot CB_x - AB_x \cdot CB_z \\ n_z &= AB_x \cdot CB_y - AB_y \cdot CB_x \end{aligned} \quad (21)$$

Cosine of the angle φ between vectors n and R is determined from the definition of scalar product:

$$n \cdot R = |n| \cdot |R| \cdot \cos\varphi \quad (22)$$

thus:

$$\cos\varphi = \frac{n \cdot R}{|n| \cdot |R|} = \frac{n_x \cdot R_x + n_y \cdot R_y + n_z \cdot R_z}{\sqrt{n_x^2 + n_y^2 + n_z^2} \cdot \sqrt{R_x^2 + R_y^2 + R_z^2}} \quad (23)$$

Eventually the value of the pressure influencing the element is:

$$\text{for } t_c < t_R \Rightarrow p(t_c) = 0 \quad (24)$$

$$\text{for } t_c \geq t_R \Rightarrow p(t_c) = p_m(t_R + t) \cdot \cos\varphi \quad (25)$$

In CAE, the above algorithm for determining the pressure of the item must be made in the form of the calculation procedure. For example, in Abaqus such a procedure is done in Fortran.

The following are illustrative graphs of the pressure on the hull of the mine destroyer, project 206FM, at two points: on the bow and stern. After including the speed of propagation of pressure waves in water, equal to 1500 m/s, in the case of 250 kg of TNT, detonated at a depth of 15 m with a distance of 20 meters in front, the pressure of the wave reaches the maximum value of 11 MPa and continually decreases. At the second point on the stern of the ship the pressure amounts to about 5 MPa, and it appears on the fuselage 0.035 s under the first point on the bow.

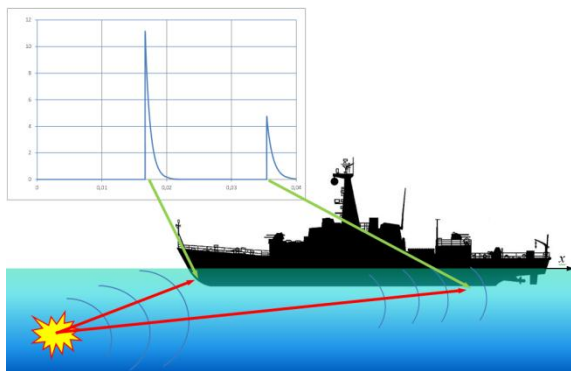


Figure 7. Pressure at two points of the ship (detonation in the distance of 20 m in front of the ship, depth of 15 m, weight of 250 kg).

6. THE SIMULATION RESULTS ON THE EFFECTS OF UNDERWATER DETONATION OF THE SHIP HULL

Characteristics presented on the figure 8 shows simulation of the pressure at the front of detonation wave as a function of mass of the TNT load and distance from the epicenter, determined by the Cole's formula.

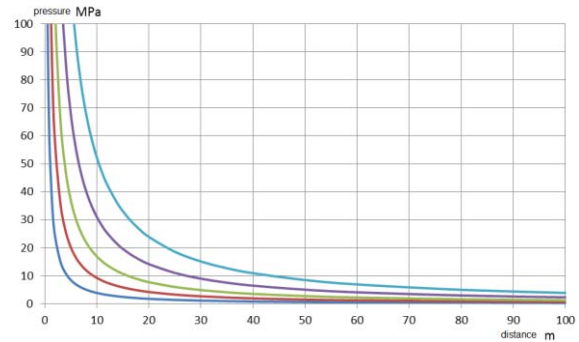


Figure 8. Pressure values at the front of the shock wave as a function of load mass of TNT of 1, 10, 50, 250, 1000 kg

Times that occur in the Cole's formulas, and is counted from the time of the wave pressures at a given point of space, does not include conveyance from the epicenter [4,6]. The pressure wave in the first phase of the explosion propagates at the speed of detonation of an estimated $V = 5000 \div 8000$ m/s. The velocity rapidly decreases to the velocity of sound in the medium [10]. After taking into account velocity of propagation of pressure waves in water of $V = 1500$ m/s, the minehunter 206 FM type and TNT load equal mass $m=250$ kg, exploded at a depth of 15 m with a distance of 20 m from the bow or the stern, the pressure wave reaches the maximum value of $p=11$ MPa and decreases along the ship to the $p=3$ MPa – figure 9. The total time of occurrence the load on the structure of the ship is 0.0376 s.

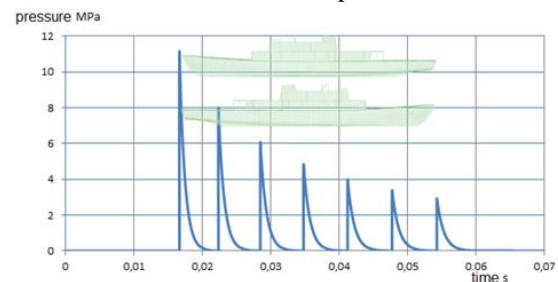


Figure 9. Pressure wave propagation along the length of the ship, detonation at a distance of 20 m before (behind) the ship.

For the same TNT load, exploded at a depth of 15 m with a distance of 20 m on the beam, the maximum shock wave pressure reaches $p=11$ MPa at amidships and decreases along the ship to the value of $p=5.9$ MPa at the bow and stern. The total time of occurrence load on the hull of the ship is more than a half shorter and equal $t=0.0124$ s. Distribution of pressure waves on the hull of the ship, coming from the TNT load exploded is presented on figure 10.

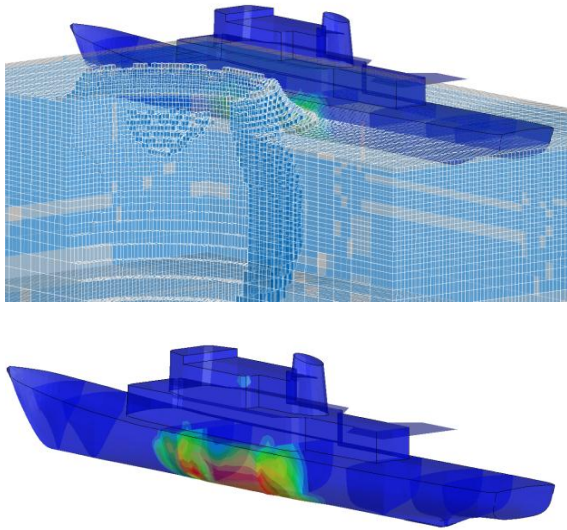


Figure 10. Distribution of shock wave (left figure) and values of pressure (right figure) on the hull coming from the TNT load explosion

Pressure wave causes the hull load over its entire length. Figure 11 shows an example of the time course of the acceleration from the explosion of 250 kg TNT load at a distance of 20 m, at a depth of 15 m from the bow of the ship.

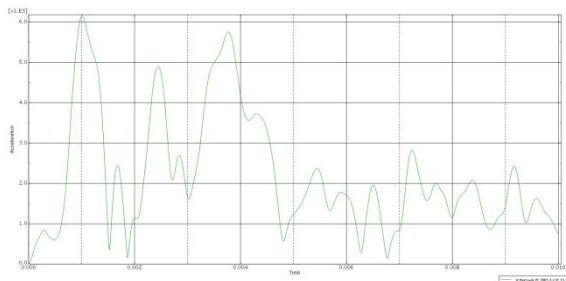


Figure 11. Acceleration received from a simulation of the keel of the explosion front of the bow the ship from a distance of 20 m, depth 15 m, TNT load mass 250 kg

CONCLUSIONS

The results of testing allowed performing simulations of a similar nature to the actual loads of underwater explosions. Virtual model of the hull of the ship responds in a similar manner to the real impacts. Most simulations were performed to calculate or estimate the strength of the hull of plastic deformation. Load model of 2 or 3 bulbs allows assessing the potential occurrence of resonance at any point of the hull. This is important in the design process because the stiffness of the fixing or changing the mass of the foundation, can arrange the marine device from the potential risks coming from the resonance of an underwater explosion.

The next step of research are modeling much more complicate structure of the hull, machinery and other equipments of mine hunter and then solving the problem of resonance between natural frequency of machines and periodical forces coming from first three bulbs effect of underwater detonation.

REFERENCES

- [1] Kacprzyk Z., Rakowski G. *Metoda elementów skończonych w mechanice konstrukcji*. Oficyna Wydawnicza Politechniki Warszawskiej, Wyd.2, Warszawa 2005 r. ISBN: 83-7207-589-1.
- [2] Szturomski B. *Podstawy Metody Elementów Skończonych*. Wydawnictwo Akademickie AMW, Gdynia 2011, ISBN 978-83-60278-5
- [3] Bathe K. J., Wilson E. L. *Numerical method in finite element analysis*. Prentice-Hall, Inc. Englewood Clifts, New Jersey, 1976 r.
- [4] Kleiber M. *Metoda elementów skończonych w nieliniowej mechanice kontinuum*. Polska Akademia Nauk, Wyd.1, PWN, Warszawa-Poznań 1985.
- [5] Zienkiewicz O. C. *The Finite Element Method in Engineering Science*. McGRAW-HILL, London 1971.
- [6] Dobrociński S. *Stabilność rozwiązań zagadnień odporności udarowej konstrukcji*. Biblioteka Problemów Eksploatacji, Akademia Marynarki Wojennej, Gdynia 2000 r., ISBN 83-7204-163-6.
- [7] Abaqus 6.10, PDF Documentation, *Theory Manual, Simulia, Dassault Systems*.
- [8] Szturomski B., Dobrociński S., Flis L. *Analiza wytrzymałościowa konstrukcji pojazdu morskiego obciążonego niekontaktowym wybuchem podwodnym*. Zesz. Nauk. AMW, ROK XLIII NR 2 (150) 2003.
- [9] Machowicz M. *Oddziaływanie powietrznej fali uderzeniowej na otoczenie*. ZN Górniczo-Hutnicza, Rok 29, Zeszyt 3, Akademia Górniczo-Hutnicza, Kraków 2005.
- [10] Cole R. H. *Underwater Explosions*. Princeton University Press, Princeton 1948.



dr hab. inż. **Andrzej GRZĄDZIELA**
Akademia Marynarki
Wojennej
Wydział Mechaniczno -
Elektryczny
ul. Śmidowicza 69
81-103 Gdynia
tel. (58) 626 27 24, e-mail
a.grzadzIELA@amw.gdynia.pl



dr inż. **Bogdan
SZTUROMSKI**

Akademia Marynarki
Wojennej
Wydział Mechaniczno -
Elektryczny
ul. Śmidowicza 69
81-103 Gdynia
tel. (58) 626 27 30, e-mail
b.szturomski@amw.gdynia.pl

d



mgr inż. **Marcin
KLUCZYK**

Akademia Marynarki
Wojennej
Wydział Mechaniczno -
Elektryczny
ul. Śmidowicza 69
81-103 Gdynia
tel. (58) 626 26 67, e-mail
m.kluczyk@amw.gdynia.pl

VIBRATION SIGNALS PROCESSING BY CELLULAR AUTOMATA FOR WIND TURBINES INTELLIGENT MONITORING

Tomasz BARSZCZ*, Andrzej BIELECKI**, Mateusz WÓJCIK***

* AGH University of Science and Technology,
Faculty of Mechanical Engineering and Robotics, Chair of Robotics and Mechatronics,
Al. Mickiewicza 30, 30-059 Cracow, Poland, e-mail: tbarszcz@agh.edu.pl

** AGH University of Science and Technology,
Faculty of Electric Engineering, Automation, Computer Science and Biomedical Engineering,
Chair of Applied Computer Science, Al. Mickiewicza 30, 30-059 Cracow, Poland,
e-mail: azbielecki@gmail.com

*** Jagiellonian University, Faculty of Physics, Astronomy and Applied Computer Science
Reymonta 4, 30-059 Cracow, Poland, e-mail: mateusz.wojcik@uj.edu.pl

Summary

In recent years wind energy is the fastest growing branch of the power generation industry. The largest cost for the wind turbine is its maintenance. A common technique to decrease this cost is a remote monitoring based on vibration analysis. Growing number of monitored turbines requires an automated way of support for diagnostic experts. As full fault detection and identification is still a very challenging task, it is necessary to prepare an early-warning tool, which would focus the attention on cases which are potentially dangerous. There were several attempts to develop such tools, in most cases based on various classification methods. The techniques that have been used so far are based on the vibration signals analysis in which the signals are considered as time series. However such approach has crucial limitations. Therefore, new approaches for wind turbines intelligent monitoring are worked out. Artificial intelligence systems are ones of promising. In this paper such approach is proposed - a vibration signal spectrum is considered as a pixel matrix which is processed using deterministic cellular automaton (DCA). It turns out that such processing allows us to detect pre-failure states.

Keywords: cellular neural networks, wind turbines, gears, intelligent monitoring

PRZETWARZANIE SYGNAŁÓW DRGANIOWYCH PRZY POMOCY AUTOMATÓW KOMÓRKOWYCH W CELU INTELIGENTNEGO MONITORINGU TURBIN WIATROWYCH

Streszczenie

W ostatnich latach energetyka wiatrowa jest najszybciej rozwijającą się gałęzią przemysłu energetycznego. Najkosztowniejsza w turbinach wiatrowych jest ich konserwacja. Popularną techniką obniżającą te koszty jest zdalny monitoring bazujący na analizie wibracyjnej. Rosnąca liczba monitorowanych turbin zmusza do znalezienia automatycznego wsparcia dla diagnozujących ekspertów. Ponieważ pełna detekcja i identyfikacja uszkodzeń jest wciąż wielkim wyzwaniem, potrzebne jest określenie narzędzia zdolnego wychwytywać jak najwcześniejsze symptomy awarii. Podejmowane były próby stworzenia takich narzędzi, opierając się na różnych metodach klasyfikacji. Używane techniki od dłuższego czasu bazują na analizie sygnałów wibracyjnych, które rozpatrywane są jako szeregi czasowe. Takie podejście, jednakże, ma istotne ograniczenia. Dlatego też poszukuje się nowych metod, które mogą być skutecznie użyte do inteligentnego monitoringu turbin wiatrowych. Systemy sztucznej inteligencji wydają się być obiecującym podejściem. W niniejszej publikacji testowana jest użyteczność tego podejścia - badane widmo sygnału wibracyjnego jest rozumiane jako macierz komórek, które konstrytuują automat komórkowy. Przetwarzanie sygnałów przy pomocy powyższego automatu pozwoli wykrywać stany przedawaryjne.

Słowa kluczowe: deterministyczne automaty komórkowe, turbiny wiatrowe, przekładnie, inteligentny monitoring

1. INTRODUCTION

In recent years wind energy is the fastest growing branch of the power generation industry. The average yearly growth in the years 1997-2003

achieved 32% in the United States and 22% in the European Union [6] and these figures will hold for at least the next decade. The distribution of costs during the life cycle of the unit for wind energy is significantly different from that of traditional, fossil

fired units [6]. First of all, initial investment costs are relatively higher, whereas in traditional units cost of fuel plays important role - usually it is the second largest cost. After commissioning, the largest cost for a wind turbine (WT for abbreviation) is its maintenance. With proper maintenance policies, wind turbines can achieve the highest level of availability in the power generation sector - even up to 98%.

Studies have shown that approximately 80% of all fractures are caused by machinery fatigue and only 20% by a static overload. Therefore, studies concerning variations of operational conditions in a wind turbine mechanical system are crucial for their engineering. Such studies have important practical application, as the wind turbine maintenance, as it has been mentioned, generates the largest part of the cost of its operation [18]. A common technique to decrease this cost is a condition monitoring [17,20,21,27], first of all continuous monitoring of the drivetrain of a wind turbine. Therefore, condition monitoring of wind turbines, including fault diagnostics, in particular at the early stage of a fault occurrence or even participatory actions, is an essential problem in wind turbines engineering in particular [17,20,24] and in rotating machinery engineering in general [3]. There were several attempts to develop various monitoring tools, in most cases based on various classification methods. Some of them are based on artificial neural networks (ANNs for abbreviation).

So far the techniques that has been used for gears monitoring are based on the vibration signals analysis in which the signals are considered as time series. However in this paper a vibration signal spectrum is considered as a pixel matrix which is processed using deterministic cellular automaton (DCA for abbreviation) - basic information about DCA and cellular ANNs, that are complex version of DCAs, can be found in [13,14,15,16,22,23,26]. Such processing allows us to detect pre-failure states.

This paper is a continuation of studies concerning monitoring wind turbines states [1,4,19], modelling its loads [2,12] and monitoring and diagnosis gears faults [6,7,8,9,10,11,28].

This article is organizing in the following way. In Section 2 wind turbines mechanics is described. Basic facts concerning deterministic cellular automata are briefly recalled in Section 3. The proposed approach and results are presented in Section 4.

2. WIND TURBINE MECHANICS

The faults which are sought in wind turbines are primarily of mechanical origin. The wind turbine with the gearbox, which is the most popular type, can be described in the following way. The main rotor with three blades is supported by the main bearing and transmits the torque to the planetary

gear. The main rotor is connected to the plate which is the gear input. The planetary gear has three planets, with their shafts attached to the plate. The planets roll over the stationary ring and transmit the torque to the sun. The sun shaft is the output of the planetary gear. The sun drives the two-stage parallel gear which has three shafts: the slow shaft connected to the sun shaft, the intermediate shaft and the fast shaft, which drives the generator. The overall gear ratio is in the range of 1:100. The generator produces alternating current of slightly varying frequency. This current is converted first into direct current power and then into alternating current power of frequency equal to the grid frequency. Electric transformations are performed by the controller at the base of the tower - see Fig.1.

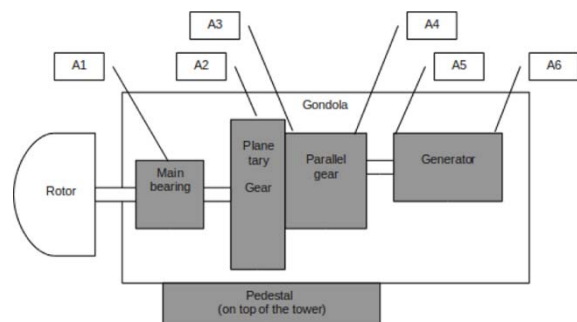


Figure 1: The mechanical structure of the wind turbine. Location of vibration measurement sensors is shown by An symbols

In the field of vibrodiagnostics, a machine operational state is understood as an accepted range of machines operational points enabling referential analysis. In practice, machine operating point is defined by values of available measurements of physical quantities such as speed, load, pressure, temperature, etc., usually called machine process parameters [19]. Typically, from each vibration record, a set of diagnostic indicators is calculated known as trends. Each trend point is a combination of representation of true machine technical condition and behaviour, machines current operating point, measurement error and random factor. In a typical condition monitoring set up, each trend is tracked against a pre-calculated threshold value. In this case, operational states (shortly called states) are used for data classification during the data acquisition process. On the basis of these states, data is combined into sets, which are assumed to represent a particular machine. Consequently, the overall number of defined diagnostic indicators and estimators is equal to the number of indicators and estimators multiplied by the number of states. Therefore, from operators point of view, it is desirable to have as little states as possible. On the other hand, from reliable-diagnostics point of view, in order to minimize the fluctuation of machines operating points, it is desirable to define ranges of states as low as possible. In this case, the state

configuration would result either in single operational state with low permissible fluctuation of operational parameters or in a large number of operational state with low permissible fluctuations of operational parameters.

3. DETERMINISTIC CELLULAR AUTOMATA

In DCAs, that are the simplest type of cellular automata, the spatial domain of the model is divided into a fixed lattice and each lattice point, a cell, has a state associated with it. The cell state at the next time step is determined solely from the earlier state of the cell and its neighbours. The lattice of cells can have any dimension but two-dimensional DCAs are considered most frequently and such DCA is used in the experiment described in this paper. The used DCA is also an automaton with completely defined rules. This means that if the initial state of the automaton is known, all subsequent states are found by iterating and updating synchronously. In these types of automata each state of the whole automaton is an array of states of cells. As it has been mentioned, cells influence and are influenced by neighbours, in the simplest case the nearest ones. However, a neighbourhood in two dimensions can be defined in several different ways. In a square lattice both only four cells, conventionally addressed as points of the compass by N,W,E,S, and also the ones that can be reached diagonally: NE,NW,SE,SW can be regarded as the nearest neighbourhood. However, the lattice can have also hexagonal organization and then each cell has six nearest neighbours. The general rule of an cellular automaton evolution is given by the equation

$$C_{t+1}(i) = F(C_{t+1}(i), C_{t+1}(j)), \quad (1)$$

where $C_{t+1}(i)$ denotes the state of the i -th cell at the t -th iteration. The index j numerates cells from the neighbourhood that is taken into consideration. Each cell can take only the finite number of states. In the simplest cellular automata, the binary ones, each cell can be only in one of the two states: 0 or 1.

4. RESULTS

The used data are real ones recorded on a 1.5 MW wind turbine, located in Germany. The data were available courtesy of the company SeaCom GmbH from Herne, Germany. The measurement system consisted of signal conditioning unit (PA8000D type from EC Electronics), data acquisition card (USB-6210 type from National Instruments) and dedicated data acquisition software. The software was developed in the LabView environment and run on the ARK-3384 embedded computer. The measured wind speed signal was acquired from the wind turbine controller. The system also has acquired the turbine output power and six vibration channels. A CA has been applied to processing signals obtained from the single vibration channel.

A fault classification system for vibration signals was created using a cellular automaton. System classifies time series of vibration signals. That series can be presented in the form of charts. A cellular automaton is designed to process that charts.

The automaton is based on a two-dimensional square lattice of cells with radius of neighbourhood equal to 1. The network topology is defined in such a way, that all the cells N,W,S,E,NW,NE,SW,SE constitute the neighbourhood - see Fig.2. Each cell has a binary value (0 or 1). The cell value represents a segment of the chart. Network is constructed using mentioned rules and after that the classification is being done in steps described in following subsections.

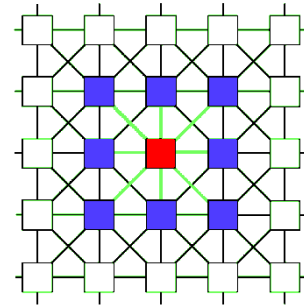


Figure 2: Two-dimensional DCA with radius of neighbourhood $r=1$: the red cell has nine neighbours - the eight blue cells and itself

The example of the vibration signal is presented in Fig.3. This time series can be divided into three intervals. The first one corresponds to the constant average trend. In the second one the average trend increases whereas in the third one the average trend has a constant value but greater than the value on the average trend in the first interval. The second interval corresponds to the failure. Therefore, the intelligent monitoring system should recognize the border between the first and the second interval as the pre-failure state.

4.1. Network initialization

The vibration signals chart is considered to be a visual pattern, not a numerical time series. Thus, it is regarded to be a binary matrix. The size of a grid cell is determined manually. Cell length and width can be different. Each grid cell reflects one network cell. If there is an experimental point inside the grid cell then that network cell is selected and is marked as 1. An example of network cells is presented in Fig.3.

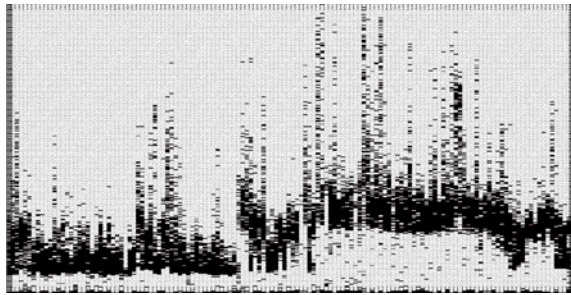


Figure 3: The DCA after initialization

4.2. Network processing

After initialization the network changes states of cells in an iteration process. Transfer function of cells is defined as the Surface Tension rule. The rule of the evolution of a cell state, defined in general by the formula (1), is given in such a way that the state of each cell $C_{t+1}(i)$ in the iteration $(t+1)$ -th is equal to:

- 0, when a sum of cells neighbouring to the cell c_t (including that cell) is one of the following: 0, 1, 2, 3 or 5,
- 1, otherwise.

After a specified number of iterations the processing is stopped.

4.3. Final rating

At the final state dominate and separate groups of cells having value 1 are counted. If there is more than one group then it means that some fault occurred. Periods of time in which the fault could have occurred are points of the time series having no cells with value equal to 1. Counting is done manually, but some algorithms to do that automatically could be specified.

A few steps of a cellular automaton state evolution are presented in figures 4, 5 and 6. There are two dominate separate groups of cells, therefore data can be marked as having a fault. The border between two obtained clusters corresponds - see Fig.6 - corresponds to the point when the average trend starts to increase - see Fig.3. Thus, the CA recognized the pre-failure state properly.

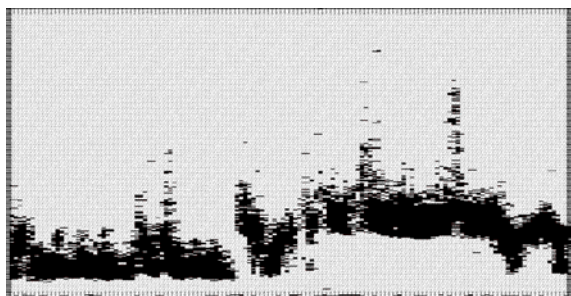


Figure 4: The cellular automaton after the first iteration

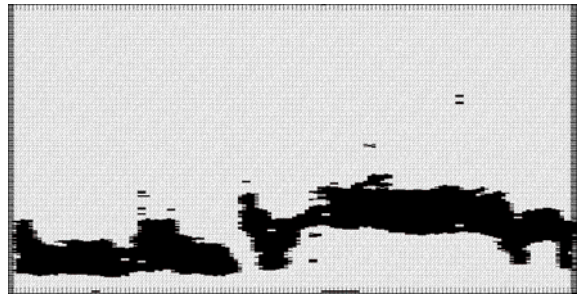


Figure 5: The cellular automaton after 10 iterations



Figure 6: The cellular automaton after 100 iterations

5. CONCLUDING REMARKS

As it has been mentioned, intelligent monitoring is crucial in wind turbines exploitation. On the other hand, there are very few attempts to create system for intelligent monitoring based on artificial intelligence - see [17] and references given there. The experiments described in this paper show that DCAs can be an effective tool for such task performing - the symptoms of a turbine damage can be detected using them. The described approach was based on the simple cellular automaton. The signal processing based on more complex systems of this type, i.e. cellular neural networks [13,14,22,23,25], should be tested as well. It should be stressed however, that the obtained results are preliminary ones - only one vibration channel has been used and, according to the lack of data obtained during the break down moment, only one case has been considered. Usually, a few vibration channels are observed simultaneously - see [2]. The monitoring module based on DCAs is planned to be a module of hybrid expert system for intelligent monitoring and fault diagnostics in wind turbines based on ANNs. Though it is planned that ART-type artificial neural networks will play a crucial role in the intelligent monitoring system, according to the results obtained in [1,4,5], the cellular automata can be used as specialised modules for detecting pre-failure states in bearings.

It should be also mentioned that the method presented in this paper has been referred to gears in wind turbines and the experiment has been performed for vibration data obtained from wind turbines. However, the method can be applied also in any rotational machines working under variable load.

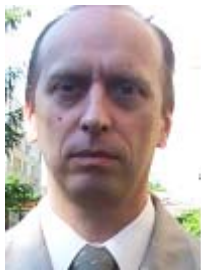
REFERENCES

- [1] Barszcz T., Bielecka M., Bielecki A., Wójcik M. *Wind turbines states classification by a fuzzy-ART neural network with a stereographic projection as a signal normalization*. Lecture Notes in Computer Science, vol.6594, 2011, 225-234.
- [2] Barszcz T., Bielecka M., Bielecki A., Wójcik M. *Wind speed modelling using Weierstrass function fitted by a genetic algorithm*. Journal of Wind Engineering and Industrial Aerodynamics, vol.109, 2012, 68-78.
- [3] Barszcz T., Bielecki A., Romaniuk T. *Application of probabilistic neural networks for detection of mechanical faults in electric motors*. Electrical Review, vol.8/2009, 2009, 37-41.
- [4] Barszcz T., Bielecki A., Wójcik M. *ART-type artificial neural networks applications for classification of operational states in wind turbines*. Lecture Notes in Artificial Intelligence, vol.6114, 2012, 11-18.
- [5] Barszcz T., Bielecki A., Wójcik M., Bielecka M. *ART-2 artificial neural networks applications for classification of vibration signals and operational states of wind turbine for intelligent monitoring*. Lecture Notes in Computer Science, 2013, accepted.
- [6] Barszcz T., Randall R.B. *Application of spectral kurtosis for detection of a tooth crack in the planetary gear of a wind turbine*. Mechanical Systems and Signal Processing, vol.23, 2009, 1352-1365.
- [7] Bartelmus W. *Mathematical modelling and computer simulations as an aid to gearbox diagnostics*. Mechanical Systems and Signal Processing, vol.15, 2001, 855-871.
- [8] Bartelmus W., Chaari F., Zimroz R., Haddar M. *Modelling of gearbox dynamics under time-varying nonstationary load for distributed fault detection and diagnosis*. European Journal of Mechanics, A/Solids, vol.29, 2010, 637-646.
- [9] Bartelmus W., Zimroz R. *Gearbox systems dynamic modelling for diagnostic fault detection*. Proceedings of the ASME Design Engineering Technical Conference, vol.4B, 2003, 625-633.
- [10] Bartelmus W., Zimroz R. *Vibration condition monitoring of planetary gearbox under varying external load*. Mechanical Systems and Signal Processing, vol.23, 2009 246-257.
- [11] Bartelmus W., Zimroz R. *A new feature for monitoring the condition of gearboxes in non-stationary operation conditions*. Mechanical Systems and Signal Processing, vol. 23, 2009, 1528-1534.
- [12] Bielecka M., Barszcz T., Bielecki A., Wójcik M. *Fractal modelling of various wind characteristics for application in a cybernetic model of a wind turbine*. Lecture Notes in Artificial Intelligence, vol.7268, 2012, 531-538.
- [13] Chua L.O., Yang L. *Cellular Neural Networks. Theory*, IEEE Transactions on Circuits and Systems, vol.35, 1988, 1257-1274.
- [14] Chua L.O., Yang L., *Cellular Neural Networks. Applications*, IEEE Transactions on Circuits and Systems, vol.35, 1988, 1275-1290.
- [15] Codd E.F., *Cellular Automata*, Academic Press Inc., Orlando, 1968.
- [16] Ermentrout G.B., Edelstein-Keshet L., *Cellular automata approaches to biological modelling*, Journal of Theoretical Biology, vol.160, 1993, 97-133.
- [17] Hameeda Z., Honga Y.S., Choa T.M., Ahnb S.H., Son C.K. *Condition monitoring and fault detection of wind turbines and related algorithms: A review*. Renewable and Sustainable Energy Reviews, vol.13, 2009, 1-39.
- [18] Hau E., *Wind turbines: Fundamentals, Technologies, Applications, Economics*, Springer, Berlin, Heidelberg, 2006.
- [19] Jabłoński A., T. Barszcz T., *Procedure for data acquisition for machinery working under non-stationary operational conditions*, Proceedings of the Ninth International Conference on Condition Monitoring and Machinery Failure Prevention Technologies, 2012, London.
- [20] Jabłoński A., Barszcz T., Bielecka M. *Automatic validation of vibration signals in wind farm distributed monitoring systems*. Measurement, vol.44, 2011, 1954-1967.
- [21] Jabłoński A., Barszcz T., Bielecka M., Brehaus P., *Automatic validation of vibration signals in wind farm distributed monitoring systems*, Measurement, vol.46, 2013, 727-738.
- [22] Kacprzak T., Ślot K., *Sieci neuronowe komórkowe*, PWN, Warszawa, 1995 (in Polish).
- [23] Kosiński R.A., *Sztuczne sieci neuronowe - dynamika nieliniowa i chaos*, WNT, Warszawa, 2002 (in Polish).
- [24] Kusiak A., Li W. *The prediction and diagnosis of wind turbine faults*. Renewable Energy, vol.36, 2011, 16-23.
- [25] Roska T., Vandewalle J., *Cellular Neural Networks*, Chichester, Wiley & Sons, 1993.
- [26] Wolfram S. *Universality and complexity in cellular automata*. Physica D: Nonlinear Phenomena, vol.10, 1984, 1-36.
- [27] Zhang Z., Verma A., Kusiak A. *Fault analysis and condition monitoring of the wind turbine gearbox*, IEEE Transactions of Energy Conversion, vol.27, 2012, 526-535.
- [28] Zimroz R, Bartelmus W, *Gearbox condition estimation using cyclo-stationary properties of vibration signal*, Key Engineering Materials, vol.413-414, 2009, 471-478.

This paper was supported by the Polish Ministry of Science and Higher Education under grant number N504 147838



Dr hab. inż. **Tomasz BARSZCZ** received the M.Sc. degree in Electric Engineering and Automatic Control from the Technical University of Gdańsk in 1993, Ph.D. in Mechatronics (1997) and D.Sc. in Automation and Robotics in 2009 from the AGH University of Science and Technology. Has long experience of application of research in numerous industries in Poland and abroad. Author of 4 books and over 150 papers. Monitoring systems developed under his supervision were installed on several hundred machines worldwide.



Dr hab. **Andrzej BIELECKI** received the M.Sc. degree in Physics and Mathematics from the Jagiellonian University in 1985 and 1992 respectively, Ph.D. in Mathematics in 1999 and D.Sc. in Mathematics in 2009. Dynamical systems theory, artificial intelligence and cybernetics are the topics of his scientific interest. He is an author of over 70 scientific papers.



Mateusz WÓJCIK, received the MSc degree in Computer Science from the Jagiellonian University. He is a PhD student at the Jagiellonian University, Faculty of Physics, Astronomy and Applied Computer Science. His scientific interests focus on artificial intelligence and machine learning.

SUPERVISING AND COMPENSATION OF THERMAL ERROR OF CNC FEED BALL SCREW

Miroslaw PAJOR¹, Jacek ZAPŁATA²

¹Institut Technologii Mechanicznej, ²Katedra Mechaniki i Podstaw Konstrukcji Maszyn,
Zachodniopomorski Uniwersytet Technologiczny w Szczecinie,
Al. Piastów 19, 70-310 Szczecin, tel.: 91-449-42-66, faks: 91-449-44-42,
miroslaw.pajor@zut.edu.pl, jacek.zaplata@zut.edu.pl

Summary

The paper presents a set allowing for on-line monitoring of machine tool feed screw temperature. Indirect supervising of the feed screw thermal elongation protects ball bearings from excessive loads. Moreover, the usage of an appropriate model in the control system of the CNC machine tool allows for the reduction of ball screw thermal errors.

Keywords: thermal error, feed screw, monitoring

NADZOROWANIE TERMICZNE ORAZ KOMPENSACJA BŁĘDÓW ODKSZTAŁCEŃ CIEPLNYCH ŚRUB POCIĄGOWYCH OBRABIAREK CNC

Streszczenie

Prezentowany w pracy układ pozwala na monitorowanie „on-line” temperatury śruby pociągowej obrabiarki. Pośredni nadzór wydłużenia cieplnego śruby zabezpiecza przed nadmiernym obciążeniem łożysk tocznych na skutek wydłużenia cieplnego śruby pociągowej. Dodatkowo zastosowanie odpowiedniego modelu w systemie sterowania obrabiarki CNC pozwala na redukcję „on-line” błędów pozycjonowania wynikających z odkształceń cieplnych śrub pociągowych obrabiarki.

Słowa kluczowe: odkształcenia cieplne, śruba pociągowa, monitoring

1. INTRODUCTION

The heat generated as a result of friction in cooperating elements of manufacturing machines is a common adverse phenomenon. An increase in the temperature of machine sub-assemblies leads to a deterioration of machine accuracy. In extreme cases generated heat can lead to seizure or even destruction of machine parts. In industrial machines the temperature measurement transmitted via LAN networks allows for remote diagnostics [1, 2, 3]. In modern CNC machine tools it is common to monitor the working temperature of the spindle bearings and temperature of motors equipped with permanent magnets [4, 5].

In CNC machine tools thermal deformations increase the volumetric error, thereby they may cause the tolerances imposed on the machined workpieces not to be met [6,7].

The aforementioned examples show the importance of the temperature monitoring in modern manufacturing. In this paper the attention is given to thermal deformations accompanying the work of the ball screw driven feed axes of CNC machine tools.

In the CNC feed axes utilising ball screws there is a need of reducing the impact of thermal phenomena on the system's functioning. For

example, the proper selection of the bearings clearance requires considering the radial thermal expansion of the shaft, which result from external heat sources. Another issue, which must be resolved by constructor, is the selection of an appropriate bearing arrangement. E.g. the “X” arrangement is characterised by the bearings load increase as a result of the shaft thermal elongation. Whereas, the bearing mounting in the “O” arrangement is characterised by a decrease in the load of bearings along with the thermal expansion of the shaft.

In the case of drive axes utilising ball screws, often apart from the pretensioning of the screw, the pretensioning of the nut-screw bearing is applied to increase the rigidity. In this case, it is important to consider the axial thermal expansion of the screw. It is, because the large mass of the machine body and existing heat flow will lead to significant difference in machine body and screw temperature. The considerable elongation of the screw relative to the body will take place if the screw is long enough, the friction moment is high due to the pretensioning of the nut, the thermal resistance between the screw and the body is high. In such case, an insufficient axial clearance in a non-locating bearing will lead to the destruction of the mechanism [9].

2. THE TEMPERATURE MONITORING AND POSITION CORRECTION SYSTEM

2.1 System of Screw Temperature Monitoring

The presented system for the feed screw temperature monitoring, designed primarily for the purpose of reducing the impact of thermal errors of the feed screw on the accuracy of the CNC machine, additionally allows for an indirect measurement of the total feed screw elongation in order to secure the machine against dangerous thermal deformation levels.

It also enables the monitoring of the feed screw ball bearing temperature. Increased temperature of the bearing unit is an alarming signal and may prove inadequate working conditions or be a symptom of failure [10, 11]. Monitoring of this temperature provides valuable information about the system wear.

In the presented set for the thermal monitoring, the NTC temperature sensors were placed in the ball screws [12] of a numerically controlled milling machine AVIA VC 760. They have been mounted within the distances of 135 mm from each other by means of a thermoconductive glue which prevents the sensors from the negative influence of external factors. The first and the last sensor are located directly under the ball bearings. The lead out of wiring (Fig.1.) takes place via an axial bore placed in the centre of the screw. The axial bore, after placing signal wires in it, was filled with adhesive silicone. Cables are thus secured against a relative rotational movement in relation to the rotating screw, caused by the inertia of the cables. This movement could result in the twisting of the wires or cables being cut by sharp steel edges.

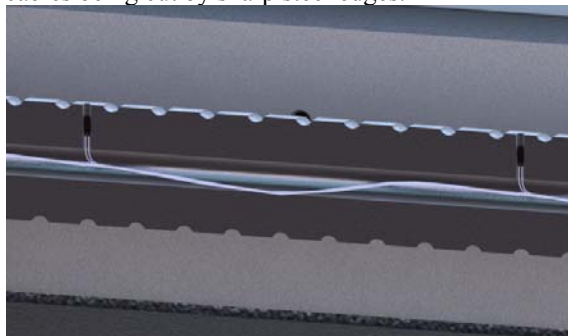


Fig. 1. Visualisation of the NTC sensors mounted in the feed screw

Leading out the signal from the screw takes place via the rotary electrical connector. In industrial application it is advisable to place a multi-path connection between the sensors and the rotary connector, allowing for fast replacement of the rotary connector worn as a result of operation or ensuring wireless data transmission.

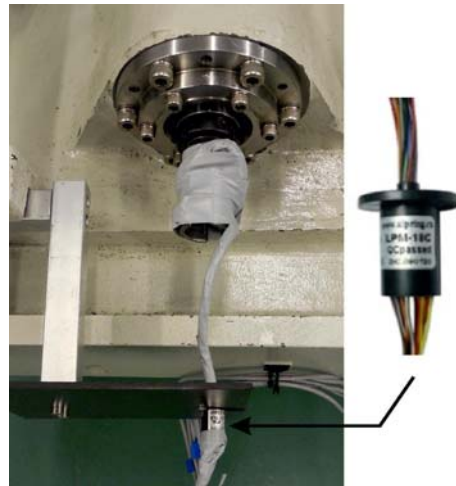


Fig. 2. Photo of the AVIA VC760 machine tool bearing node along with a connector providing the possibility of the sensor system rotation

In the presented example, a single bearing unit of the screw consists of a pair of angular bearings in the back to back arrangement. Bearing units of the screw, along with the screw itself, were preloaded by means of tightening the bearing nuts with a tension wrench, providing the preload suggested by the manufacturer. Rolling bearing interface between the nut and the screw has been initially pretensioned by gear supplier.

2.2. Control System

The temperature measurement for the purposes of monitoring may be conducted and analysed regardless of the work of the CNC machine tool control system. However, the compensation of thermal deformations on-line requires a continuous data flow between the control system of CNC machine and the module calculating the position corrections. This is caused by the dependence of the position correction from the present position of the table and a temporary distribution of the screw temperature function.

In the constructed set, the resistance temperature signals are subject to acquisition by means of National Instruments measurement converters, and then sent through the ITP/UDP protocol to the PLC of the machine tool.

In the industrial application, the data acquisition module type would be dependent on the measurement modules offered by the vendor of the machine control system. It should be noted that usually the most convenient and reliable solution is the application of modules directly recommended by the control system manufacturers.

The algorithm of the control system including thermal deformation correction implemented in a manner unnoticeable to the machine tool operator can be created on the basis of the structure of virtual axes (Fig. 3).

The architecture of virtual axes has been implemented by B&R for precise synchronisation of multi-axis drives [5]. In this solution, the virtual axis, which is only a software unit, is a master unit for the slave physical units. Transmitting the set position via the Powerlink interface, at intervals of 400ms, to the slave units ensures synchronisation.

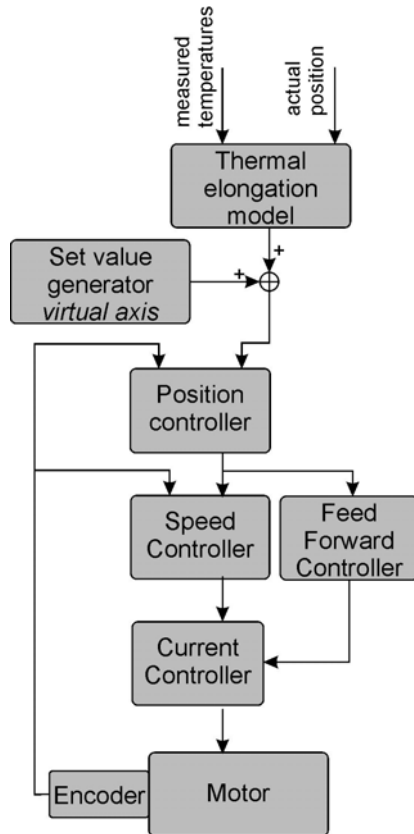


Fig. 3. The diagram of the control system of a single axis

The aforementioned structure has been implemented in the presented solution. B&R ARNCO libraries containing the full structures of the CNC drives, have been used for this purpose. The structure includes i.e. G-code interpreter, trajectory generator, drive regulator and complex geometric error compensation structures. A virtual, 3-axis CNC structure was created. It sends the set positions summed with the thermal deformation corrections to slave physical units operating in the follow-up system. In this way, it was possible to introduce on-line corrections of the drives positions.

2.3. Positioning Accuracy Measurement Set

The measurement of the positioning accuracy was performed with a Renishaw XL80 laser interferometer. First interferometer mirror was mounted on the machine tool table and the second one on the headstock. Additionally, sensors measuring the temperature of the moving table, the temperature of the body on which the table moves, and the temperature of headstock columns were

installed. A picture of the measurement station is presented in Fig. 3.



Fig. 4. AVIA VC760 machine tool equipped with screws with temperature sensors during the measurement of positioning accuracy

3. MODEL OF DEFORMATIONS

3.1. Introducing the Model of Screw Deformations

It is assumed that the ball screw and the bearings can be modelled as a one-dimensional heated bar restrained on both sides by springs (Fig. 5).

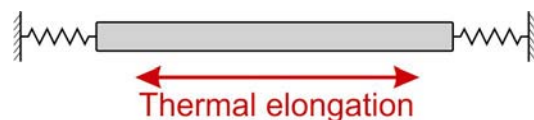


Fig. 5. Model of feed screw deformations

The screw temperature was approximated by a linear spline which adopts the values recorded by the temperature sensors in the nodes. Integrating the screw temperature in the function of its length and multiplying the obtained value by the thermal expansion coefficient provides us with the information on the screw elongation.

It was assumed that the rigidity of both bearings unit is the same and that their rigidity is constant as they deform.

In order to calculate the displacement of a point located on the screw, it was necessary to transform

the CNC control system coordinates to the coordinate system connected directly with the physical location of the nut on the bolt.

3.2. Tuning the Model

In order to tune the analytical model, a series of the measurements lasting about 3 hours were conducted. Initially, the positioning accuracy of the machine being in a state of thermal equilibrium with the environment was measured. Then, a cyclic movement of the table was turned on at a speed of 50mm/s, acceleration of 50mm/s², within the range of 150mm÷300mm, lasting about 1.5h. Friction heat generated in the ball gear caused the screw thermal elongation. Then a series of measurements of positioning accuracy, distributed evenly over a period of 1.5h, was performed. During that time, the system was cooled by the natural heat exchange with the environment.

While the study, it was noted that the change of the temperature of the table, caused by the heat flow from the nut, causes a distortion of the measurement. Installing a sensor for the measurement of the table temperature allowed to introduce a correction based on the known thermal expansion coefficient, the measured geometrical dimensions and the recorded temperature.

4. EXPERIMENTAL VERIFICATION

For the purposes of verification, two measurement cycles lasting 6 and 3 hours respectively were carried out. In the first cycle, initially, the positioning accuracy of the machine being in a state of thermal equilibrium with the environment was measured. Subsequently, a cyclic movement of the table was turned on at a speed of 50mm/s, acceleration of 50mm/s², within the range of -150mm÷300mm, lasting about 1.5h. Then, 5 series of measurements of positioning accuracy were performed, evenly distributed within 1.5h. During this time, the system was cooled by the natural heat exchange with the environment. Next, the cyclic movement of the table was started again, this time within the range of 500mm÷650mm. And then 6 series of positioning accuracy measurements were performed. In total, when the first cycle was carried out, we performed 12 measurement series.

Selected measurements of positioning accuracy and the corresponding screw temperatures are shown in Fig. 6. and Fig. 7.

In the second measurement cycle lasting about 3h, initially, the positioning accuracy of the machine being in a state of thermal equilibrium with the environment was measured. Then, a cyclic movement of the table was turned on at a speed of 50mm/s, acceleration of 50mm/s², within the range of 300mm÷500mm lasting about 1.5h. Subsequently 5 series of measurements of positioning accuracy were performed, evenly distributed within 1.5h.

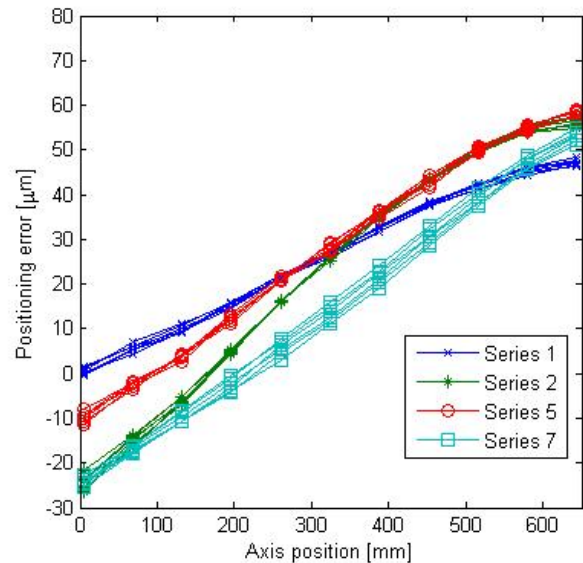


Fig. 6. Positioning error recorded during 1 measurement cycle

Error of the first measurement series (Fig. 6) performed in the conditions of thermal equilibrium with the environment shows that the screw was tensioned. This effect, as a geometric error, can be easily compensated. Due to the numerous literature concerning the subject [13, 14, 15], this issue was omitted in this paper.

Heating of the screw causes an increase in the inclination of the positioning inaccuracy curve, its distortion and vertical shift. This is caused by the non-linear screw temperature distribution and elastic flexibility of the angular bearings maintaining the screw.

Fig. 7. shows the temperatures recorded by the sensors placed in the screw during the performance of positioning accuracy measurements. Series 1 corresponds to the thermal equilibrium with the environment. Series 2 corresponds to the temperature distribution with the maximum value reached after the first heating of the screw. Series 7 corresponds to the distribution with a maximum temperature values, reached after the second heating of the screw. The temperature maxima correspond to the places where the nut slid during the cyclic movement. All data shown in Fig. 6., Fig. 7, Fig. 8. and Fig. 9. correspond to first cycle.

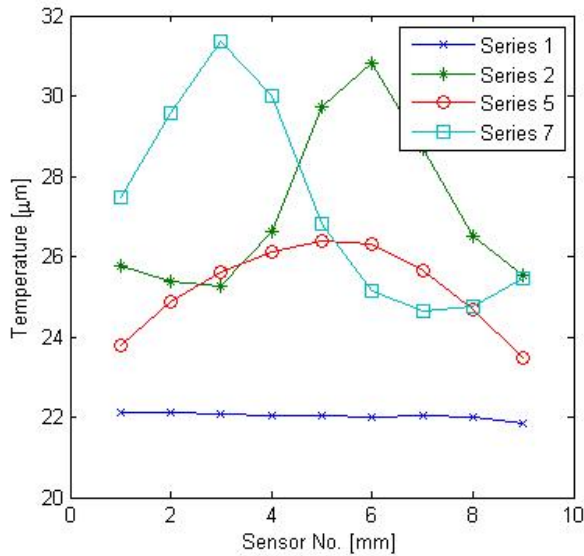


Fig. 7. Screw temperatures recorded during 1 measurement cycle

Calculation of the position correction (Fig. 8.) on the basis of the previously presented model allows for the compensation of the occurring thermal errors.

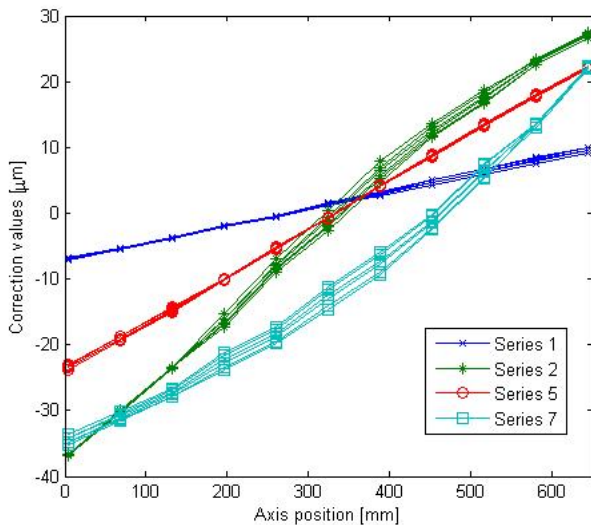


Fig. 8. Temperature corrections calculated for 1 measurement cycle

Application of the correction allows for a reduction of the thermal error from about 50μm to about 10μm (cf. Fig. 6 and Fig. 9). Further improvement of the positioning accuracy may be achieved easily by removing geometric errors.

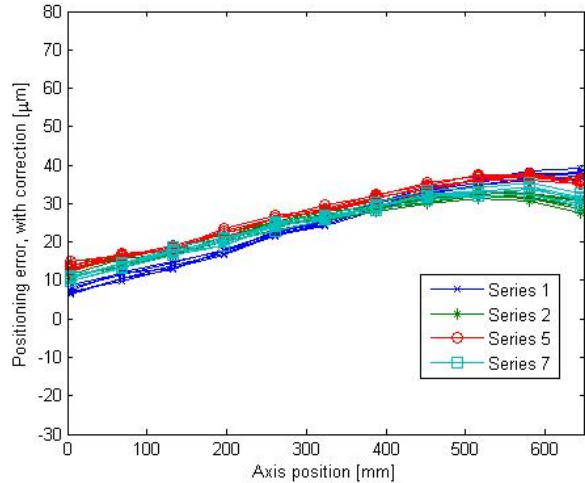


Fig. 9 Positioning error after the introduction of thermal errors during 1 measurement cycle

5. CONCLUSIONS

The application of the virtual axes architecture in the control system allows for freely correcting of the axis movement. It is possible to insert geometric errors correction and thermal error corrections into control system. Owing to the extensive literature in the subject of geometric errors, this issue was omitted in presented paper, focusing on the introduction of a on-line thermal error correction. In the presented example, the error connected with thermal deformation was reduced from about 50μm to about 10μm.

The proposed solution, owing to its accuracy, is close to the accuracy achieved by the solutions based on magnetic or optical scales (positioning accuracy at the level of $\pm 2 \div 5 \mu\text{m}$ [16]).

The target solution is to be 100% competitive and even better in terms of price than the solutions using linear encoders. It is believed that more accurate modelling of the thermal deformation error can be achieved by taking into account the characteristics of non-linear rigidity of the bearings. Due to time-consuming identification of the parameters of such a model, it may be advantageous to utilise neural networks to such a modelling.

The sensors installed in the screw can be used to monitor the work of the bearing nodes, whereas the calculated total elongation of the screw allows for the protection of the bearing nodes against excessive load as a result of strains introduced by thermal deformations.

LITERATURE

- [1] Hoske M. T.: „Zdrowie” maszyn. Control Engineering Polska, Czerwiec 2006, wydanie elektroniczne
- [2] www.astor.com.pl
- [3] www.ec-systems.pl
- [4] www.beckhoff.com
- [5] www.br-automation.com/pl
- [6] Mayr J., Jędrzejewski J., et al.: *Thermal issues in machine tools*. CIRP Annals - Manufacturing Technology 61, 2012, p. 771–791
- [7] Li J. W., et al.: *Thermal-error modeling for complex physical systems: the state-of-arts review*. International Journal of Advanced Manufacturing Technology 42, 2009, p. 168–179
- [8] Xu Z. Z., et al.: *Thermal error forecast and performance evaluation for an air-cooling ball screw system*. International Journal of Machine Tools & Manufacture 51, 2011, p. 605–611
- [9] Lechrich K., Kosmol J.: *Modelowanie odkształceń cieplnych osi posuwów szybkich metodą elementów skończonych*. Modelowanie Inżynierskie 32, 2006, p. 339–344
- [10] Dwojak J., Rzepiela M.: *Diagnostyka i obsługa techniczna łożysk tocznych: poradnik*. wydawnictwo Biuro Gamma, Warszawa, 2003
- [11] www.skf.com
- [12] Pajor M., Zapłata J.: *Compensation of thermal deformations of the feed screw in a CNC machine tool*. Advances in Manufacturing Science and Technology, 2011 Vol. 35, No. 4, 2011, p. 9–17
- [13] Majda P.: *Pomiary i kompensacja błędów geometrycznych obrabiarek CNC*, Inżynieria Maszyn, ISSN 1426-708X, Vol. 16, No. 1–2, Wrocław 2011, p.126–134
- [14] Pietruszewicz K., Pajor M., Urbański Ł.: *Dynamic corrections of the tooling errors possibilities within the mechatronic actuator for motors with permanent magnets*. Archiwum technologii Maszyn i Automatykacji vol. 31 nr 2, 2011, p. 181–190.
- [15] Schwenke H., et al.: *Geometric error measurement and compensation of machines—An update*. CIRP Annals - Manufacturing Technology 57, 2008, p. 660–675
- [16] www.heidenhain.com/



Prof. of the WPUT, **Mirosław PAJOR**, PhD. Eng., Head of the WPUT Institute of Mechanical Technology and Head of the WPUT Mechatronics Centre. Interests: machine dynamics, intelligent control and diagnostic systems of CNC machine tools.



Jacek ZAPŁATA, M.Sc. PhD student of the WPUT Faculty of Mechanical Engineering and Mechatronics. Research assistant at the Department of Mechanics and FMC. Interests: heat deformations of machine tools, IR measurements, robotics.

SIMPLIFIED DYNAMIC MODEL OF ROTATING BEAM

Rafał HEIN, Cezary ORLIKOWSKI

Faculty of Mechanical Engineering,
Department of Mechanics and Mechatronics
Gdansk University of Technology,
Narutowicza Street 11/12, 80-233 Gdansk
fax: (+48) 58 347 21 51, email: rahe@pg.gda.pl

Summary

In the paper a hybrid model of rotating beam is presented. It was obtained by using two methods: modal decomposition and spatial discretization. Reduced modal model was built for the system without the load related to inertia forces that occur during beam rotation. This inertia load was next modeled by using the method of simply spatial discretization and combined with reduced modal model. This approach allows to obtain accurate low-order model of rotating beam.

Keywords: mechanical system, modelling, vibration, modal analysis, model reduction.

UPROSZCZONY MODEL DYNAMICZNY WIRUJĄCEJ BELKI

Streszczenie

W artykule przedstawiono hybrydowy model wirującej belki. Otrzymano go stosując dwie metody: dekompozycji modalnej oraz dyskretyzacji przestrzennej. Zredukowany model modalny zbudowano dla układu bez obciążenia wynikającego z działania sił bezwładności występujących podczas ruchu belki. Oddziaływanie to uwzględniono stosując metodę dyskretyzacji przestrzennej. Takie podejście umożliwia otrzymanie dokładnego modelu niskiego rzędu wirującej belki.

Słowa kluczowe: układy mechaniczne, modelowanie, drgania, analiza modalna, redukcja modeli.

[1] INTRODUCTION

Rotating flexible structure can be considered as a physical model of elastic linkage, manipulator arms, helicopter rotor and others. Such structures are distributed or distributed-lumped parameter systems. An rotating Euler-Bernoulli or Timoshenko beam was studied by many authors [1-5,8,9,16-22].

By application of finite element method (FEM) it is possible to obtain adequate accurate mathematical model. However FEM models are usually high order ones. In some applications for example in automatic control systems design procedures, low order models are preferred.

Designers greatly benefit from the availability of very small models that capture the behaviour of a complex system with almost the same accuracy as a high order model. A simple but adequate model of a system reflects the basic properties and provides good inside into the process.

The purpose of the paper is to build the model of a beam vibrating in horizontal plane. Two methods of modelling has been applied – modal decomposition and spatial discretization. Modal model of Euler-Bernoulli beam can be constructed in very simply way by application of known eigenvalues and eigenfunctions. The distributed inertia forces were

modelled by application of simple lumping technique. Hence, finally obtained model is hybrid one.

General idea of the proposed modelling has been presented in [10]. In the method a reduced modal model is built for a part of considered system excluding elements and phenomena that make difficulties in modal decomposition and analysis. These phenomena are next modelled by application of spatial discretization method. In this way one obtains two submodels which are next combined with one another into the hybrid model. The methodology was successfully applied by authors for many different dynamic systems analysis [10-14].

This paper describe the first attempt of hybrid modelling application for rotating beam.

Fig. 1 presents considered Euler-Bernoulli beam. External moment causes body rotation and small elastic deformation.

For the considered system following equation of motion can be derived [21]

$$(I_H + I_B)\ddot{\phi} + \rho A \int_r^{r+l} xy_u dx = M \quad (1)$$

$$\rho y_{tt} + EI y_{xxxx} = \dot{\varphi}^2 y_{xx} \rho A \int_x^{r+l} \xi d\xi - \ddot{\varphi} \rho A x + \quad (2)$$

$$-\dot{\varphi}^2 (xy_x - y) \rho A$$

where

$$I_B = \rho A \int_r^{r+l} x^2 dx$$

is the moment of inertia of the

undeformed beam and:
 M – external moment, φ – rigid body rotation, r – hub radius, l – length of beam, I_H – hub moment of inertia, EI – flexural rigidity, y – transverse displacement of the beam, ρ – density, A – cross section area.

The boundary conditions are:

$$y(x, t)|_{x=r} = 0, \quad y_x(x, t)|_{x=r} = 0,$$

$$EI y_{xx}(x, t)|_{x=r+l} = 0$$

$$EI y_{xxx}(x, t)|_{x=r+l} = 0$$

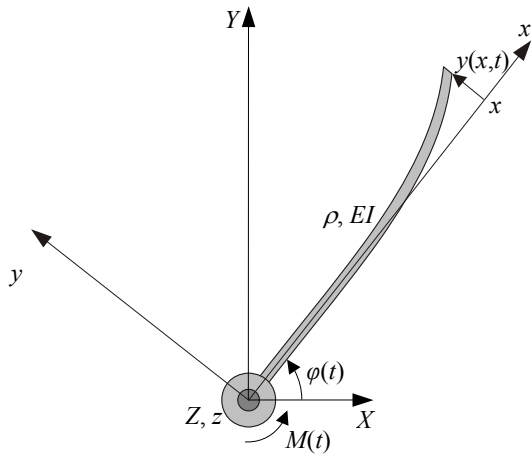


Fig. 1. Euler-Bernoulli beam rotating in horizontal XY plane

In the case of sufficiently small angular speed one can reduce equations (2) to the linear form and finally we have:

$$(I_H + I_B) \ddot{\varphi} + \rho A \int_r^{r+l} xy_{tt} dx = M \quad (3)$$

$$\rho A y_{tt} + EI y_{xxxx} = -\ddot{\varphi} \rho A x \quad (4)$$

Considering beam rotating in vertical plane it is necessary to take into account distributed gravity force which causes a distributed moment dependent on the angular position of rotating beam and transverse distributed load - Fig. 2.

In such case the set of equation describing rotating beam are following

$$(I_H + I_B) \ddot{\varphi} + \rho A \int_r^{r+l} xz_{tt} dx + \rho A g \int_r^{r+l} \cos(\varphi + z_x) x dx = M \quad (5)$$

$$\rho A z_{tt} + EI z_{xxxx} = -\ddot{\varphi} \rho A x - \rho A g \cos(\varphi + z_x), \quad (6)$$

with boundary conditions:

$$z(x, t)|_{x=r} = 0, \quad z_x(x, t)|_{x=r} = 0,$$

$$EI z_{xx}(x, t)|_{x=r+l} = 0$$

$$EI z_{xxx}(x, t)|_{x=r+l} = 0$$

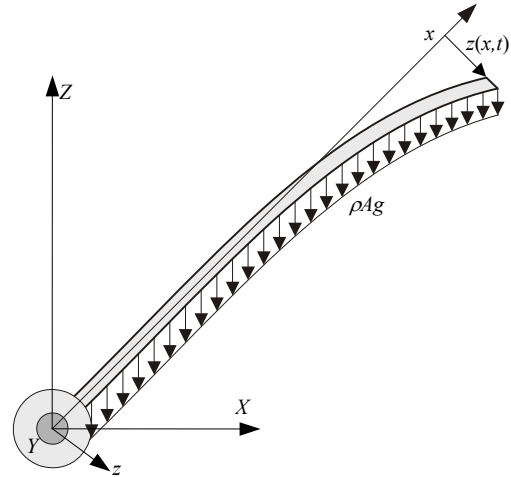


Fig. 2. Beam rotating in vertical ZX plane

Very interesting situation from modelling point of view appears when we assume that a flexible link performs motion in the horizontal and the vertical planes. Let us consider situation when driving rigid hub rotates around vertical axis - Fig. 3.

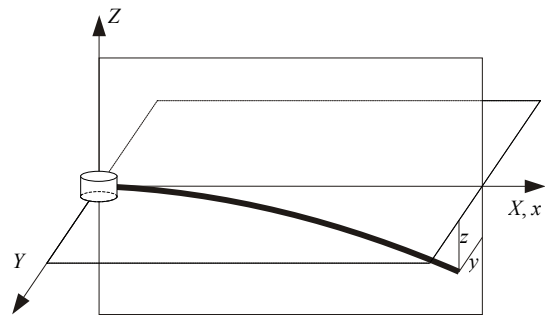


Fig. 3. Beam rotating in horizontal plane YX and transverse displacements in two perpendicular planes YX, ZX

In such case elastic deformations in the horizontal plane are excited by external moment and in the vertical plane are caused by weight of the beam which acts as a distributed force. Such loads cause that combined transverse and torsional vibration appear. Equation describing such system are following [16]:

in the horizontal plane

$$\rho A y_{tt} + EI y_{xxxx} = -\ddot{\varphi} \rho A x \quad (7)$$

and in the vertical plane

$$\rho A z_{tt} + EI z_{xxxx} = -\rho A g \cos z_x. \quad (8)$$

Torsional displacement $\psi(x,t)$ occurs owing the combined horizontal and vertical transverse displacement. Corresponding equation is as follows

$$\rho I_0 \psi_{tt} - G I_0 \psi_{xx} = E I z_{xxx} y_x - E I y_{xxx} z_x \quad (9)$$

with the boundary conditions:

$$\begin{aligned} y(x,t)|_{x=r} = 0, \quad y_x(x,t)|_{x=r} = 0, \quad E I y_{xx}(x,t)|_{x=r+l} = 0, \\ E I y_{xxx}(x,t)|_{x=r+l} = 0, \quad z(x,t)|_{x=r} = 0, \quad z_x(x,t)|_{x=r} = 0, \\ E I z_{xx}(x,t)|_{x=r+l} = 0, \quad E I z_{xxx}(x,t)|_{x=r+l} = 0, \\ \psi(x,t)|_{x=r} = 0, \quad \psi_x(x,t)|_{x=r} = 0. \end{aligned}$$

In this paper the simplest case of motion of the flexible link described by linear equation (3,4) is considered.

2. MODELLING

2.1. FEM model

Applying finite difference method [15] one can obtain following lumped parameters model of the system presented in Fig. 2. Instead of equation (4) we can obtain

$$M \ddot{y} + K y = f \quad (10)$$

where y, f are vectors of displacement and load respectively.

Assuming n finite elements we have

$$y = [y_1 \quad \dots \quad y_n]^T,$$

and

$$f = [f_1 \quad \dots \quad f_n]^T,$$

After discretization, equation (4) can be presented in the form

$$\ddot{\phi} = \frac{1}{I_H + I_B} \cdot \left(M - \sum_{i=1}^n \rho A y_{ii}(x_i) x_i \Delta x_i \right) \quad (11)$$

and

$$f_i = \rho A x_i \Delta x_i \ddot{\phi}, \quad (12)$$

where:

Δx_i – length of the i -th finite element,
 x_i – coordinate of i -th finite element,
 $i=1, \dots, n$.

Graphical form of the model (10-12) is presented in Fig. 4.

It was obtained on basis of equation (10) after its Laplace transformation with zero initial conditions, where s is the argument of Laplace transformation and I - identity matrix.

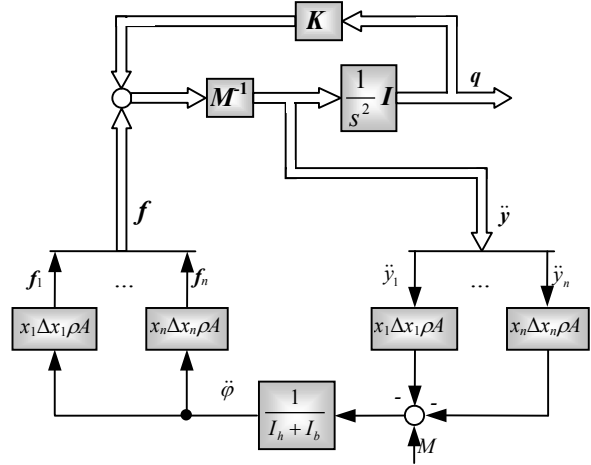


Fig. 4. Graphical representation of FEM model of considered system

2.2. Modal reduced model of beam

The model described by equation (10) can be written in modal representation as:

$$M_m \ddot{q}_m + K_m q_m = f_m, \quad (13)$$

where:

$$M_m = \Phi^T M \Phi = \text{diag}(m_1, \dots, m_r, \dots, m_n),$$

$$K_m = \Phi^T K \Phi = \text{diag}(k_1, \dots, k_r, \dots, k_n),$$

$$q_m = \text{col}(q_{m1} \quad \dots \quad q_{mr} \quad \dots \quad q_{mn}), \quad f_m = \Phi^T f,$$

$$\Phi = \text{col}(\varphi_1, \dots, \varphi_r, \dots, \varphi_n), \quad \varphi_i = \text{col}(Y_{i1}, \dots, Y_{ir}, \dots, Y_{in})$$

in which:

m_i – modal coefficients of inertia, k_i – modal coefficients of stiffness φ_i – eigenvectors of matrix $M^{-1}K$, Y_{ij} – eigenvector components.

By solving (13) we can next obtain the solution of (10) in the following form:

$$y = \Phi q_m, \quad \dot{y} = \Phi \dot{q}_m, \quad \ddot{y} = \Phi \ddot{q}_m \quad (14)$$

Modal model (13) can be reduced by removing those rows and columns in M_m, K_m which are insignificant to the system's dynamic. Thus, after such approach we obtain:

$$M_{mr} \ddot{q}_{mr} + K_{mr} q_{mr} = f_{mr}, \quad (15)$$

where:

$$\left. \begin{aligned} M_{mr} &= \text{diag}(m_1, \dots, m_r), \quad K_{mr} = \text{diag}(k_1, \dots, k_r), \\ q_{mr} &= \text{col}(q_{m1}, \dots, q_{mr}), \quad f_{mr} = \Phi_r^T f, \\ \Phi_r &= \text{col}(\varphi_1, \dots, \varphi_r). \end{aligned} \right\} (16)$$

An approximate solution of (1) by the application of reduced order model (7) can be obtained from the formulas:

$$y = \Phi_r q_{mr}, \quad \dot{y} = \Phi_r \dot{q}_{mr}, \quad \ddot{y} = \Phi_r \ddot{q}_{mr}. \quad (17)$$

Obtained reduced model of beam can be directly coupled with the discrete model of distributed load (11, 12). Graphical form of the final hybrid reduced model is presented in Fig. 5.

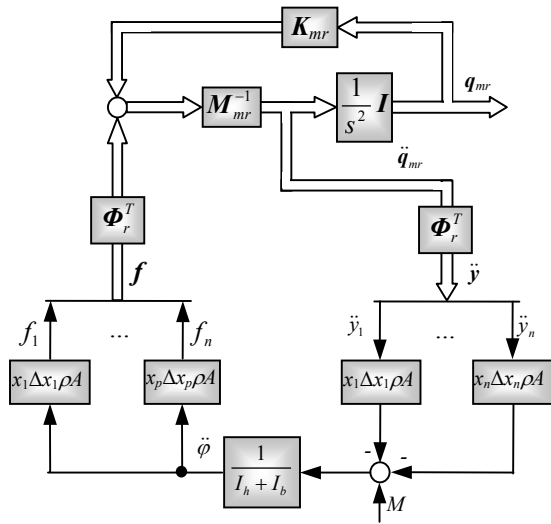


Fig. 5. Graphical representation of hybrid model described by (12,13,16)

Grace to diagonalization it is possible to present the modal model in the detailed form – Fig. 6. It must be mentioned that two submodels reduced modal model of beam and model of inertia load are coupled in n power ports. The pair of signals (f_i, y_i) are related to the i -th port. The order of the whole model depends on the number of retained modes in the modal model but it does not depend on the number of ports. It means that inertia loading can be modelled by using any number of finite elements.

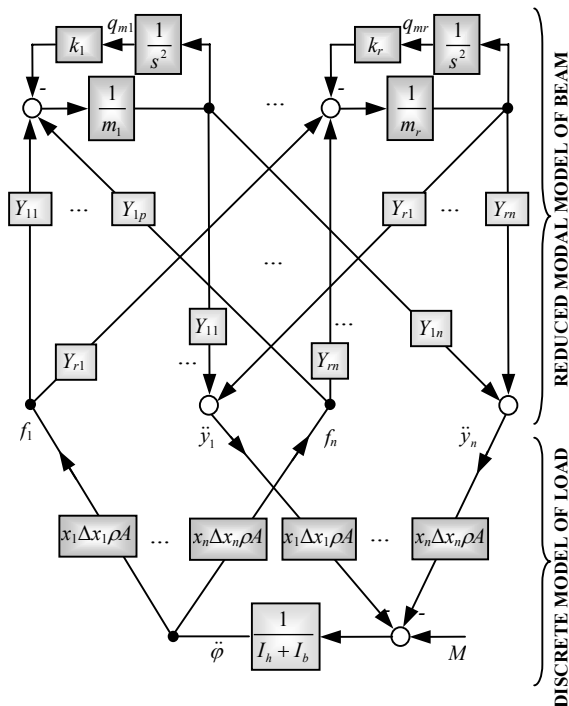


Fig. 6. Hybrid reduced model

3. Simulation and results

Simulations were performed using the Matlab-Simulink package applying the following physical data: Young modulus of elasticity $E=69 \cdot 10^9$ [Pa], mass density $\rho=2700$ [kg/m³], length of beam $l=0.62$ [m], hube radius $r=0.03$ [m], cross section dimensions: $h=0.002$ (height), $b=0.015$ (width).

Fig. 4 and Fig. 5 (or 6) present complete mathematical models in the form accepted by mentioned software tool. Model from Fig. 4 was considered as reference (full) model of the given system. Fig. 7 presents frequency response related to not rotating beam (without inertia load) – dotted line, and modal reduced model of the beam – continuous line. Reduced model has 3 retained modes.

Frequency characteristics obtained for the reference model and hybrid reduced model (both of them related to the rotating beam) are presented in Fig. 8. The frequency characteristics of the full (reference) model of the investigated system is presented by dotted line. It is compared to the characteristic related to the proposed hybrid model – continuous line. Obtained results prove that proposed method enables to obtain accurate low order model in the frequency range related to the number of retained modes.

Presented frequency characteristics (Fig. 7-8) were obtained for the moment M as the input signal and the beam displacement at its free end.

Fig. 9b presents time response of the system. The output signal $u=\phi l + y(l+r)$ (Fig. 9c) was obtained for the input signal M in the form presented in Fig. 9a.

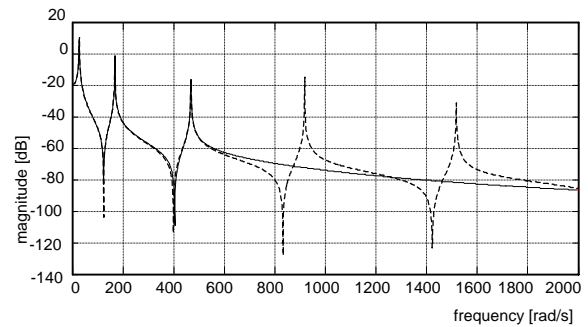


Fig. 7. Comparison of frequency characteristics of full (reference) model and modal reduced model

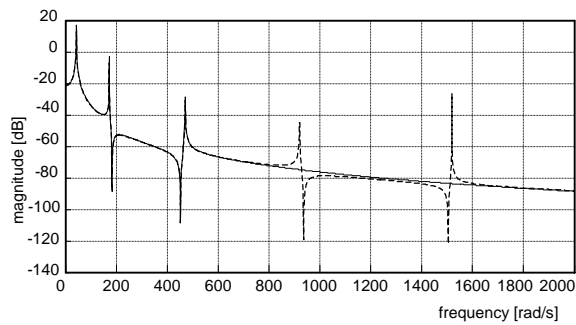


Fig. 8. Frequency response of the whole system

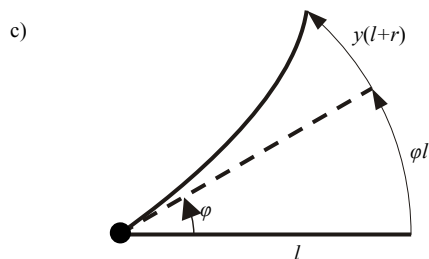
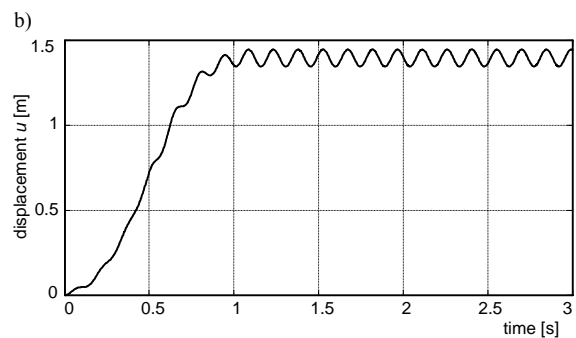
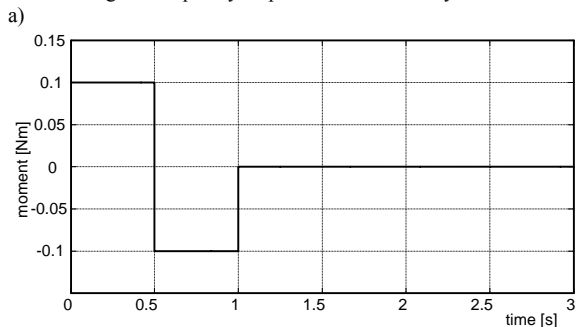


Fig. 9. Time response of the hybrid, reduced model

4. Conclusion

A hybrid modelling procedure for analysis the dynamics features of rotating beam is proposed in the paper. Two modelling techniques are used: modal decomposition and spatial discretization. The final reduced (low order) model is obtained in the following way. First, the finite element method (spatial discretization) is applied to obtain lumped parameter model of the whole investigated system. Next, modal decomposition and reduction is applied for model of beam without inertia load which results from beam rotation. Finally reduced modal model of beam is combined with the model of inertia load. Some simulation results presented in the paper

provide that presented method of modelling is efficient and enables obtain low order model with assumed accuracy.

The presented method of modelling is the first step of application the proposed method to modelling rotating beam.

Further works will be related to the beam rotating in a vertical plane and next to the beam moving in both horizontal and vertical planes.

The last case is very interesting because a torsional vibrations appear as the effect of coupling bending vibrations in two perpendicular planes.

Proposed methodology of hybrid modelling enables to include effects of linear or nonlinear coupling between submodels.

REFERENCES

- [2] Al-Said, S., Naji, M., and Al-Shukry, A.: *Flexural Vibration of Rotating Cracked Timoshenko Beam*, J. Vib. Control, Vol. 12, pp. 1271–1287, 2006
- [3] Ansari M., Esmailzadeh, Jalili N.: *Exact frequency analysis of a rotating cantilever beam with tip mass subjected to torsional-bending vibrations*, Journal of Vibration and Acoustics, Vol. 133, 2011
- [4] Barbosa E.G., Gões L.C.S.: *Modeling and identification of flexible structure using bond graphs applied on flexcam quanser system*, ABCM Symposium Series in Mechatronics, Vol. 3, pp. 129-138, 2008
- [5] Bercin, A.N., Tanaka, M.: *Coupled Flexural-Torsional Vibrations of Timoshenko Beams*, J. Sound Vib., Vol. 207, pp. 47–59, 1997
- [6] Furta, S. D.: *Linear Vibrations of a Rotating Elastic Beam With an Attached Point Mass*, J. Eng. Math., Vol. 46, pp. 165–188, 2003
- [7] Gawroński W., Kruszewski J., Ostachowicz W., Tarnowski J., Wittbrodt E.: *The finite element method in the dynamics of structures* [in Polish], Arkady, Warsaw 1984
- [8] Kruszewski J., Gawroński W., Wittbrodt E., Najbar F., Grabowski S.: *The rigid finite element method* [in Polish], Arkady, Warsaw 1975
- [9] Lin S. M.: *Dynamic Analysis of Rotating Nonuniform Timoshenko Beams with an Elastically Restrained Root*, Journal of Applied Mechanics, Vol. 66, pp. 742-749, 1999
- [10] Lin, S., Mao, I., and Lin, J., 2007, *Vibration of a Rotating Smart Beam*, AIAA J., 45, pp. 382–389
- [11] Orlikowski C.: *Modelling, analysis and synthesis of dynamic systems by application of bond graphs*. Gdańsk University of Technology Press, Gdańsk, 2005 [in Polish]
- [12] Orlikowski C., Hein R.: *Modal reduction and analysis of gyroscopic systems*. Solid State Phenomena 164 (2010) 189-194.
- [13] Orlikowski C., Hein R.: *Reduced model of gyroscopic system, Selected Problems of Modal Analysis of Mechanical Systems*, Editor T. Uhl,

- Radom: Publishing House of the Institute for Sustainable Technologies National Research Institute, 2009, AGH, Kraków 2007,
- [14] Orlikowski C., Hein R.: *Modelling and analysis of rotor with magnetic bearing system, Developments in mechanical engineering*, Editor J. T. Cieśliński, GUTP, Gdansk 2008,
- [15] Orlikowski C., Hein R.: *Hybrid, approximate models of distributed-parameter systems*. The 12th Mechatronics Forum Biennial International Conference. Part 2/2, Zurich, June 28-30, 2010 / H. Wild, K. Wegner. - Swiss Federal Institute of Technology, p. 163-170, 2010
- [16] Rao S. S.: *The finite element method in engineering*, IV ed., Elsevier, 2005
- [17] Sutton R.P., Halikias G.D., Plummer A.R., Wilson D.A.: *Modelling and H^∞ control of a single-link flexible manipulator*, Proc Instn Mech Engrs, Vol. 213, Part I, pp. 85-104, 1999
- [18] Turhan Ö., Bulut G.: *On Nonlinear Vibrations of a Rotating Beam*, J. Sound Vib., Vol. 322, pp. 314–335, 2009
- [19] Yardimoglu B.: *Vibration Analysis of Rotating Tapered Timoshenko Beams by a New Finite Element Model*, Shock Vib., Vol. 13, pp. 117–126, 2006
- [20] Yigit A., Scott R.A., Ulsoy A.G.: *Flexural motion of a radially rotating beam attached to a rigid body*, Journal of Sound and Vibration, Vol. 121, No. 2, pp. 201-210
- [21] Yuksel S., and Aksoy T. M.: *Flexural Vibrations of a Rotating Beam Subjected to Different Base Excitations*, Gazi University Journal of Science, Vol. 22, pp. 33–40, 2009
- [22] Zhu W.D., Mote C.D.: *Dynamic modeling and optimal control of rotating Euler-Bernoulli beams*, Journal of Dynamic Systems, Measurement and Control, Vol. 119, pp. 802-808, 1997
- [23] Zhu W.D.: *Dynamical analysis and optimal control of a flexible robot arms*, M.Sc. Thesis, Arizona State University, Tempe, AZ, 1988

The research is supported from the science budget resources in 2011-2014 as the research project (N N501 120240)



Rafal HEIN, D.Sc. Eng. is an assistant professor at the Faculty of Mechanical Engineering, Gdańsk University of Technology. His research interests focus on the modelling of dynamic mechanical and mechatronic systems



Cezary ORLIKOWSKI, D.Sc. Ph.D. Eng. is an assistant professor at the Faculty of Ocean Engineering and Ship Technology, Gdańsk University of Technology. In addition, he is also working as professor and he is a Deputy Rector in The State School of Higher Professional Education in Elbląg. His current research interest include mechatronics and dynamic systems modelling.

CHOSEN ASPECTS OF MICRO MILLING MACHINE DIAGNOSTICS

Bogdan BROEL-PLATER, Paweł DWORAK, Krzysztof JAROSZEWSKI

Katedra Automatyki Przemysłowej i Robotyki Wydział Elektryczny ZUT w Szczecinie
ul. 26-go Kwietnia 10, 71-126 Szczecin, fax. +48914495341, bbp@zut.edu.pl

Summary

The paper deals with the one of the designed diagnostic issue for micro milling machine. The short description of designed and set in motion micro machine for milling is presented. Geometrical construction is deliberated as well as a drive and measurement systems are depicted. Moreover capabilities of the machine are compared to conventional ones and advantages of presented machine are listed. The machine supervisory control system, which base on artificial intelligence diagnostic system is described. Conducted in design process deliberations about types and structures of the net and form and source of the signals are presented. The last part of the paper includes conclusions and final remarks.

Keywords: micro cutting machine, diagnostics, artificial intelligence.

WYBRANE ASPEKTY DIAGNOSTYKI MIKROFREZARKI

Streszczenie

W artykule przedstawia się jedno z zagadnień diagnostycznych związanych z mikrofrezarką. Zaprezentowany został także krótki opis zaprojektowanej i uruchomionej maszyny do mikro frezowania. Rozważona została konstrukcja geometryczna maszyny oraz przedstawione zostały systemy pomiarowe i napędowe. Ponadto porównuje się właściwości tej maszyny z rozwiązaniami konwencjonalnymi i wymienia się jej wady i zalety. Opisano bazujący na sztucznej inteligencji system diagnostyczny oraz system nadzoru maszyny. Prezentuje się rozważania przeprowadzone w procesie projektowania sieci dotyczące typu i struktury sieci oraz formy i źródła sygnałów. Ostatnia część artykułu zawiera wnioski.

Słowa kluczowe: maszyna do mikro obróbki, diagnostyka, sztuczna inteligencja.

1. INTRODUCTION

The production of the precise miniature component is stimulated by increasing requests from e.g. aircraft industry, electronic industry or biomedicines [1], [10], [11]. Moreover global tendency to devices miniaturization and very fast development of mechatronics cause increase importance of the micro machining processes; in particular large interest of the Micro Electro - Mechanical Systems (MEMS) that contain precise mechanic components with high shape ratio, sizes of a few micrometers to a few millimeters and very often characterize by lack of the axial symmetry [11]. Moreover mechanic components of such systems have to be made of the difficulty machined materials such as high alloy steel, ceramic or titanium compounds. Obtaining required precision of manufacturing such elements is impossible using classical technology as: molding, pressing, hammering, electro or chemical erosion and even laser tooling, but only using micro cutting [11]. That is why, among many technique of micro components production there is observed the growing interest of micro cutting, which arises with large potential of

that method in the zone of the realization of the geometrically complex elements. Especially high rate of adoption such machines takes place in case of tooling "micro shapes" in the area of micro element.

The micro cutting technique, in case of unitary production, allows for projection of the 3D free face with relatively little costs effort. It all causes a large applicability of micro cutting, for instance in case of micro mold manufacturing [2]. Another advantage of such tooling technique is relatively high efficiency, low harmfulness for environment, relatively low cost of devices and their exploitation.

Nowadays the operations of micro cutting are leaded on high precision machines characterized by the high efficient of stiffness with systems for temperature control [3], [4], [5]. Mainly from cost reduction point of view the strong tendency is actually observed due to build tooling machines characterized by small dimensions and possibility to move it easily [6], [7], [8], [9]. Unfortunately such construction are incomparable worst in contrast with conventional precision tooling machine from stiffness, precision and vibration moving by basis damping point of view. For that reason the development of new construction of micro machines

for tooling is very important and actual topic. The researches on the micro cutting subject, both in Poland and all over the world, are still pioneering kind [12]. However, there are brands offering specified commercial solutions of micro cutting machines, which are quite expensive and have rather only individual character.

The rest of the paper is organized as follows. In section 2 a micro milling machine is presented. The machine diagnostic system is described in section 3. Supervisory system and its hardware solution are presented in section 4. Brief conclusions are drawn in section 5.

2. MACHINE DESCRIPTION

Described prototype of machine for micro tooling was built as an effect of realization of the grant partly supported by the Grant No N R03 0050 06/2009 "Construction of a prototype system for testing micromachining – researches and modeling of process" financed by the Polish Ministry of Science and Higher Education. The basis of the machine composes of specially produced stabile granite corps (Absolute Black Granite) on which the electro-spindle with controlled rotary velocity (100.000 RPM) and precise system of liner motion are mounted. What is more, the machine is equipped with condition system stabilizing temperature of the machine. That micro milling machine has three numerically controlled axes and is equipped in adequate measurement apparatus, among others: precocious multi axes dynamometer for measuring cutting forces, digital viewing microscope Keyence, model VHX-600ESO with high zoom and acoustic measurement system. The workspace such designed machine is limited to cuboid with size of 100x100x50 mm and the errors of positioning in near the value of 0.5 μm . The rest operation parameters are similar to other construction existing on the market, nevertheless expected price is many times lower, due to using ready-made modules with made by own control system and with individual construction of the corps. One of the most important properties of the constructed machine is monitoring system with diagnostic algorithms based on artificial intelligence. Generally in nowadays construction of such machines monitoring systems are quite rarely integrated in machine control system.

Design works on the machine were started from selection of kinematic structure, which has essential influence on technological precision possible to obtain by the machine; it is mean precision of relative tool and tooling object motion. For that reason two selected geometrical structures were taken into consideration.

Conducted simulation gave the possibility to compare the structure with vertical and horizontal spindle due to precision of projection the tool to tooling object. As a criterion for that comparison the lowest value and dispersion of volume error were

chosen. Finally all conducted analysis lead to choosing the horizontal structure as better one especially in the view of precision of the projection of the tool and tooling object relative position. In the machine the spindle is horizontally moving along the Z axis and the tooling object could be moving on the surface Y-X. A computer comparative analysis of the machine construction with other ones known from literature shows that the chosen construction would meet with the highest ratio all requirements regarded: stiffness, dynamic and precision of tool position projection due to tooling object.

The constructions on each line moving axis were used commercial high precision drives of Aerotech brand from USA: "Y" axis working horizontally based on model ANT95-50-LV, "Z" axis based on model ANT95-50-L; "X" axis based on model ANT130-110-L. The drives working under control of the controller Epaq model EPAQ-S-FPB-XX-/1-MP10MI-MP10M-MP10M-MP10.

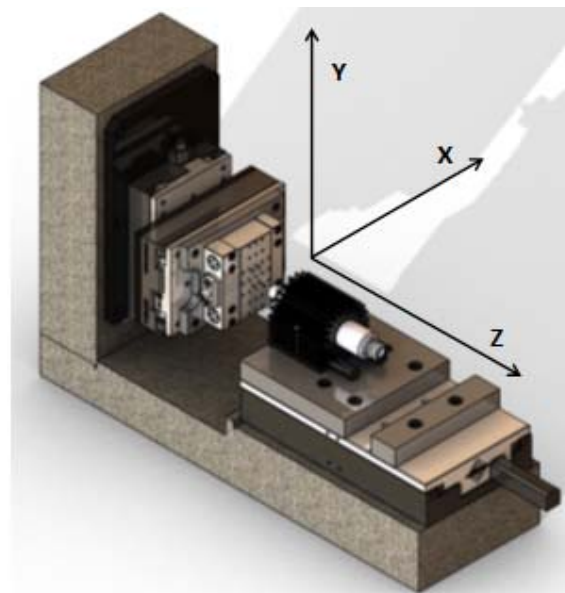


Fig. 1. Project of the milling micro machine with pointed out axes

The main driven system consist of commercial electro spindle type 4015 DC, which was made by SycoTec brand from Germany, controlled by controller and supplier e@syDrive 4425. Moreover, that system requires supplying of compressed (0.5-0.8 bar) air of adequate clarity due to protect ceramic bearing from pollutants. Additionally servo drive of vertical axes is using pneumatic cylinder actuator for supporting the operations of electrical linear motor. For that reason there were designed pneumatic installation for the machine. The main component of that installation is rotary vane compressor for continuous work, model Gast 74R130-P114H201X, moreover there are air filters, valves and pressure reducers.

One of the most important parameter of correct leading process of micro milling is supporting constant temperature of machine and tooling object.

Due to these requirements the machine is installed in closed cover, inside which the temperature and humidity are stabilized by maintained-free air conditioner made by Schroff brand. The machine is presented in the figure number 2.

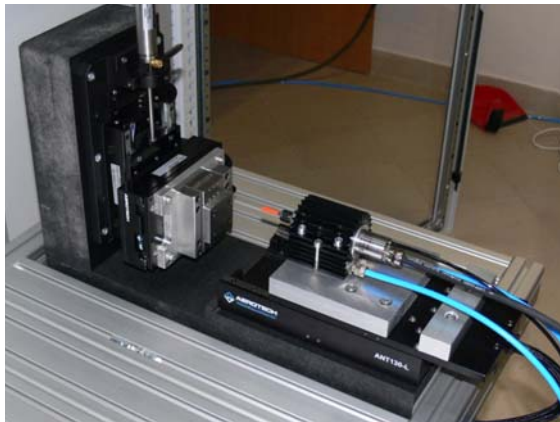


Fig. 2. The machine for micro milling

Summing up description of the micro machine for milling operation list of main features is depicted:

- small dimensions,
- very high precisions of tooling,
- very high stiffness and thermal stability,
- high rotary velocity of the tool – high coercion frequency during milling process.

For that machine the control and supervision system were designed and implemented. The scheme of the system is shown in the figure number 3.

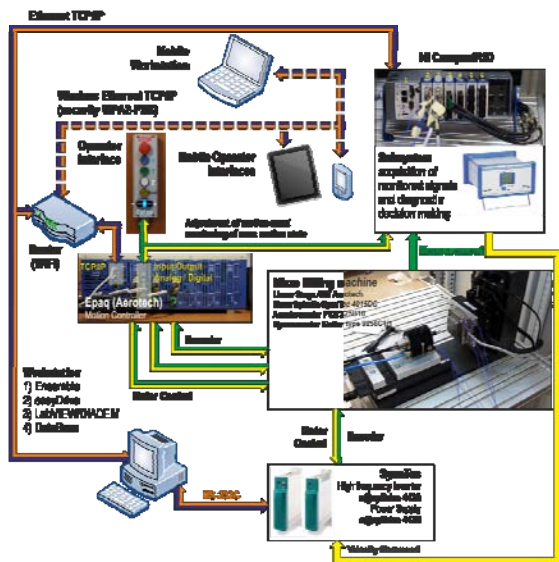


Fig. 3. Structure of the machine control and supervising system

The knowledge about course and character of the micro milling process, get on the way of experiment, were used to make conception of the intelligent diagnostic system. Seeing that micro milling process in comparison with classical tooling in macro scale is relatively poorly known, and what is more is characterized by many specific features only using

recorded experimental data and its analysis could be the source of the diagnostic system concept.

3. DIAGNOSTIC SYSTEM FOR MICRO MACHINE FOR MILLING

One of the micro tools features is that they could be very easily destroyed, due to its small dimensions, e.g. 0.1 mm. Especially during installation in the spindle the tool could be damaged. For that reason it is very important to validate the state of micro tool (due to after mounting it in the grip of electro spindle, and of course before starting the tooling process.

The zoomed in edges of new (undamaged) and damage tools are presented in the figures number 4 and 5, respectively.

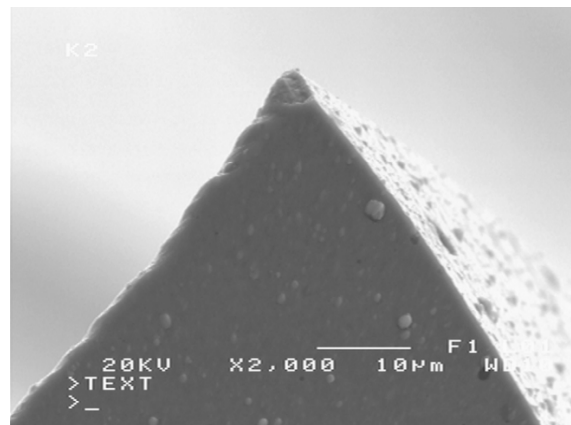


Fig. 4. Zoomed in edge of the new tool Kyocera 2FESM005-10-04

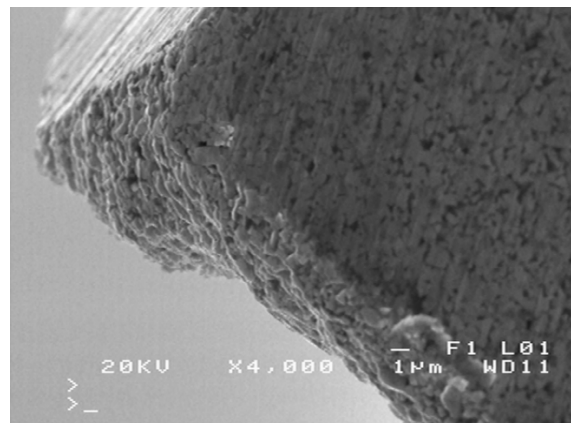


Fig. 5. Zoomed in edge of damage tool.

Designed, for leading such diagnostic procedure, system is based on analysis of measured, using miniature accelerometers (model 325B10 made by PCB brand) attached to the servo drive corps, spindle vibrations signals. It is assumed that the measurements are made when the proper spindle velocity is achieved. In the figure number 6 the example of time domain signals in the axis “Y”, recorded at the speed of 24,000 RPM, for the three diagnosed states are presented.

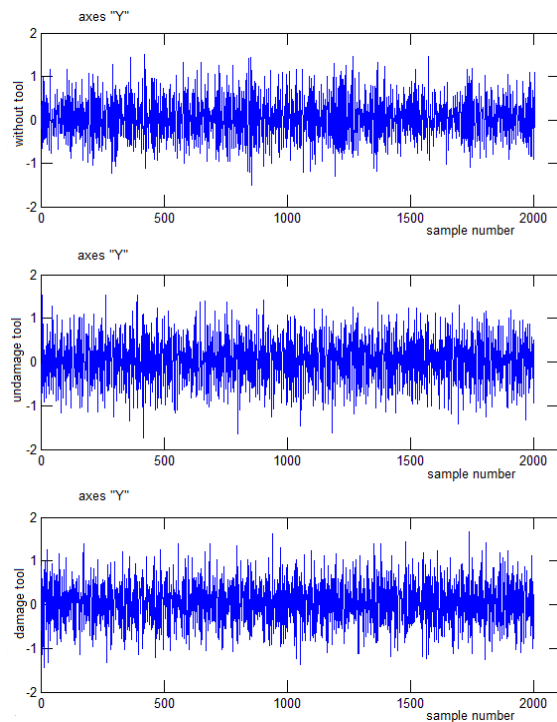


Fig. 6. Time domain signal in the axes "Y"

The proper velocity related to the sampling parameters, the spread of the FFT window and expected value of first harmonic of the vibration signal. Assuming that in the spindle is mounted the tool with 2 edges and the measurements are conducted with sample rate of 51,200 SPS resulted in obtaining the spindle velocities values: 96,000 RPM, 48,000 RPM, 24,000 RPM and 12 000 RPM as a guaranties correct form of the diagnostic signals. For that signals parameters the integer number of samples per period for first harmonic and integer number of periods of first harmonic in the window set up for FFT are obtained. The value 4096 samples for FFT analysis were chosen due to guarantee on the one hand high speed of working diagnostic algorithm and on the other hand as that one which allows to obtain enough thin bands (high enough resolution) in spectral characteristic. The figure number 4 presents examples of the spectrum charts with different FFT window spread. Moreover into investigation was taken the issue of using window before FFT. Windows such as Tukey or Taylor among others are using in case of eliminations negative influence of FFT algorithm assumptions. All kinds of window available in Matlab environment were checked and it was found that it is enough to us the rectangle kind of window. The spectral characteristics for different type of window are presented in the figure number 7.

The diagnostic system is using the information obtained from the results of the leaded in advance spectral analysis (FFT). Similar approach to the diagnostic issue is presented for instance in [1]. Such procedure of analyzing the spectral signals could be

leaded not only before starting tooling, but also each time when the micro tool do not have a contact with the tooling object due to the program path.

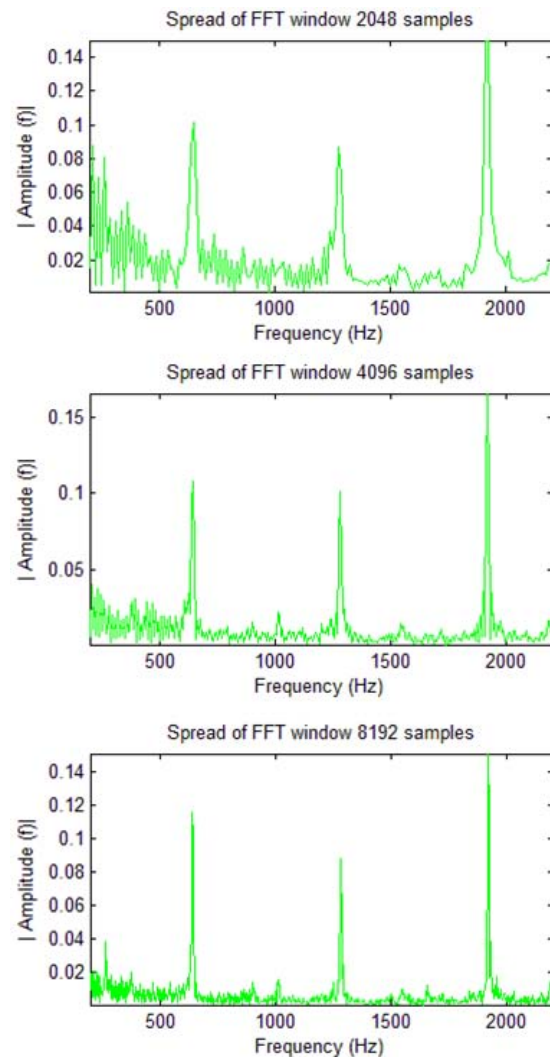


Fig. 7. Spectral characteristic for different spreads of the FFT window

Such test and analysis could give us a chance to state if in the grip there is no tool or in the grip is the tool which is undamaged or damaged. The spectral charts for those cases are presented in figure 8. To achieve efficiently working diagnostic system recognizing mentioned above three potential states it is necessary to collect data reflecting different tools occurring on the market. Due to find the best source of diagnostic information not only spectra recorded signals were taken into consideration but also signals forming by using the mathematic operation on the elementary, recorded signals. To find the best form of symptoms following signals were investigated:

- signal recorded in the "X" axis,
- signal recorded in the "Y" axis,
- signal formed as a result of summing signals recorded in axes "X" and "Y",
- signal counted as a amplitude of resultant vector formed from signals recorded in the axes "X" and "Y", i.e. $\sqrt{(X^2+Y^2)}$,

- signal counted as a amplitude of resultant vector formed from signals recorded in the axes X, Y and Z, i.e. $\sqrt{X^2+Y^2+Z^2}$.

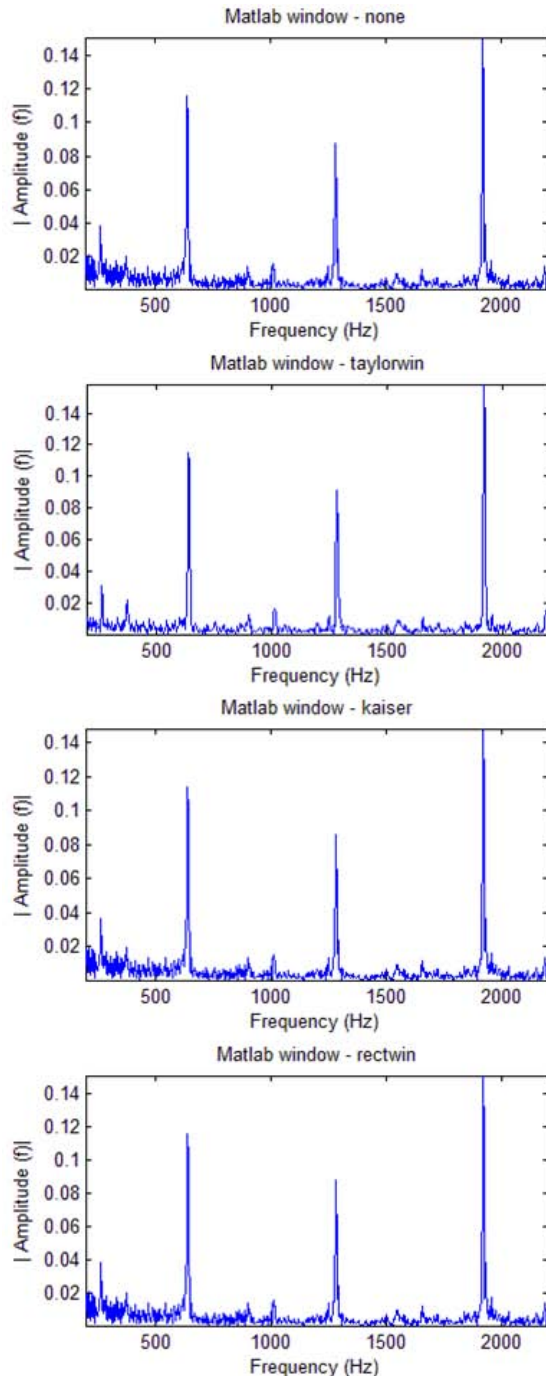


Fig. 8. The spectral characteristics for different type of window

For mentioned above signals spectral characteristic were counted and chosen parameters of that characteristic were used to assemble learning patterns for the process of learning artificial neural networks. What is more analyze of the shape of many plotted spectral characteristic leads us to the view that more efficient neural system could be designed using proportions of the characteristic parameters (integral of specific areas around main

harmonics on the spectral characteristic) then just directly parameters. The investigated relations:

- quotients of area value around first, second, third harmonic and the sum of whole chart area ($1h/\text{sum}$, $2h/\text{sum}$, $3h/\text{sum}$),
- quotients of area around second harmonic and area around first harmonic with quotient of area around third harmonic and area around first harmonic ($2h/1h$, $3h/1h$),
- quotients of sum area around first and third harmonic and area around second harmonic with sum area around second and third harmonic and area around first harmonic ($(1h+3h)/2h$, $(2h+3h)/1h$). For the speed 24.000 RPM the first, second and third harmonic are 400 Hz, 800 Hz and 1200 Hz, respectively.

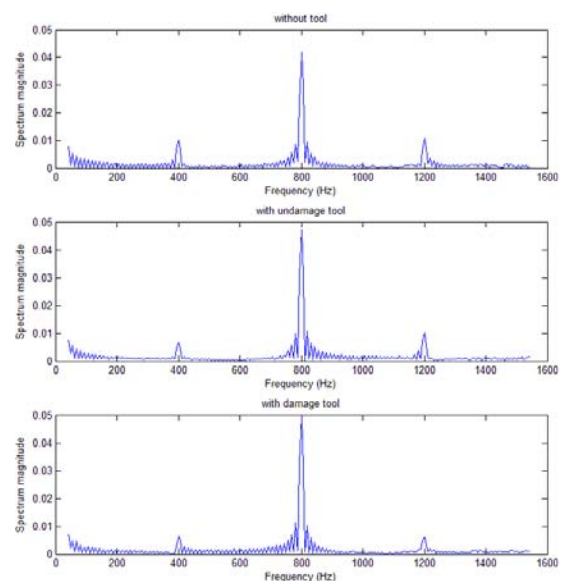


Fig. 9. The spectral characteristics for different machine states

Moreover analysis of the charts shows that the plots are not constant from window to window. For that reason for diagnostic system also average values and deviations counted for spectral characteristic were taken into account.

Having all above described assumptions about form of potentially useful signals the structures and types of neural networks were chosen. Only forward kinds of nets were investigated. Table number 1 presents the list of researched neural networks.

Looking for the net capable to correct recognition of the machine state above listed types and structures of the nets were researched in addition with combination of also previously described form of input signals.

Finally as the best kinds of nets were calculated nets:

- with signal on the input:
- rotary velocity 24,000 RPM,
- with operation 2h/1h, 3h/1h (2 dimensional input vector),
- measurement of the acceleration in the „X” axis,
- feed-forward type,

- only 1 hidden layer with 3 neurons,
- with outputs coded as -10 / 10.

Table 1. The list of examined structures of the nets

no.	input	Number of neurons in the layer				output
		1 st	2 nd	3 rd	4 th	
1	2, 3, 4, 6	3				3 in case of the network recognized each of the three states
2		6				
3	due to the set of the signal treated as a symptoms	9				
4		12				
5		15				
6		18				
7		6	3			
8		9	3			
9		9	6			
10		12	6			
11		12	9			1 in case of the network recognized only state one from three
12		15	9			
13	9	6	3			
14	12	6	3			
15	12	9	3			
16	12	9	6			
17	15	9	6			
18	15	12	3			
19	15	12	6			
20	12	9	6	3		

Conducted test using wider (then during learning) sets of signals gave the results:

- the net recognized state “without tool” works with error equal to 0,
- the net recognized state “undamaged tool” works with error equal to 7,8%,
- the net recognized state “damaged tool” works with error equal to 8,0%,
- the net recognized all states works with error equal to 5,2%.

As a final solution, advisory diagnostic system is proposed in which operator would be obtaining information from all four nets. The operator in case of detecting dysfunction of the system is supported by concluding system based on fuzzy logic techniques. Such a diagnostic algorithm were implemented and tested during common operations, what is described in the next paragraph more detailed. The main implementation environment for that control and supervisory system is LabView by National Instruments.

Many more diagnostic issues were also investigated. Among others one of the important issues is to detect the point when the ending touching the object and the micro milling starts. Another one is to determine before starting the tooling if the program were written accurately and the machine and the tool do not have path with collisions. Moreover observation of actual spindle velocity in contrast with set up is next important symptom of the machine state let us to validate the efficiency of the spindle system. Algorithms for diagnosing mentioned machine states are still under investigation and implementation.

4. SUPERVISION SYSTEM FOR THE MACHINE

The main tasks of supervision system are acquisition, monitoring, analyzing and recording data during operation and communication with control system. The hardware structure was divided into three main parts, which is showed in the figure 10.

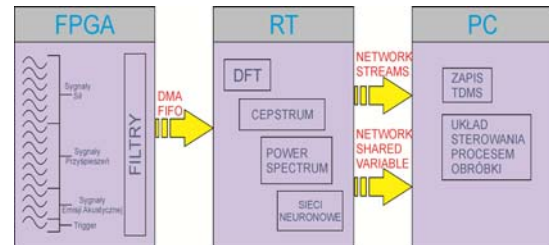


Fig. 10. Hardware structure

The FPGA module in controller PAC cRIO 9022, first section, is responsible for acquisition and filtering of the signals measured on the machine. That solution gives us a chance to measure very fast changing signals as force and acceleration with sampling rate 51,200 SPS and filtering them in real time. The second section based on working in real time regime another cRIO 9022 instance. The DMA channels are used to transfer huge amounts of data in short time without charging controller’s CPU. Transition data to the third instance is realized using “Network Streams” protocol. That last instance (PC computer) is responsible for recording all collected data. That instance is dedicated to data analysis and diagnostic tasks.

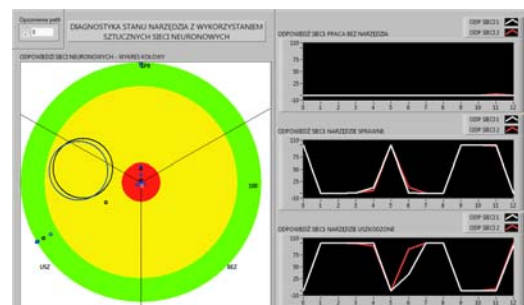


Fig. 11. The view of diagnostic screen

The important component of implemented supervision system is Human – Machine Interface. Such an interface delivers many functions improving comfort of operators work. It was assumed that HMI would have been realized on two wireless panels. To expand supervisory system on remote devices working under Windows operating system LabView Mobile Module from LabView National Instruments were used. The module supports Shared Variable Engine and cooperates with Data Acquisition devices. As an operator panel tablet Acer Inconia Tab W500 and smartphone HTC HD2 were chosen.

The interface implemented on PC and operator panel displaying results of diagnostic analysis. The example of such view is presented in the figure 11.

5. SUMMARY

As it was described a micro machine for milling were designed, assembled and tested. On the basis on the recorded signals analysis of diagnostic procedure were done. Due to that analysis diagnostic system using neural networks were designed in Matlab and implemented in LabView. Tests shows that the best results are obtained when the decision about actual state of the machine is make on the basis of combined answers from 4 nets.

The study has been supported by the Grant No N R03 0050 06/2009 "Construction of a prototype system for testing micromachining – researches and modeling of process" financed by the Polish Ministry of Science and Higher Education.

REFERENCES

- [1] L. Wang, R. X. Gao, *Condition Monitoring and Control for Intelligent Manufacturing*. Springer-Verlag, London, 2006.
- [2] R.T. Howe, *Micro systems research in Japan*. World Technology Evaluation Center (WTEC), 2003.
- [3] www.moriseiki.com
- [4] www.kugler-precision.com
- [5] www.kernmicrotechnic.com
- [6] Y. B. Bang, K. Lee and S. Oh, "5-Axis micro milling machine for machining micro parts", *Advanced Manufacturing Technology*, 2004.
- [7] Y. Okazaki, N. Mishima and K. Ashida, "Microfactory-concept, history, and developments", *Journal of Manufacturing Science and Engineering*, vol. 126, pp 837–844, 2004.
- [8] E. Kussul, T. Baidyk, L. Ruiz-Huerta, A. Caballero-Ruiz, G. Velasco and L. Kasatkina, "Micromechanical engineering: a basis of the low-cost manufacturing of mechanical micro devices using micro equipment", *Journal of Micromechanics and Microengineering*, vol. 6, pp. 410–425, 1996.
- [9] E. Kussul, T. Baidyk, L. Ruiz-Huerta, A. Caballero-Ruiz, G. Velasco and L. Kasatkina, "Development of micromachine tool prototypes for microfactories", *Journal of Micromechanics and Microengineering*, vol. 12, pp. 795–812, 2002.
- [10] Brandon C. Gegg, C. Steve Suh, Albert C. Luo, *Machine Tool Vibrations and Cutting Dynamics*, Springer 2011.
- [11] Ki Bang Lee, *Principles of Microelectromechanical System*, Willey 2010.
- [12] Rolf Iserman, *Fault Diagnosis Applications*, Springer 2011



Bogdan BROEL-PLATER received the M.Sc. and Ph.D degrees in control engineering in 1975 and 1986, respectively. Currently assistant professor in the Department of Control Engineering and Robotics, Faculty of Electrical Engineering, West Pomeranian University of Technology, Szczecin. Main scientific interests: programmable logic controllers, industrial application of fuzzy-logic control, mechatronics.



Pawel DWORAK received the M.Sc. and Ph.D degrees in control engineering in 1999 and 2005, respectively. Currently assistant professor in the Department of Control Engineering and Robotic, West Pomeranian University of Technology, Szczecin. Main scientific interests: multivariable control systems, adaptive control, process data acquisition and visualization, industrial applications of modern control algorithms.



Krzysztof JAROSZEWSKI received the M.Sc. and Ph.D. degrees in control engineering in 2001 and 2007, respectively. Currently assistant professor in the Department of Control Engineering and Robotic, West Pomeranian University of Technology, Szczecin. Main scientific interests: artificial intelligence, especially neural networks, control systems and visualization, industrial diagnostic.

RESEARCH ON STRUCTURE AND DIRECTIONAL DISTRIBUTION OF VIBRATION GENERATED BY ENGINE IN THE LOCATION WHERE VIBRATIONS PENETRATE THE HUMAN ORGANISM

Rafał BURDZIK

The Silesian University of Technology, Faculty of Transport
Kraśińskiego 8, 40-019 Katowice, Poland fax./tel. 6034166 rafal.burdzik@polsl.pl

Summary

The paper presents the results of investigation on directional distribution of vibration generated by engine. The vibration are strongly correlated to comfort and safety of driving. The results of the research enable analyzing the vibration propagation from engine to human body. The structures and directional distribution of the vibrations have been registered in the location where vibrations penetrate the human organism.

Keywords: vibration propagation, vibration structure, car vehicle

BADANIA STRUKTURY I ROZKŁADU KIERUNKOWEGO DRGAŃ POCHODZĄCYCH OD SILNIKA W MIEJSCACH WNIKANIA DO CIAŁA KIEROWCY

Streszczenie

W artykule przedstawiono wyniki badań kierunkowego rozkładu drgań generowanych przez silnik pojazdu na postoju. Komfort i bezpieczeństwo jazdy są ściśle powiązane z drganiami pojazdu. Uzyskane wyniki badań umożliwiają precyzyjną analizę propagacji drgań od silnika do organizmu człowieka. Drgania rejestrowano w 3 osiach w miejscach konstrukcyjnych, w których drgania przenoszone są na ciało człowieka.

Słowa kluczowe: propagacja drgań, struktura drgań, pojazd samochodowy

1. INTRODUCTION

The vibrations are inseparable phenomena during operating and driving by all means of transport. Vehicles in motion are forced to vibration mainly by the road. There are many of different vibration sources in vehicles as well. Some of them are main source of vibration during operating but without any movement. The motor engine should be considered as one of the most important vibration generator when the car doesn't drive [1-4].

In order to examine vibration related phenomena occurring in a moving vehicle or a stationary one with its engine on, one should start with identification of vibration sources. Vibration sources in a vehicle are dynamic forces but also free vibrations as well as forced, self-induced, parametrical, non-parametrical, random and stationary ones, all generated by the driving unit, the power transmission system and the road. Due to the properties of vibration related phenomena, they may be analysed from the perspective of diagnostics, degradation and impact on men.

The information capacity of the vibration signal is very large. It can give the information about comfort and safety. Analysis of vibration related phenomena is a solution commonly applied in Structural Health Monitoring (SHM) systems [5-12]. One may distinguish between two major approaches

to detection and positioning of defects in SHM systems, i.e. global [13] and local [14] methods. The vibrations have to be considered as results of dynamics system, material properties and construction [15-17].

2. VIBRATION OF CAR VEHICLE AND HUMAN PERCEPTION

During operating of vehicles there are many vibration generated by the different sources. Motor engine should be considered as the vibration generator as well. This kind of machine generate a disturbing force of one sort or another, but the frequency of the disturbing force should not be at, or near, a natural frequency of the structure otherwise resonance will occur, with the resulting high amplitudes of vibration and dynamic stresses, and noise and fatigue problems. There are two basic types of structural vibration: steady-state vibration caused by continually running machines such as engines, air-conditioning plants and generators either within the structure or situated in a neighbouring structure, and transient vibration caused by a short-duration disturbance such as a lorry or train passing over an expansion joint in a road or over a bridge.

Ride comfort is extremely difficult to determine because of the variations in individual sensitivity to

vibration. Therefore many researchers have concentrated their efforts on reducing the amount of vibration from vehicles. Some interesting researches were conducted for the low frequency discomfort for human analysed [18]. Ride vibrations are transmitted to the driver buttocks and back by the seat. The floor panel, pedal and steering wheel transmit additional vibrations to the feet and hands of the driver. These vibrations are producing a level of discomfort for driver.

Human perception of vibration is very good. A human organism may then be perceived as a complex spring-mass system of a large number of degrees of freedom and diversified properties characterising elasticity, damping, masses, frequency of free vibrations of individual components and human organs. The division of human perception of vibrations determines the subjective and psychosomatic responses as well as disturbances in the system functioning. As regards the location where vibrations penetrate the human organism, one may speak of general and local vibrations. General vibrations are transferred into the human organism via feet in a standing position or via the pelvis, the back and feet in a sitting or lying position. Local vibrations affect the human organism through upper limbs. Perception of the impact of wave related phenomena, such as noise and vibrations, on a human being is a complex matter, also in terms of the very nature of the said phenomena. The vibration energy affecting the human organism originates in the direct penetration area exclusively, therefore, what matters for the vibration perception is the energy affecting a unit of surface area in a unit of time. It is a real challenge in structural design to ensure that the perception threshold level is not exceeded. An indication of the likely human response to vertical vibration is shown in Fig. 1.

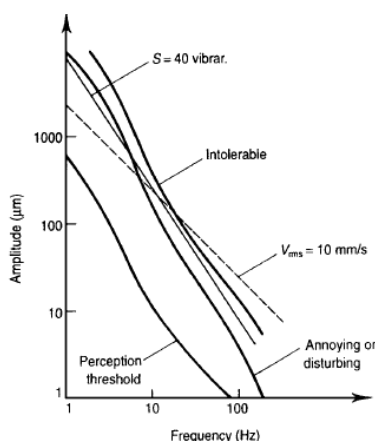


Fig. 1. Human response to vibration [19]

It shows harmonic vibration amplitude as a function of frequency. As it is presented the lines for constant velocity have smaller slopes than lines for constant vibration intensity. Therefore standards based on constant velocity give increased weight to lower frequency vibrations which are more likely to

induce structural resonance and damage than frequencies above 50 Hz.

The perception of vibrations occurring in automotive vehicles depends on physical characteristics and the current state of the man, the location and the area of the vibration penetration into the organism, the time-frequency structure of the penetrating vibrations which enables assessment of the exposure time for vibrations of specific frequencies.

3. RESEARCH

Under the studies in question, active experiments were undertaken featuring measurements of vibration accelerations in a three directions in three selected points to analyse propagation of vibration generated by engine to driver feet and back.. It were recorded the vibration in three orthogonal axes (X,Y,Z). The purpose of the research was analysis of the car body vibration generated from motor engine. The experiments were conducted on the car vehicle which was placed on the special test racks. It allows eliminate the road roughens impact on the suspension and in result to car body. The paper presents some results of measurements vibration of motor engine, floor of the car under the driver foots and driver seat. It enables to analyse the way of vibration transfer from the source to driver. Ride vibrations are transmitted to the driver buttocks and back by the seat. The floor panel transmit additional vibrations to the feet of the driver. These vibrations are producing a level of discomfort for driver.

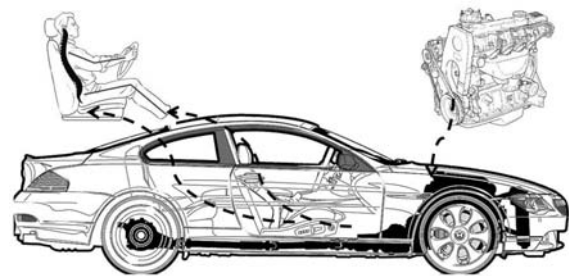


Fig. 2. Engine vibration transfer into human organism

The established scope of research enables to observe changes of the vibration for chosen points on the vibration propagation way from engine. The three orthogonal axes were analysed separately. The comparison of the acceleration of vibration signals allows determine which directions of the vibration propagation is parent. The proposed methodology allows estimate influence of vibration generated by engine on human perception of vibration. Rotating machinery such as motors can generate disturbing forces at several different frequencies such as the rotating speed and blade passing frequency. Reciprocating machinery such as compressors and engines can rarely be perfectly balanced, and an

exciting force is produced at the rotating speed and at harmonics.

The acceleration of vibration sensors type ADXL were used. The ADXL are complete acceleration measurement systems on a single, monolithic IC. It was used the dual-axis accelerometer (Fig. 3 and 4).



Fig. 3. ADXL sensors on engine block



Fig. 4. ADXL sensors on floor panel and seat

The established scope of research enables to observe changes of the vibration for idle gear rotational speed increase. The idle gear rotational speeds founded during research were:

- 750 rpm,
- 1500 rpm,
- 2000 rpm,
- 3000 rpm.

The signals are nonstationary so to analyze the human perception as the exposure to vibration in chosen frequency band the time-frequency transformation have to be made. The STFT signal distribution has been depicted in Fig. 16-17. It allows observing how long vibration in chosen frequency band is propagating to the structure.

4. RESULTS

The registered signals are nonstationary so to analyze the human perception to vibration in chosen frequency band the time-frequency transformation have to be made. It enables comparison of structure of vibration for different direction and rotational speed. The STFT signal distribution has been depicted in Figures bellow. It allows observing how long vibration in chosen frequency band is propagating to the structure.

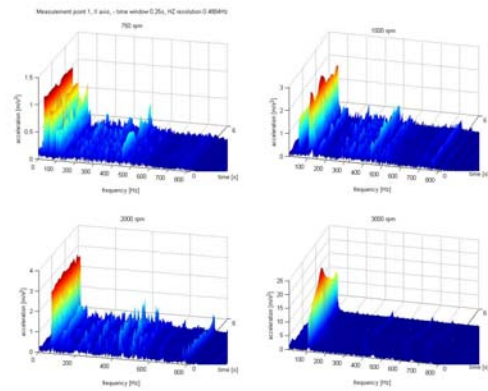


Fig. 5. t-f distribution of the vibration for different rotational speed of engine, block of engine X axis

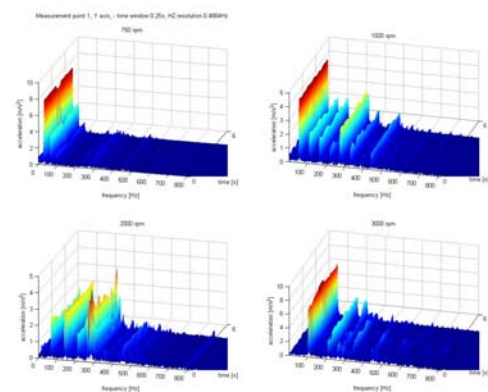


Fig. 6. t-f distribution of the vibration for different rotational speed of engine, block of engine Y axis

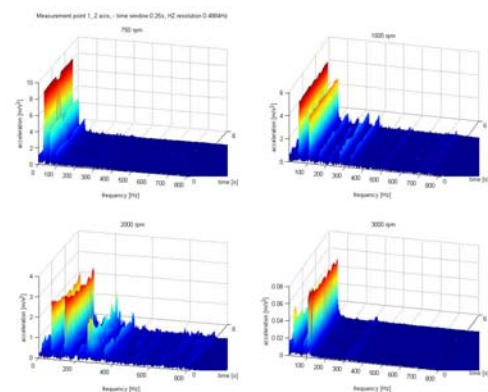


Fig. 7. t-f distribution of the vibration for different rotational speed of engine, block of engine Z axis

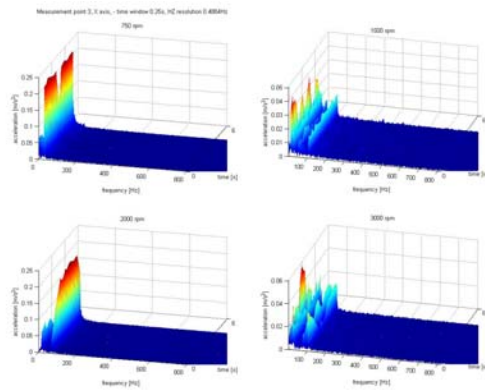


Fig. 8. t-f distribution of the vibration for different rotational speed of engine, floor panel X axis

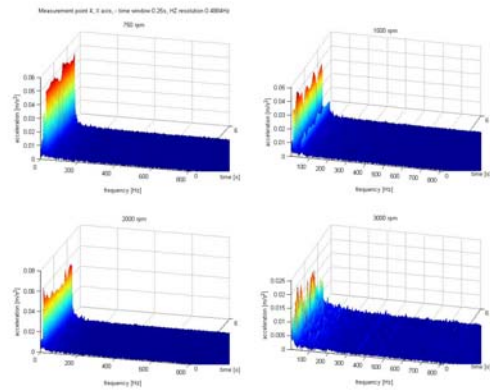


Fig. 11. t-f distribution of the vibration for different rotational speed of engine, driver seat X axis

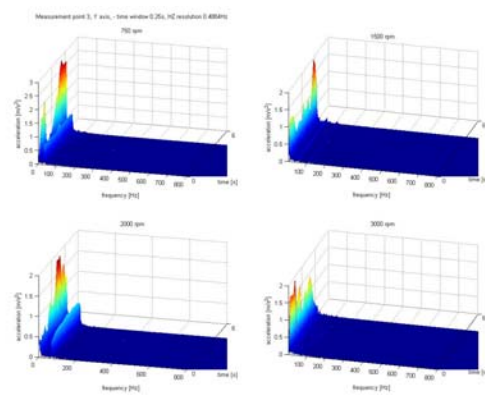


Fig. 9. t-f distribution of the vibration for different rotational speed of engine, floor panel Y axis

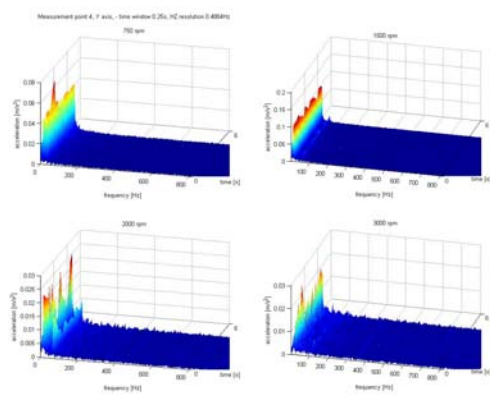


Fig. 12. t-f distribution of the vibration for different rotational speed of engine, driver seat Y axis

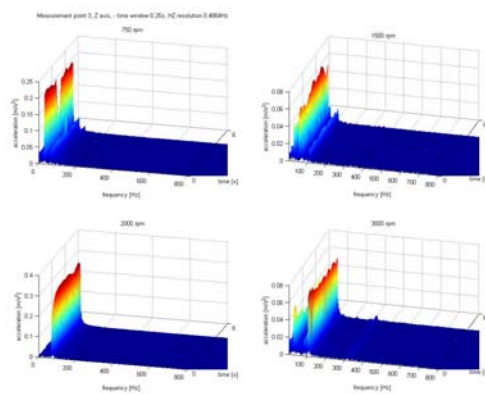


Fig. 10. t-f distribution of the vibration for different rotational speed of engine, floor panel Z axis

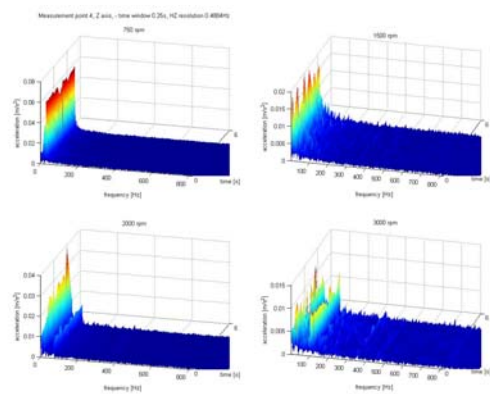


Fig. 13. t-f distribution of the vibration for different rotational speed of engine, driver seat Z axis

4. CONCLUSION

The results of the research enable analyzing the vibration propagation from engine to human body. The structures and directional distribution of the vibrations have been registered in the location where vibrations penetrate the human organism. The vibration of floor panel and seat have got much more less higher frequencies components. It can't be define that increase of rotational speed of the engine causes the vibration increase.

6. LITERATURE

- [1] Burdzik R. *Material vibration propagation in floor pan*. Archives of Materials Science and Engineering, AMSE vol. 59/1 January 2013, s, 22-27.
- [2] Burdzik R., Doleček R.. *Research of vibration distribution in vehicle constructive*. Perner's Contacts vol. VII no. 4, 2012, pp. 16-25.
- [3] Burdzik R., Stanik Z., Warczek J. *Method of assessing the impact of material properties on the propagation of vibrations excited with a single force impulse*. Archives of Materials and Metallurgy 57(2), 2012, pp. 409-416.
- [4] Burdzik R. *Monitoring system of vibration propagation in vehicles and method of analysing vibration modes*. J. Mikulski (Ed.): TST 2012, CCIS 329, Springer, Heidelberg, 2012, s. 406-413.
- [5] Jasinski M., Radkowski S. *Use of the higher spectra in the low-amplitude fatigue testing*. Mechanical Systems And Signal Processing 25(2) (2011) 704-716.
- [6] Figlus T., Wilk A. *Comparison of the sound pressure measurement and the speed measurement of the gearbox vibrating surface*. Journal of Transport Problems vol. 7 issue 1, 2012, pp. 37-42.
- [7] Tuma J. *Gearbox noise and vibration prediction and control*. International Journal of Acoustics and Vibration vol. 14 issue 2 (2009) 99-108.
- [8] Pojawa B. *The energetic diagnostics of naval propulsion system with naval gas turbine*. Diagnostyka 2(50), 2009, pp. 55-58.
- [9] Michalski R., Wierzbicki S. *An analysis of degradation of vehicles in operation*. Maintenance and Reliability 1(37), 2008, pp. 30-32.
- [10] Cempel C., Tabaszewski M. *Multidimensional vibration condition monitoring of non-stationary systems in operation*. Mechanical Systems and Signal Processing 21 (3), 2007, pp. 1233-1241.
- [11] Cempel C. *Singular values of symptom observation matrix of a system in operation as indicators of system damage*. Diagnostyka 4(60), 2011, pp. 27-38.
- [12] Urbanek J., Barszcz T., Uhl T. *Comparison of advanced signal-processing methods for roller*

bearing faults detection. Metrology and Measurement Systems, 19(4), 2012, 715-726.

- [13] Uhl T., *The use and challenge of modal analysis in diagnostics*. Diagnostyka vol. 30 i. 2, 2004, pp. 151-160.
- [14] Raghavan A., CES. Cesnik. *Review of guided – waves structural health monitoring*, The Shock and Vibration Digest 39, 2007, pp. 91-114.
- [15] Blacha L., Siwiec G., Oleksiak B. *Loss of aluminium during the process of Ti-Al-V alloy smelting in a vacuum induction melting (VIM) furnace*. Metalurgija 52 (3), 2013, p. 301-304.
- [16] Folega P., Siwiec G. *Numerical analysis of selected materials for flexsplines*. Archives of Metallurgy and Materials 57 (1), 2012, p. 185-191.
- [17] Mencik J. *Determination of parameters of visco-elastic materials by instrumented indentation*. Part 3: rheological model and other characteristics, Chem. Listy 104, 2010, pp. 275-278.
- [18] Wyllie I.H., Griffin M.J. *Discomfort from sinusoidal oscillation in the pitch and fore-and-aft axes at frequencies between 0.2 and 1.6Hz*. Journal of Sound and Vibration 324, 2009.
- [19] Beards C.F. *Structural Vibration: Analysis and Damping*. Halsted Press, New York 1996.
- [20] Niziński S., Wierzbicki S., Ligier K., *Model matematyczny procesu eksploatacji pojazdów mechanicznych*. WITPIS, Sulejówek, 2002.
- [21] Wierzbicki S., *Evaluation of on-board diagnostic systems in contemporary vehicles*. Diagnostyka 2 (4)/2011, p.35-40



Rafal BURDZIK is Ph.D. in Department of Automotive Vehicle Construction, Faculty of Transport, Silesian University of Technology. His research interests are: noise and vibration in transport, machinery diagnostic, digital analyse of signals, logistics and forwarding. He is the member of PAN Commission of Transport - member of the Bureau, the Secretary. He is the member of PTDT.

THE UNCERTAINTY OF DETERMINING SHOCK ABSORBER DAMPING CHARACTERISTIC ON INDICATOR TEST STAND

Łukasz KONIECZNY, Rafał BURDZIK, Jan WARCZEK

The Silesian University of Technology, Faculty of Transport
Kraśińskiego 8, 40-019 Katowice, Poland fax./tel. 6034166 lukasz.konieczny@polsl.pl

Summary

The paper presents the research results of twin-tube hydraulic front shock absorber used in the column McPherson. It was conducted on indicator test stand. The force vs displacement and force vs. velocity diaphragms were determined. Loop diagrams are set of average for several full cycles shock absorber (compression and decompression). For this average the uncertainty of shock absorber damping characteristics was determined.

Keywords: shock absorber, damping characteristic

NIEPEWNOŚĆ WYZNACZANIA CHARAKTERYSTYKI TŁUMIENIA AMORTYZATORA NA STANOWISKU INDYKATOROWYM

Streszczenie

W ramach referatu przedstawiono wyniki badań amortyzatora hydraulicznego dwururowego przedniego stosowanego w kolumnie McPhersona przeprowadzonych na stanowisku indykatorowym. W ramach badań wyznaczono wykresy pracy oraz wykresy prędkościowe. Wykresy pętlicowe stanowią realizacje średnie wyznaczone dla kilkudziesięciu pełnych cykli pracy amortyzatora (sprężanie i rozprężanie). Dla tak wyznaczonych realizacji średnich określono niepewność wyznaczenia charakterystyki tłumienia amortyzatora.

Słowa kluczowe: amortyzator hydrauliczny, charakterystyka tłumienia

1. INTRODUCTION

The objective assessment of the technical condition of the shock can be examined on indicator shock absorber test stand. Such examination can generate the work graph of the shock absorber (force-displacement) and a velocity graph (force-linear velocity) and determine damping characteristics. Example of testing of MTS shock absorber test stand has been depicted in Fig. 1.



Fig. 1. MTS shock absorber test stand

Determination of the damping characteristics can be achieved by two ways. The first based on designated force-displacement diagram at a constant stroke and variable angular velocity. Forced damping value assuming the maximum speed of the piston at compression and decompression can receive points for the shock absorber damping characteristics as shown in Fig. 2.

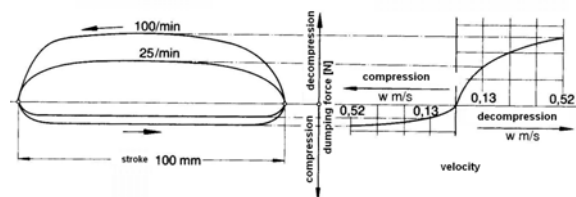


Fig. 2. Determined shock absorber characteristics with variable angular velocity and constant stroke [3]

In the second approach, the angular velocity is constant and the value of the stroke is changing (Fig. 3) The damping characteristic is determined the same way as in the first case, assuming a value for the maximum damping piston velocity (separately compression and decompression).

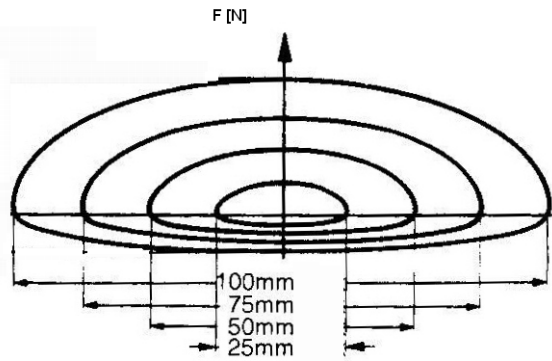


Fig. 3. Determined shock absorber characteristics with variable stroke and constant angular velocity [3]

The implementation of the calculation of the characteristics of the first and second approach may lead to some discrepancies in the designed characteristics (authors confirmed that in the publication [5]).

These differences result from differences in the components designated maximum velocity, i.e. the value of the stroke and the angular velocity. For the assumed constant linear speed for large values of stroke at low frequencies is much larger pumped fluid than is the case with short strokes and high-frequency excitation. Therefore, it was proposed to develop the characteristics of the graph $F(v)$ to the plane of $F(s, v)$ – force vs stroke and linear velocity (Fig. 4).

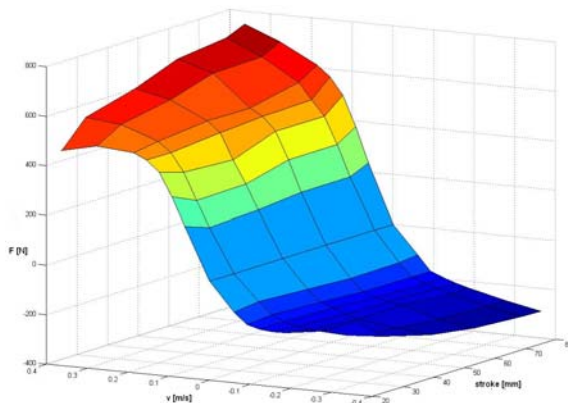


Fig. 4. Shock absorber damping force as a function of velocity and stroke

2. RESEARCH ON INDICATOR TEST STAND

The research on twin-tube hydraulic front shock absorber used in the MsPherson strut were carried out on indicator test stand. The Figure 5 shows view of the indicator test stand with mounted shock absorber.



Fig. 5. Indicator test stand

The measuring system diagram is shown in Figure 6.

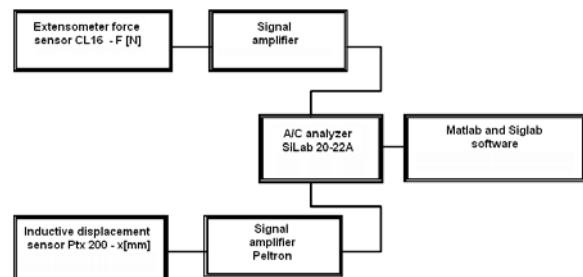


Fig. 6. Measurement system

The force sensor CL 16 accuracy class of 0.5% is relative to the result of a measurement in the range of 10% to 100% range of the sensor. Displacement transducer is characterized by a basic error of 0.5% of the measuring range. The analyzer SigLab 20-22 overall accuracy: $\pm 0.0025\%$ of full scale.

After mounting the shock absorber to the test stand, and checking the correctness of the assembly process followed warm up of the cold oil in shock absorber (work for about 60 [s]). After an initial warm-up followed data acquisition process.

Measurements were made for 13-teen different angular velocities (frequency set on inverter) of excitation and constant stroke 50 [mm]. The plots of force vs. displacement (Figure 7) and force vs. linear velocity (Figure 8) are averaged loop.

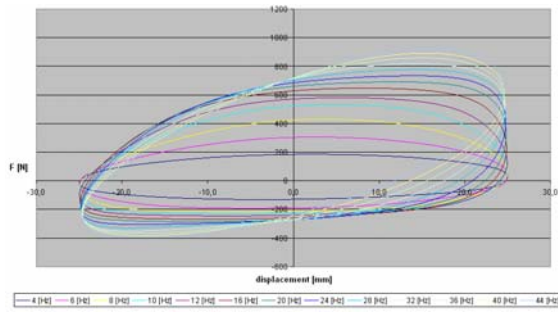


Fig. 7. Force vs. displacement (frequency set on inverter in [Hz])

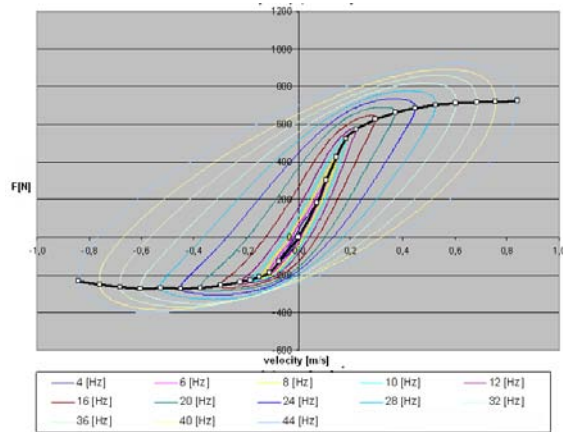


Fig. 8. Force vs. velocity (frequency set on inverter in [Hz]) and damping characteristic (black line)

The figure 8 contains marked damping characteristics designated for the maximum velocity limit (black line).

The averaged loop diagram were determining by the procedure as follow. The minimum number of 25 full cycles consisting of compression and decompression were recorded. The figures 9 and 10 shows imposed the single loop recorded at the time of forces and displacements.

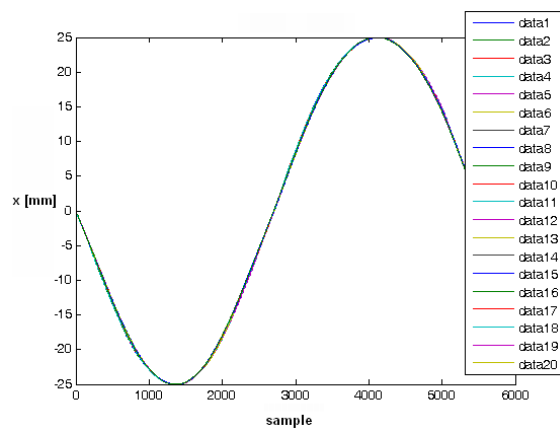


Fig. 9. Imposed displacements single loop recorded at time.

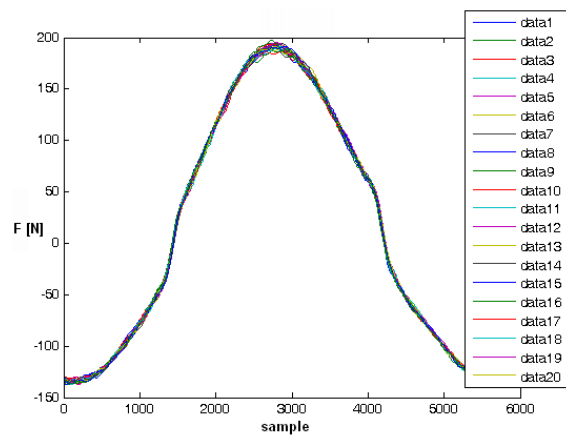


Fig. 10. Imposed forces single loop recorded at time

The value of force when displacement is zero (the position in the middle of the stroke -maximum linear velocity) is taken to the damping characteristics (separately compression and decompression). Sample values of forces for maximum velocity (for frequency 0.48 Hz) recorded in subsequent cycles shows figure 11.

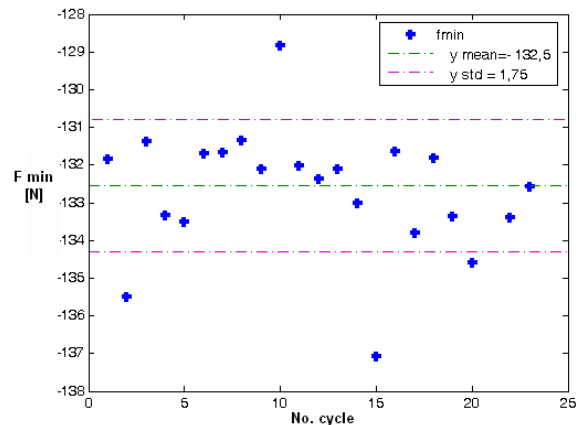


Fig. 11. Sample values of forces for maximum velocity in subsequent cycles

In the laboratory practice the normal distribution is assumed to 2σ estimate (ie with a probability $p \approx 0.95$) for the statistics of the measurements. Figure 12 and 13 show the damping characteristics for compression and decompression with the area of uncertainty.

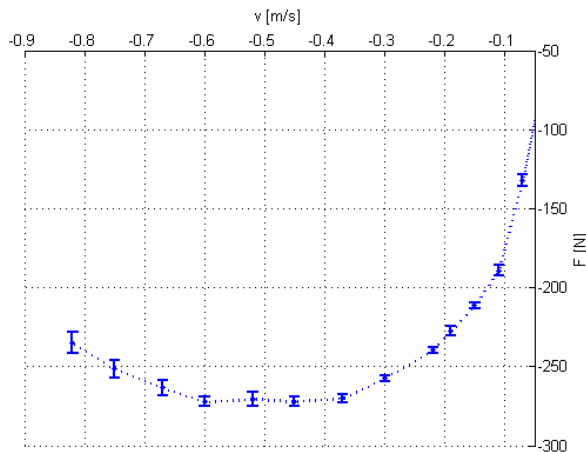


Fig. 12. Damping characteristics with the area of uncertainty for compression

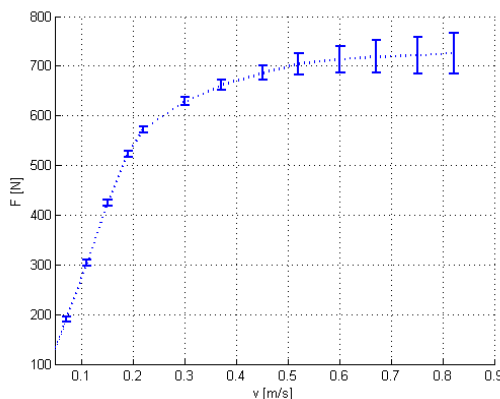


Fig. 13. Damping characteristics with the area of uncertainty for decompression

3. SUMMARY

Determination of the damping characteristics based on the average value of force for point of maximum velocity is affected of a small uncertainty of 5%. This value is also related to the accuracy of determining the representative loop. Small uncertainty of loop changes for a constant excitation provides quality of the shock absorber.

LITERATURA

- [1]. Dixon J. C. *The shock absorber handbook*. Society of Automotive Engineers, USA 1999
- [2]. Gardulski J., Warczek J.: *Investigation on force in frictional kinematic pairs to assess their influence on shock absorber characteristic*. Transport Problems, volume 3, Issue 1, Gliwice 2008 s.19-24.
- [3]. Konieczny Ł.: *Badania amortyzatorów hydraulicznych na zmodyfikowanym stanowisku indykatorowym*. Zeszyty Naukowe Politechniki Śląskiej, s. Transport, z.61 Wydawnictwo Politechnik Śląskiej, Gliwice 2007 s.151-156.
- [4]. Konieczny Ł., Śleziak B.: *Wpływ wybranych parametrów na charakterystyki tłumienia*

amortyzatorów hydraulicznych. Zeszyty Naukowe Politechniki Śląskiej, s. Transport, z.64 Wydawnictwo Politechnik Śląskiej, Gliwice 2008 s.145-150.

- [5]. Konieczny Ł., Burdzik R., Warczek J.: *Determinations of shock absorber damping characteristics taking stroke value into consideration account*. Diagnostyka 2010 nr 3, s. 51-54.
- [6]. Lanzendoerfer J.: *Badania pojazdów samochodowych*. WKiŁ, Warszawa 1977.
- [7]. Michalski R, Wierzbicki S.: *An analysis of degradation of vehicles in operation*. Eksploatacja i Niezawodność – Maintenance and Reliability 2008; 1(37): 30-32.
- [8]. Reipell J., Betzler J.: *Podwozia samochodów – podstawy konstrukcji*. WKiŁ Warszawa, 2001, Sikorski J.: *Amortyzatory – budowa – badania – naprawa*. WKiŁ, Warszawa 1984.



Lukasz KONIECZNY is Ph.D. in Department of Automotive Vehicle Construction, Faculty of Transport, Silesian University of Technology. His research interests are: machinery vibrodiagnostic, digital analyse of signals, simulation researches of vehicle suspension dynamic, hydro-pneumatic suspensions. He is the member of PTDT.



Rafal BURDZIK is Ph.D. in Department of Automotive Vehicle Construction, Faculty of Transport, Silesian University of Technology. His research interests are: noise and vibration in transport, machinery diagnostic, digital analyse of signals, logistics and forwarding. He is the member of PAN Commission of Transport - member of the Bureau, the Secretary. He is the member of PTDT.



PhD Eng. **Jan WARCZEK** is a researcher in Department of Vehicle Car Construction, Faculty of Transport Silesian Technical University Research interests: diagnostics and experimental simulation using vibroacoustics methods, dynamics of vehicle suspensions, method of active vibration reduction.

MODEL OF RAIL CRACK BASED ON A DISCRETE SET OF LOOPS WITH CURRENT

Vitalij NICHOGA*, Igor STOROZH*, Liubomyr VASHCHYSHYN**

* Lviv Polytechnic National University

S. Bandery Str., 12, Lviv, 79013, UKRAINE, e-mail: nich@org.lviv.net

** Karpenko Physico-Mechanical Institute of the NAS of Ukraine

Naukova Str., 5, Lviv, 79601, UKRAINE, e-mail: myalternative@inbox.ru

Abstract

This article describes the model of the crack in the railway rail, for the magnetic crack detection system, based on interpretation of the magnetized material as a set of loops with current. Calculated field distributions along the rail with crack are shown.

Key words: rail, crack, model

MODEL PĘKNIĘCIA SZYNY KOLEJOWEJ BAZUJĄCY NA DYSKRETNYM PĘTLACH PRĄDOWYCH

Streszczenie

W artykule został opisany model szczeliny w szynie kolejowej, dla magnetycznych systemów wykrywania pęknięć, bazujących na interpretacji materiałów magnetycznych z pętlami prądowymi. Przedstawione zostały obliczone rozkłady pola wzdłuż szyny z pęknięciami.

Słowa kluczowe: kolejowe, pęknięcia, model

1. INTRODUCTION

It is known that the magnetic field leakage diagnostic of the railway is based on research distortion of the magnetic field that occurs in areas of defects.

If the metal of construction of rail is homogeneous in its magnetic properties, its permeability is equal to μ and the magnetic induction B , of magnetizing field, almost enclosed in the rail. In fact if the rail has a defect in the form of cracks perpendicular to the direction to magnetic

field, the magnetic permeability of the defective area is much less than the permeability of the rail.

Consequently, the redistribution of magnetic flux in the area of the cracks: one part of the magnetic flux passing through the crack, the second - through the airways of the defect and the third part will go below the crack. Consequently, the resulting magnetic field above the crack is sharply inhomogeneous (distorted).

Magnetized matter can be regarded as a certain volume filled with elementary contours with current. [1] Under the influence of the external magnetic field, these contours are oriented so that the directions of their fields match. (Fig.1. a)

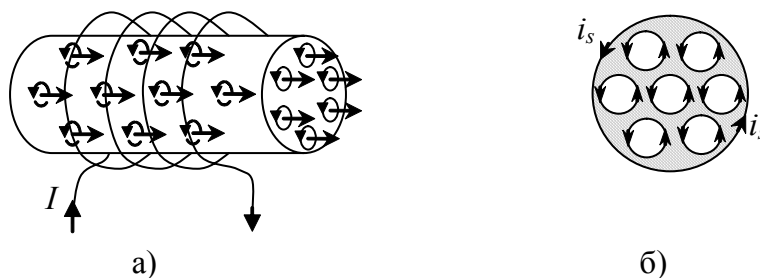


Fig.1. Ferromagnetic body under the magnetic field: a) general view, b) cross section

If we consider the cross section of a magnetized body, transverse contour currents can be presented so that the direction of currents neighboring elementary circuits opposite and, in the case of a

homogeneous field and a homogeneous substance, their effects are mutually compensated (fig.1.b). Uncompensated currents remain only on the surface of the body. These currents are continuously

distributed along the surface of the body. Their value depends on the value magnetizing field and parameters of substance, but does not depend on the size of the body.

Based on the above, rails, magnetized in the longitudinal direction, can be regarded as a single-

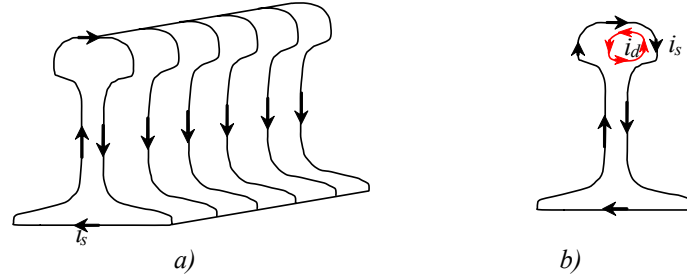


Fig. 2. Currents that occur on the surface of the rails during magnetization with the longitudinal magnetic field (a), the formation of current defect (b)

If there is a defect in the rail, a region whose properties differ from the parameters intact rails, so the internal currents are others. As a result, this area internal currents will not be fully compensated, or just be missing, which is convenient to simulate entering a new loop with the current of defect i_d , whose direction is opposite to the direction of current on the surface of the rail i_s . This will change the scattering field and allow localizing defect.

This representation will allow for known magnetomotive force of magnetizing system of crack detector wagon, magnetic core and rail parameters to calculate the magnetic flux in the rail. Next, replacing magnetized rail with system of loops with currents, these currents can be calculated by determining in advance of their own and mutual inductance by mutual arrangement. The resulting field is a superposition of the fields from all the loops of the model. [1].

2. ADEQUACY OF THE PROPOSED MODEL

To confirm the adequacy of the model calculation was carried out for the signal from the rail junction. The simulation results (fig.3.) coincide with the signal from the rail joint, which was obtained experimentally by averaging signals from 100 rail joints (fig.4.).

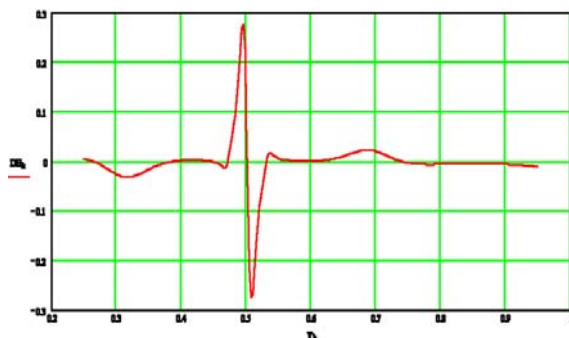


Fig.3. Waveform of rails joint

layer solenoid of the complex form which is evenly distributed winding shape coincides with the shape of the rail. Fig.2 schematically shows the surface currents on the surface of the rails resulting magnetization.

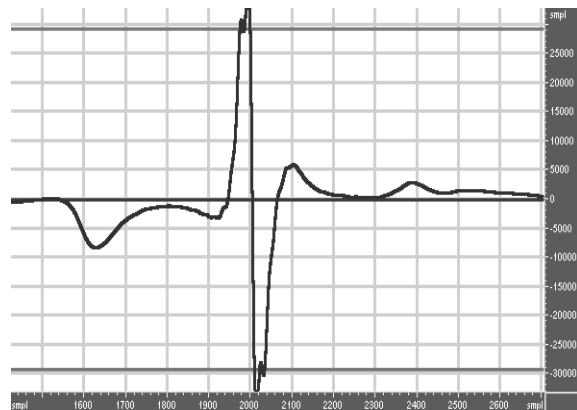


Fig.4. Averaged waveform of 100 rails joints

On the figures 5-7 simulated waveform of crack laying at different depth under surface is presented. The typical change of its shape, depending on depth, can be observed. Such shape corresponds to the shape of waveforms represented in literature [2,3].

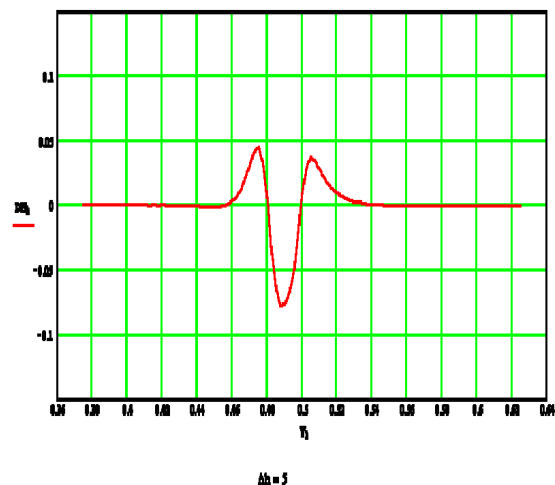


Fig.5. Waveform of crack laying at 5mm under surface.

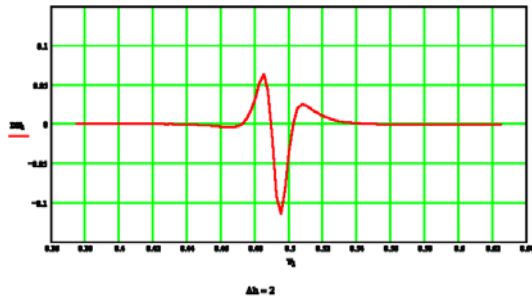


Fig.6. Waveform of crack laying at 2mm under surface.

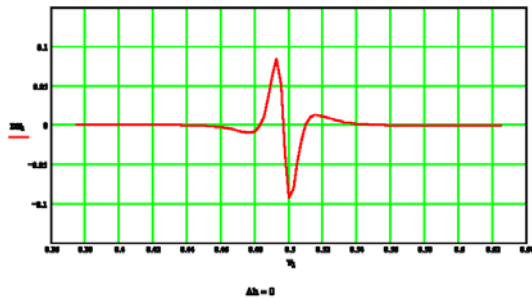


Fig.7. Waveform of crack disclosed to the surface.

Proposed model allows easily simulate the signal from crack caused by longitudinal exfoliation. The result of such simulation, which corresponds to the real signals [2,3], is shown on the figure below.

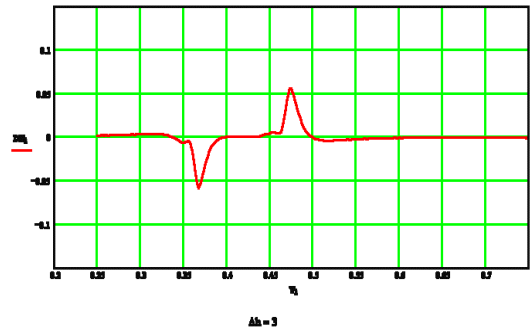


Fig.8. Waveform of signal from longitudinal crack laying at 2mm under surface

Also based on simulated signal from the transverse cracks basis for wavelet analysis of defectoscopic signals was created, which showed better result for the sensitivity to changes in scale than the model based on the magnetic charges.

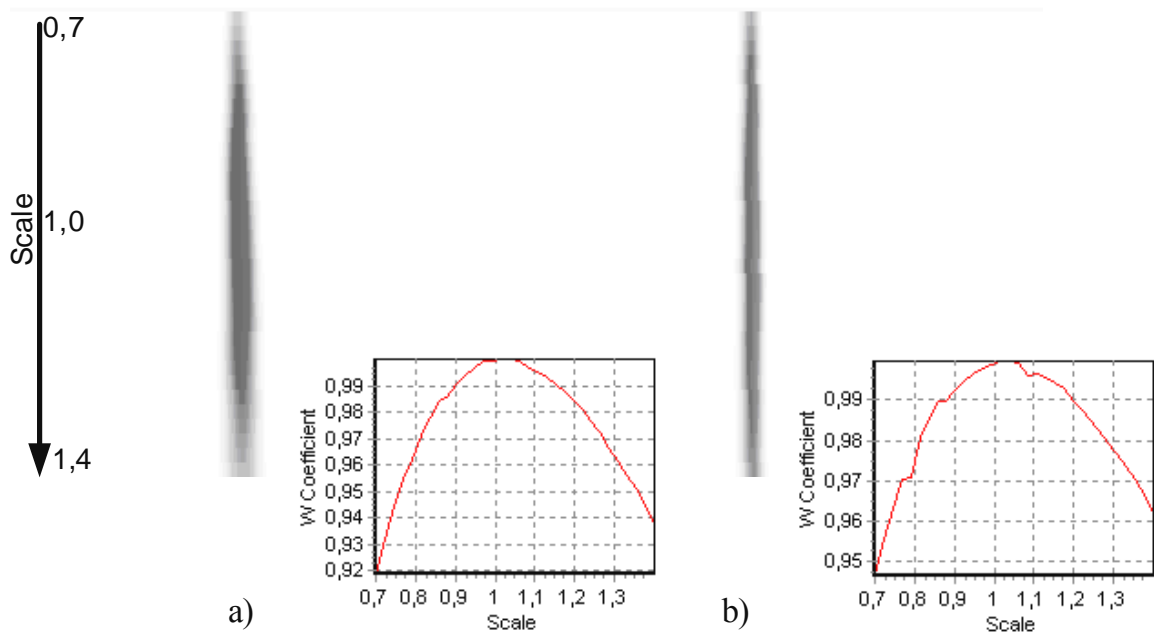
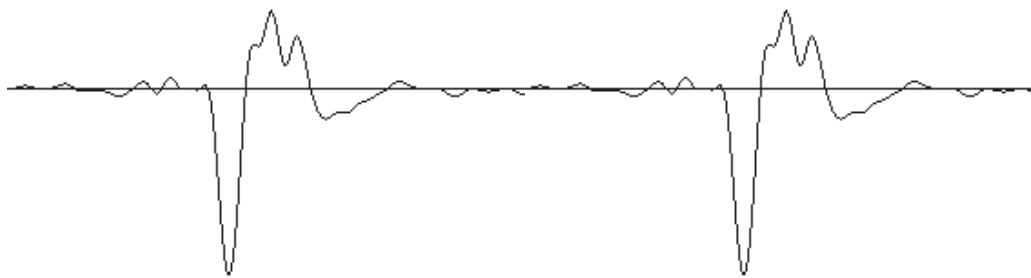


Fig. 9. Wavelet spectrum of the transverse crack waveform using mathematical models based on current loops (a) and magnetic charges (b) as wavelet basis.

3. CONCLUSION

The mathematical model allows creating basis functions for wavelet analysis to further use for automatic recognition of signals from rail defects - cracks and more accurately predicting the type of cracks form signal. Basis functions are used for creating a bank of signals that are necessary for the further development of the algorithm for automatic detection the signal from the real defects in railroad rails.

REFERENCES

- [1] Нестеренко А. *Введение в теоретическую электронехнику*. Наукова думка, Київ 1969
- [2] Гурвич А.: *Неразрушающий контроль рельсов при их эксплуатации и ремонте*. Транспорт, Москва 1983
- [3] Брандис М. *Руководство по дефектоскопии рельсов*. Valacron 2005



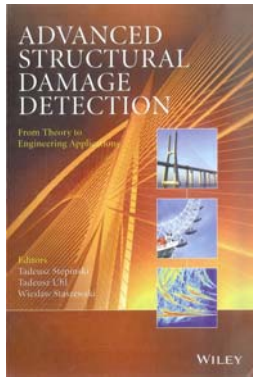
Vitalij NICHOGA,
doctor of technical sciences, professor of the Department of Radio-Electronic Devices and Systems of the Institute of Telecommunications, Radio electronics and Electronic Technics. Basic directions of scientific researches are selection and processing defectoscopic signals.
E-mail: nich@org.lviv.net



Igor STOROZH,
junior scientific worker of Lviv Polytechnic National University. Basic direction of scientific researches is data acquisition hardware and digital signal processing.
E-mail: igor-com-ua@yandex.ru



Liubomyr Vashchyshyn,
postgraduate of the Department of Selection and Processing of Stochastical Signals. Basic direction of scientific researches is processing defectoscopic signals.
E-mail: myalternative@inbox.ru



Tadeusz Stepinski
Tadeusz Uhl
Wieslaw Staszewski

**Advanced Structural
Damage Detection:
From Theory to
Engineering Applications**

*John Wiley & Sons, Ltd.,
2013*

Structural Health Monitoring (SHM) is the interdisciplinary engineering field devoted to the monitoring and assessment of structural health and integrity. SHM technology integrates nondestructive evaluation techniques using remote sensing and smart materials to create smart self-monitoring structures characterized by increased reliability and long live length. Its applications are primarily systems with critical demands concerning performance where classical onsite assessment is related to high costs, difficult or even impossible. This book reports result of the research project MONIT conducted at AGH – University of Science and Technology in Krakow and supported by The European Regional Development Fund in the frame of the program Innovative Economy. Written by academic experts in the field, this book provides students, engineers and other interested technical specialists with a comprehensive review of recent developments in various monitoring techniques and their applications to SHM. Providing a comprehensive review of main SHM techniques it contributes to an area which is a subject of intensive research and development. This book offers both theoretical principles and feasibility studies for a number of SHM techniques. It presents a number of new/novel data processing algorithms and demonstrate real operating prototypes.

Diagnostyka

APPLIED STRUCTURAL HEALTH, USAGE AND CONDITION MONITORING

Obszar zainteresowania czasopisma to:

- ogólna teoria diagnostyki technicznej
- eksperymentalne badania diagnostyczne procesów i obiektów technicznych;
- modele analityczne, symptomowe, symulacyjne obiektów technicznych;
- algorytmy, metody i urządzenia diagnozowania, prognozowania i genezowania stanów obiektów technicznych;
- metody detekcji, lokalizacji i identyfikacji uszkodzeń obiektów technicznych;
- sztuczna inteligencja w diagnostyce: sieci neuronowe, systemy rozmyte, algorytmy genetyczne, systemy ekspertowe;
- diagnostyka energetyczna systemów technicznych;
- diagnostyka systemów mechatronicznych i antropotechnicznych;
- diagnostyka procesów przemysłowych;
- diagnostyczne systemy utrzymania ruchu maszyn;
- ekonomiczne aspekty zastosowania diagnostyki technicznej;
- analiza i przetwarzanie sygnałów.

Wszystkie opublikowane artykuły uzyskały pozytywne recenzje wykonane przez niezależnych recenzentów.

Topics discussed in the journal:

- General theory of the technical diagnostics,
- Experimental diagnostic research of processes, objects and systems,
- Analytical, symptom and simulation models of technical objects,
- Algorithms, methods and devices for diagnosing, prognosis and genesis of condition of technical objects,
- Methods for detection, localization and identification of damages of technical objects,
- Artificial intelligence in diagnostics, neural nets, fuzzy systems, genetic algorithms, expert systems,
- Power energy diagnostics of technical systems,
- Diagnostics of mechatronic and antropotechnic systems,
- Diagnostics of industrial processes,
- Diagnostic systems of machine maintenance,
- Economic aspects of technical diagnostics,
- Analysis and signal processing.

All the published papers were reviewed positively by the independent reviewers.

Redaktorzy działowi:

dr hab. inż. Tomasz BARSZCZ, prof. AGH
dr hab. Andrzej BIELECKI, prof. AGH
prof. dr hab. inż. Wojciech CHOLEWA
prof. dr hab. Wojciech MOCZULSKI
prof. dr hab. inż. Stanisław RADKOWSKI
prof. dr hab. inż. Wiesław TRAMPCZYŃSKI
prof. dr hab. inż. Tadeusz UHL

Kopia wszystkich artykułów opublikowanych w tym numerze dostępna jest na stronie www.diagnostyka.net.pl

Druk:

Centrum Graficzne „GRYF”, ul. Pieniężnego 13/2, 10-003 Olsztyn, tel. / fax: 89-527-24-30

Oprawa:

Zakład Poligraficzny, UWM Olsztyn, ul. Heweliusza 3, 10-724 Olsztyn
tel. 89-523-45-06, fax: 89-523-47-37

Wszystkie opublikowane w czasopiśmie artykuły uzyskały pozytywne recenzje, wykonane przez niezależnych recenzentów.

Redakcja zastrzega sobie prawo korekty nadesłanych artykułów.

Kolejność umieszczenia prac w czasopiśmie zależy od terminu ich nadesłania i otrzymania ostatecznej, pozytywnej recenzji.

Wytyczne do publikowania w DIAGNOSTYCE można znaleźć na stronie internetowej:

<http://www.diagnostyka.net.pl>

Redakcja informuje, że istnieje możliwość zamieszczania w DIAGNOSTYCE ogłoszeń i reklam.

Jednocześnie prosimy czytelników o nadsyłanie uwag i propozycji dotyczących formy i treści naszego czasopisma.

Zachęcamy również wszystkich do czynnego udziału w jego kształtowaniu poprzez nadsyłanie własnych opracowań związanych z problematyką diagnostyki technicznej. Zwracamy się z prośbą o nadsyłanie informacji o wydanych własnych pracach nt. diagnostyki technicznej oraz innych pracach wartych przeczytania, dostępnych zarówno w kraju jak i zagranicą.